Università degli Studi di Firenze

DOTTORATO DI RICERCA IN

"*Scienze Fisiologiche e Nutrizionali*"

CICLO XXV

COORDINATORE Prof. Poggesi Corrado

Impact of sarcomeric protein mutations associated to myopathies on the mechanics and energetics of myofibril contraction

Settore Scientifico Disciplinare BIO/09

Dottorando

Dott. ssa Ferrara Claudia

Tutore

Prof. Poggesi Corrado

Prof. ssa Tesi Chiara

Anni 2010/2012

Contents

Chapter 1: Introduction

1.0 Myopathies

Muscle diseases, also called myopathies, are pathologies of the cross-striated muscle that affect muscle fiber function, both cardiac and skeletal, ultimately resulting in muscle weakness. "Myopathy" originates from the greek words "myo" meaning muscle, and "pathos" meaning suffering. Myopathies may have different origins. Congenital myopathies are usually caused by mutations in muscle specific genes coding for proteins, mainly present in the sarcomere.

1.1 Structure of sarcomeres

The striated pattern in muscle cells is the result of the arrangement of thick and thin filaments into myofibrils. Myofibrils form the contractile apparatus inside each muscle fiber in which every myofibril has a parallel, longitudinal disposition and cylindrical shape of diameter around 1 µm. In each myofibril, the contractile apparatus is organized in single units, the sarcomeres, that repeat logitudinally every 2-2.5 µm along myofibrils and fiber and, in physiological state, aligne with sarcomeres of parallel myofibrils. The striations that caracterize both cardiac and skeletal muscle and determine the repeating pattern of the sarcomere, are formed by alterning regions of higher and lower optical density, due to thick and thin filaments arrangement in each myofibril, named A and I bands, respectively. The sarcomer is bounded by optical dense Z-discs at the centre of each I-band. The A-band is positioned around the lighter H-zone, Figure 1, (Gregorio CC and Antin PB, 2000). The muscle shortening is associated to the reduction of width of I-band and H-zone, without any variation of A-band width (Squire JM, 1997). So, when sarcomere shortens, reduction of the distance between neighbouring Z-line is related to the sliding of actin thin filaments towards the center of the sarcomere, causing the increase of overlapping of thin and thick filament, without any variation in the length of both filaments (Huxley AF, 1957; Huxley HE, 1969; Squire JM, 1997). Thick and thin filaments are fomed by polimerization of the two principal contractile proteins, myosin and actin, respectively. Actin and myosin form the ‘molecular motor’ in muscles. Myosin works as an enzyme performing ATP hydrolysis under the allosteric control of actin such that actin binding initiates ATP product release and force generation in the myosin power stroke (see below).

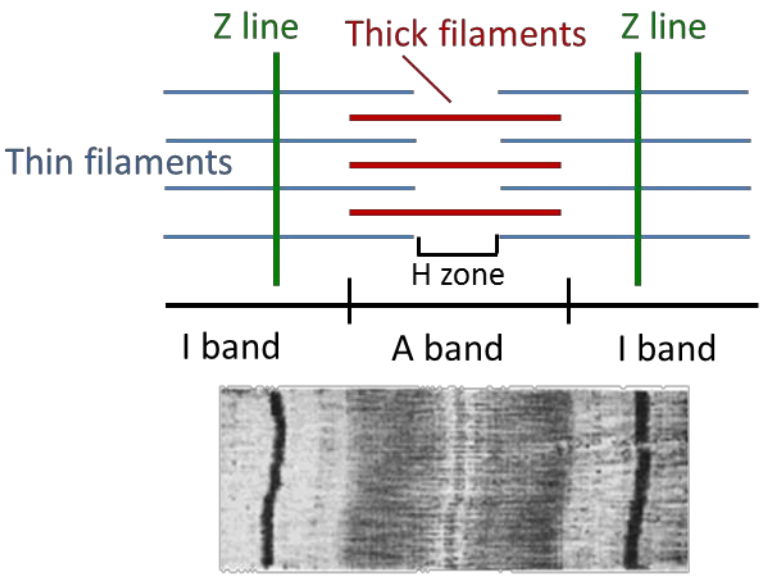

Figure 1. Structure of the sarcomere, the contractile unit of myofibrils. In each sarcomere, contractile proteins actin and myosin are organized in thin and thick filaments.

1.2 Chemo-meccanical cycle

The sliding filament mechanism, i.e. the shortening of muscle due to sliding of thin on thick filaments, is coupled to the development of force along the sarcomere longitudinal axis and is driven by the myosin molecular motor, which hydrolyzes ATP and cyclically interacts with the actin thread, forming “cross-bridges”. This is the cross-brige chemomechanical cycle (Gordon AM et al., 2000). The reaction pathway can be described as a series of coupled biochemical and mechanical events. The structure of the myosin head (as depicted in Figure 2 and 3 with the light chain binding domain that can move like a lever arm relative to the actin-binding, catalytic domain) is designed to achieve the efficient conversion of biochemical energy into force production. ATP binding to a myosin head (M) causes a rapid, almost irreversible dissociation of the myosin head from actin (A). Following detachment from actin, the ATP is hydrolyzed to ADP and inorganic phosphate (Pi) both remaining tightly bound to the myosin head. The free energy of ATP hydrolysis is not released but remains within the structure of the M.ADP.Pi complex. The hydrolysis is, in fact, accompanied by a major conformational change that represents a “repriming” of the power stroke; both the hydrolysis and the conformational change are reversible. ADP and Pi will remain bound to the myosin head until the myosin binds again to an actin site. The affinity of M.ADP.Pi for actin is significantly higher than that of M.ATP. If an actin site is within the reach of the myosin head, this will bind rapidly and reversibly to the actin site in the presence of ATP. The interaction of the M.ADP. Pi complex with actin can promote a

major change in conformation (the power stroke) which is accompanied by the dissociation of Pi. If the filaments carry an external load (e.g., isometric conditions), then the power stroke results in the distortion of an elastic element. The location of the elastic element is unknown and is described in Figure 2, for simplicity, as part of the S2 region connecting the myosin head to the rod. The dissociation of Pi is a reversible event and Pi can rebind to reverse the power stroke. The final step of the chemo-mechanical coupling is a strain-dependent mechanism of ADP release leading to an AM complex which is rapidly dissociated by new ATP binding. ADP release can be very fast if the external load on the sarcomeres is small, while it is much slower for high loads (isometric conditions). The features of this transition likely differ between myosin designed for efficient fast shortening vs efficient load bearing. In this generally accepted scheme, transitions of crossbridges from force-generating to nonforce- generating states involved in isometric force relaxation comprise both forward (ADP release and ATP binding) and backward (Pi rebinding and reversal of the power stroke) steps.

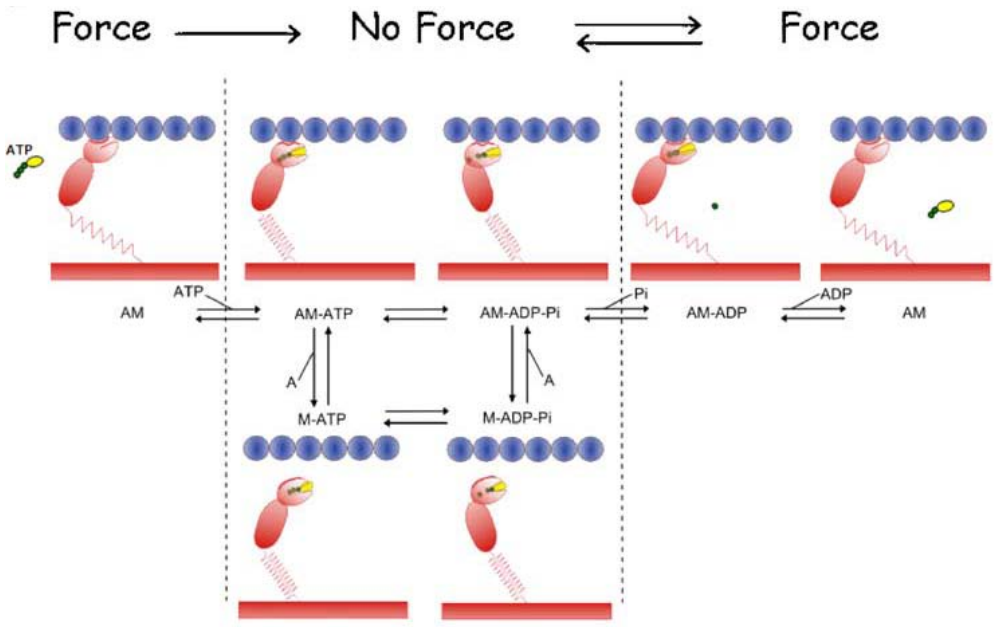

Figure 2. Reaction pathway for acto-myosin ATPase and energy transduction cycle.

1.3 Thick filament proteins

The sarcomeric thick filaments (Figure 3) are mainly composed by the motor protein myosin II. Myosin II is a polymer (6 chains) which is composed of two heavy chains (Myosin Heavy Chain, MHC of ≈ 200 kDa each), interconnected by a long twisted tail domain, and 4 light chains (LC). The extending domains of the myosin heavy chain are called the two myosin 'heads'. Two myosin light chains (MLC-1 and MLC-2) of ≈ 20 kDa are bound to the neck region of each head. The myosin 'head' is also called cross-bridge, since it bridges the gap between the thick myosin filaments and the thin actin filaments in muscle. The four light chains consist of two essential light chains (ELC, the MLC-1) and two regulatory light chains (RLC, the MLC-2) (Gordon AM et al., 2000). Each cross-bridge has ATPase activity, that is activated by interaction with actin. Force and filament movement depend on the energy released from ATP hydrolysis. In the presence of Ca^{2+}, the myosin cross-bridges bind to actin, that promote the release of Pi and than ADP. During this process a structural transition in the cross-bridge, suggested to be a change of tilt or change of shape, is thought to produce a relative sliding force between thin actin and thick myosin filamens. The cross-bridge can be released from actin when it binds another ATP molecule.

In the heart, two different isoforms of MHC are present: α-myosin heavy chain (α-MHC) and β-myosin heavy chain (β-MHC). Human myosin is mainly composed of β-MHC and up to 5% of α-MHC.

Another important component of the thick filament is cardiac Myosin Binding Protein C (cMyBP-C), a sarcomeric protein associated with the thick filaments, located in the cross-bridge containing A-bend of the sarcomere (Figure 1). To cardiac MyBP-C has been assigned a role in assembly and stability of the sarcomere as well as in the modulation of contraction (Oakley CE et al., 2004). It has been demonstrated that cMyBP-C knockout mice are viable but show significant cardiac hypertrophy, myocyte disarray and fibrosis (Harris S, Foord SM, 2000). Two models have been proposed for the arrangement of cMyBP-C in the sarcomere. In the firs 'collar' model it is suggested that cMyBP-C molecules forme a ring around the thick filament (Moolman-Smook J et al., 2002). The second model proposes that the C-terminal of the molecule runs parallel to the myosin backbone, while the N-tetminal domain interacts with neighbouring actin filaments (Squire JM et al., 2003; Whitten AE et al., 2008). The C-terminal region of cMyBP-C also contains binding sites for the giant protein titin (see below).

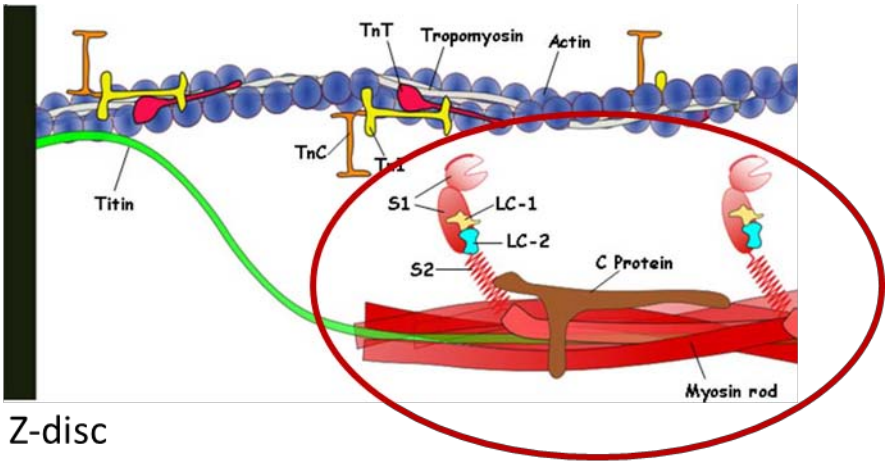

Figure 3. Figure describing the schematic structure of half-sarcomere: red inset represents thick filament. Abbreviations: S1,S2= S1 and S2 portions of myosin head; LC-1 and 2= Myosin light chain 1,2. C protein= myosin binding protein C. Modif. from Ferrantini et al., 2010

1.4 Thin filament proteins

The thin filament (Figure 4) consists mostly of the≈ 45 kDa globular protein G -actin. G-actin monomers polymerise spontaneously to form the backbone of the thin filament, F-actin. F-actin is a double helix. The actin helix appears as two right-handed helices which twin slowly around each other (Squire JM 1997; Holmes KC et al., 1990). In striated muscle, tropomyosin (Tm) is wrapped around the F-actin backbone as an α-helical coiled-coil dimer. Tm modulates the actin-myosin ineractions and functions to stabilize the actin structure. It comprises 284 aminoacid chains each spanning seven actin monomers and containing seven quasi-repeating regions. The Tm molecules are linked together through a head-to-tail association, which allows adjacent Tm molecules to function as a cooperative unit that spans 7 actin monomers. The Ca^{2+} binding protein complex, troponin (Tn), is bound to Tm (Kobayashi T, Solaro RJ, 2005; Wolska BM, Wieczorek DM, 2003). The thin filament is so comprised of actin, Tm and Tn in a 7:1:1 ratio. Troponin is a heterotrimer, which consists of three subunits: troponin C (TnC), the Ca^{2+} binding subunit; Troponin I (TnI), an inhibitor of the acto-myosin reaction that shuttles between tight binding to actin and tight binding to the Ca^{2+}-TnC; and troponin T (TnT), which is bound to Tm. Troponin subunits are present in different isoforms which distribution is tissue specific (fast skeletal muscle and slow skeletal muscle; miocardial) and also depend on development stage (Schiaffino and Reggiani; 1996), (see Table 1). In cardiac muscle specific isoforms are present for all three subunits: cTnC, cTnI and cTnT.

Gene	Isoforms	Pattern of expression
TnC-fast	TnC-f	Fast skeletal m.
TnC-slow/cardiac	TnC-s/c	Slow skeletal m., heart
TnT-fast	TnT-1f, -2f, -3f, -4f and developmental isoforms	Fast skeletal m., developing skeletal m.
TnT-slow		Slow skeletal m.
TnT-cardiac	TnT-1s, -2s TnT-1c, -2c, -3c, -4c	Developing skeletal m., heart
TnI-fast		Fast skeletal m.
TnI-slow	TnI-f TnI-s	Slow skeletal m., developing heart
TnI-cardiac	TnI-c	Heart

Table 1. Myofibrillar protein isoforms and their expression pattern in mammalian striated muscles

The interactions among the Tn subunits, Tm and actin are Ca^{2+} sensitive and allows for Ca^{2+} induced conformational changes within the troponin complex, modification of the Tm position on the actin filament and the initiation of contraction (Gordon AM et al., 2000). During relax phase (or "diastolic phase" in the heart), the intracellular Ca^{2+} concentration is low and under these conditions TnI binds to actin-Tm and inhibits the binding of myosin and thereby force generation. During activation (or "systole" in the heart) , intracellular Ca^{2+} concentration increases and Ca^{2+} can bind to TnC. This induces conformational changes in TnC and ultimately causes a redistribution of cross-bridges towards the force generating state (Solaro RJ and Van Eyk J, 1996).

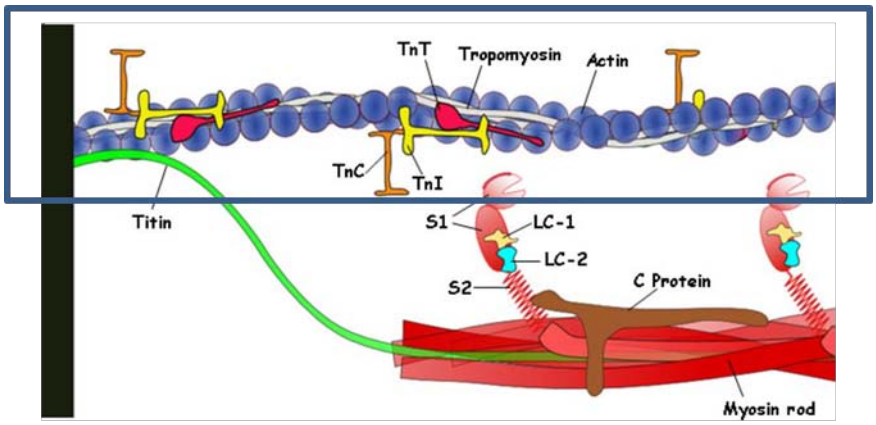

Figure 4. Same scheme of half-sarcomere of Figure 3: blue inset shows thin filament. Abbreviations: TnT= troponin T; TnC= troponin C; TnI= troponin I. Modif. from Ferrantini et al., 2010

1.5 Giant structural proteins

Titin is the largest protein found in mammals (Labeit et al., 1990) with a molecular weight of≈ 3700 kDa depending on isoform composition. At the N-terminus titin is anchored in the Z-disc and to the thin filament and at the C-terminus it is bound to the thick filament. The region of titin located in the I-band is a complex molecular spring element, which consists of a PEVK domain (rich in proline (P), glutamate (E), valine (V) and lysine (K)), tandem Ig segments and variable N2B and N2A elements (Le Winter MM et al., 2007). Titin is a major determinant of passive tension in cardiomyocytes. The passive tension results from extension of the I-band region of titin, which elongates as sarcomere length increases (Figure 5). The N2B element alone is present in the stiffer N2B isoform, while both the N2A and N2B elements make up the more compliant N2BA isoform. Both isoforms are co-expressed within the cardiac sarcomere and their ratio determined the passive stiffness of cardiomyocytes (Le Winter MM, Granzier H, 2010).

Like titin, also nebulin (Figure 5) is a giant sarcomeric protein (~800 kDa) involved in structure stability and contractile performance. A single nebulin molecule spans nearly the entire length of the thin filament. Nebulin is present only in skeletal muscle. In cardiac muscle it is replaced by a related protein, Nebulette, which is shorter and has lower MW , around a sixth the size of nebulin, and only localizes in the Z-disc (Pappas CT et al., 2011). An accurate description of nebulin and of the skeletal muscle pathologies related to nebulin is given below.

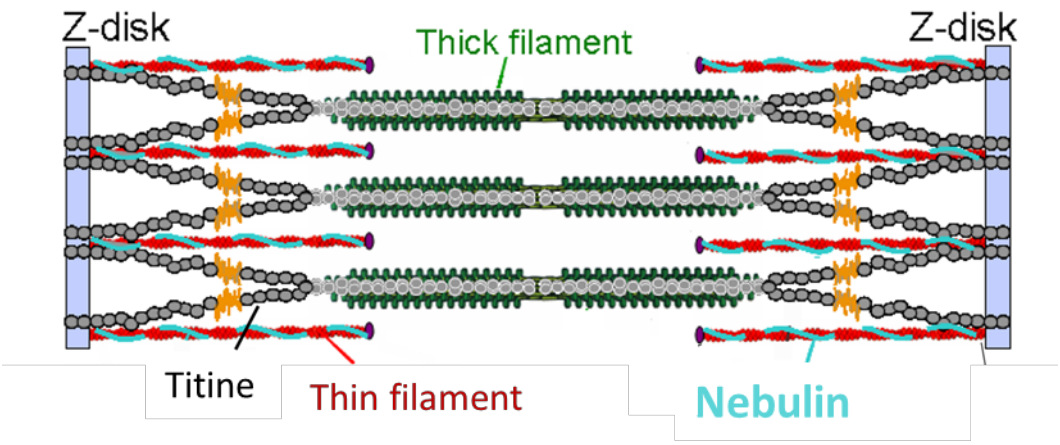

Figure 5. This picture resumes the sarcomeric structure and highlights position of main structural proteins of sarcomere like titine (gray) and nebuline (light blue).

1.6 Steric block hypothesis and conformational states of thin filament

A three-state model of the thin filaments has been proposed by Geeves et al. (1984) to explain the regulation of the interaction between actin, Tn, Tm and myosin (Figure 6). Tm can occupy three distinct positions on actin filament. Under relaxing condition, in absence of Ca^{2+}, Tm sterically blocks the interaction between actin and myosin heads in a 'blocked state'. Herein, not even weak myosin binding is possible. When Ca^{2+} starts to be present, Ca^{2+} starts to bind to TnC. This causes serial structural changes in all the components of Tn that allows movement of Tm to another position on actin filament and thereby the probability of formation of strong cross-bridges starts to increase. This is called 'closed or activated state'. Further increasing of Ca^{2+} concentration and the transition from weak to strong cross-bridges pushes Tm further to the 'open or activated state', further increasing the probability of strong mechanical transition and allowing full activation of thin filament and force generation by strong cross-bridges formation (Gordon et al., 2000; Lehman et al., 1997; Lehman et al., 1995).

A

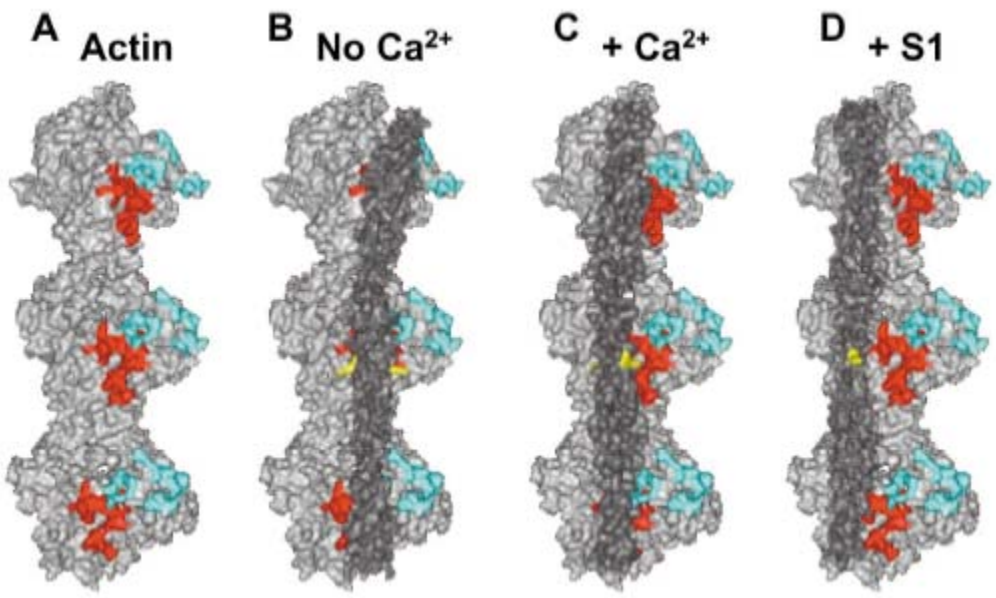

B

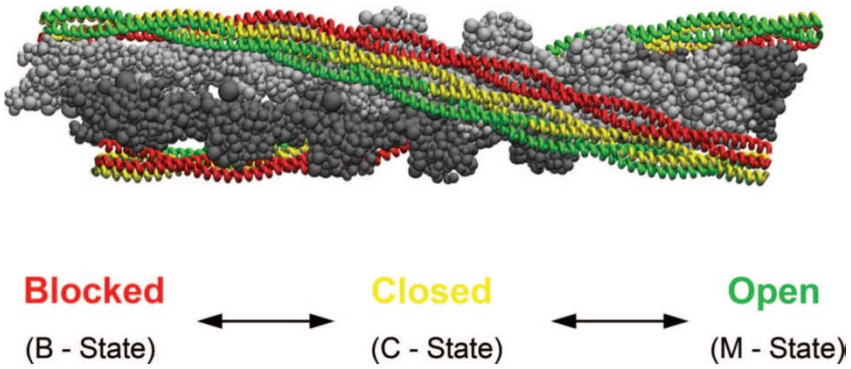

Figure 6. The 3-state model of myofilament activation. A, Actin residues are light gray, except for residues (1–4, 24–25, 95–100; shown in light blue) making weak electrostatic interaction with myosin and residues (144–148, 340–346, 332–334; shown in red) forming stronger attachments with myosin. In B–D, a surface rendering of a cardiac tropomyosin segment (residues 61–112 of each tropomyosin strand) in dark gray. Arg90 of tropomyosin in each strand is shown in yellow to illustrate the putative rolling motion of tropomyosin. (Gordon et al., 2000). B, The 3 average positions of Tm are depicted. Tm residues at the outer actin domain in the blocked state (red), Ca^{2+} binding to cTnC results in an azimuthal shift to the weakly bound closed state (yellow) in the actin inner domain, and myosin binding drives the final shift to the force-producing open state (green).

1.7 Calcium sensitivity

The Ca^{2+} concentration that produce half maximal active tension gives an information of the sarcomeric concentration of Ca^{2+} necessary to trigger the contraction and is indicated as c_{50Ca2+}, usually expressed as pCa50 (-log c_{50Ca2+}). It is an index of the apparent sensibility to calcium of the tension generation mechanism. pCa50 is directly related to the amount of Ca^{2+} that binds to TnC, but does not reflect strictly the affinity for Ca^{2+} of regulatory binding sites on TnC. A reduction of c_{50Ca2+} caused by TnC increased affinity for Ca^{2+}, is directly related to the increase of the amount of Ca^{2+} bound to TnC as well as to the tension developed during contraction at submaximal level of Ca^{2+}. In addition to factors that directly affect the affinity of TnC for Ca^{2+}, c_{50Ca2+} could be influenced by upstream regulation mechanisms like structural or covalent modifications (e.g. kinase or phpsphatase activity of enzymes) of TnI, TnT or Tm as well as factors affecting crossbridge kinetic parameters or crossbridge number recruited to generate force even independently of the amount of Ca^{2+} bound to TnC.

1.8 Cooperativity

The regulatory mechanism of contraction can be modulated by sarcomeric mechanisms of cooperativity that seems to be intrinsic in activation and contraction processes. In both skeletal and cardiac contraction, the relation between Ca^{2+} concentration and isometric tension is very steep, much steeper than expected from simple kinetic equilibrium between Ca^{2+} ions and binding sites on TnC. This is likely due to cooperative interactions playing a pivotal role in the triggering of contraction after Ca^{2+} release. A cooperativity mechanism is intrinsic to the three state model, previously described. With formation of strong acto-myosin interactions, Tm filament shifts to “open state”, and this produces an increase in activation of the thin filament, that means an increase in the number of strong interactions and in tension developed, independently to the amount of Ca^{2+} bound to TnC. A second cooperativity system is strictly related to the amount of Ca^{2+} bound to its sites on TnC. The coupling of adjacents regulatory units, likely due to head to tail interaction of Tm units along thin filament, could be responsible of cooperativity. Ca^{2+} that binds to TnC in a regulatory unit, could increase the affinity for Ca^{2+} of one or more neighbour regulatory units, triggering a feedback in activation of thin filament. This hypothesys has been tested by various experiments on skinned skeletal fibers (Brandt PW, 1997; Kreutziger KL, 2008; Kreutziger KL, 2011) based on removal of TnC from striated muscle or introduction of recombinant inactivated TnC, unable to bind Ca^{2+} in some regolarory units.

The presence of inactive regulatory units obtained by this approache breaks off the signaling continuity along the filament, showing not only an expected reduction of active tension developed during contraction, but also a reduction of the slope of tension-pCa relationship and then of cooperativity of activation (Brandt PW, 1997).

1.9 Familial Hypertrophic Cardiomyopathy: general features

HCM is a genetic and clinical pathology classified as a "*disease of the sarcomere"* leading to left ventricular hypertrophy, diastolic dysfunction and sudden death.

Cardiovascular disease is the first cause of death, sickness and morbidity in the European Union (EU) and the United States (US). There are both acquired and genetic bases for cardiovascular disease, with most disease being multifactorial and a result of the interaction of numerous environmental and genetic factors. However there are a number of single gene disorders of the cardiovascular system, inherited in a simple Mendelian fashion. The most prevalent cardiovascular single gene disorder is familial hypertrophic cardiomyopathy (FHC) which has a reported frequency of 1:500 (Maron BJ, 2002) and thus is likely to be present in approximately 4 million people within the EU and the US. FCM is an autosomal dominant inherited heart disease, which results in hypertrophy of the left ventricle in the absence of other cardiac or systemic disease (such as hypertension or aortic stenosis). It is a disease characterized morphologically by left ventricular wall and septal hypertrophy, resulting in a decreased left ventricle volume (Elliott P et al., 2004).

The hallmark of FHC, left ventricular (LV) hypertrophy usually develops at puberty or early adulthood, but can be present at birth, or develop as late as the 6th decade (Maron BJ, 2002). The distribution of LV hypertrophy in FHC is typically regional and asymmetric, develops in virtually all imaginable patterns within the ventricle (Klues HG et al., 1995), and may involve the right ventricle and papillary muscles. For reasons that remain unknown, the basal anterior septum and anterolateral free wall are almost always involved, and generally represent the site of maximum wall thickness values (Maron MS et al., 2009). These range from very mild (13-15 mm) to extreme hypertrophy (30 mm or more), with an average of 21 to 23 mm in large FHC cohorts (Nistri S et al. 2006; Olivotto et al., 2003b). Obstruction of the left ventricular outflow tract is present at rest in approximately 25% of patients and in a higher proportion during exercise.

Histologically, areas of myocyte disarray and interstitial fibrosis are characteristic of the disease. Although not unique to FHC, myocyte disarray is considered a main feature of the disease, and is always found at autopsy or in myectomy specimens (Basso C et al., 2000). Disarray can be defined as a profound derangement of myocyte alignment, with loss of the physiological, parallel orientation of the cells. The functional consequences of disarray may affect LV mechanics by interfering with the physiological homogeneity of contraction and relaxation (Ho et al., 2002), and represent a potential substrate for ventricular arrhythmias (Basso et al., 2000).

Variable and sometimes striking patterns of intra-myocardial fibrosis have been described in FHC hearts based on pathological studies (Basso et al., 2000) and, more recently, by cardiac magnetic resonance (CMR) techniques allowing in vivo visualization of areas of late gadolinium enhancement (LGE) (Maron MS et al., 2009; Olivotto et al., 2008). LGE localizes preferentially to the most hypertrophied regions of the ventricle, often represented by the basal and mid-septum, and are more often found in patients with diffuse and severe hypertrophy. Preliminary evidence points to LGE areas as a potential substrate of ventricular arrhythmias (Adabag et al., 2008).

Another pathophysiological hallmark of FHC is microvascular dysfunction. In the past decade, a number of studies have demonstrated that in FHC patients the coronary vasodilator reserve is markedly impaired not only in the hypertrophied septum, but also in the least hypertrophied LV free wall (Camici and Crea, 2007; Olivotto et al., 2006). In the absence of epicardial coronary stenoses, this finding is indicative of diffuse microvascular dysfunction, in line with pathologic evidence of marked and widespread remodeling of the intramural coronary arterioles (Basso et al., 2000), which show smooth muscle hyperplasia and disorganized elastic fibres, causing deformation and irregular narrowing of the vessel lumen. Microvascular dysfunction is the most important substrate for recurrent ischemia in FHC, and has been shown to represent an important predictor of long-term prognosis and adverse LV remodeling (Camici and Crea, 2007; Olivotto et al., 2006), (See Figure 7).

Although systolic contractility is preserved and features of hypercontractility are observed at the whole heart level, outflow obstruction and impaired relaxation can cause progressive forward and backward heart failure and an increased incidence of ventricular arrhythmia can lead to sudden cardiac death.

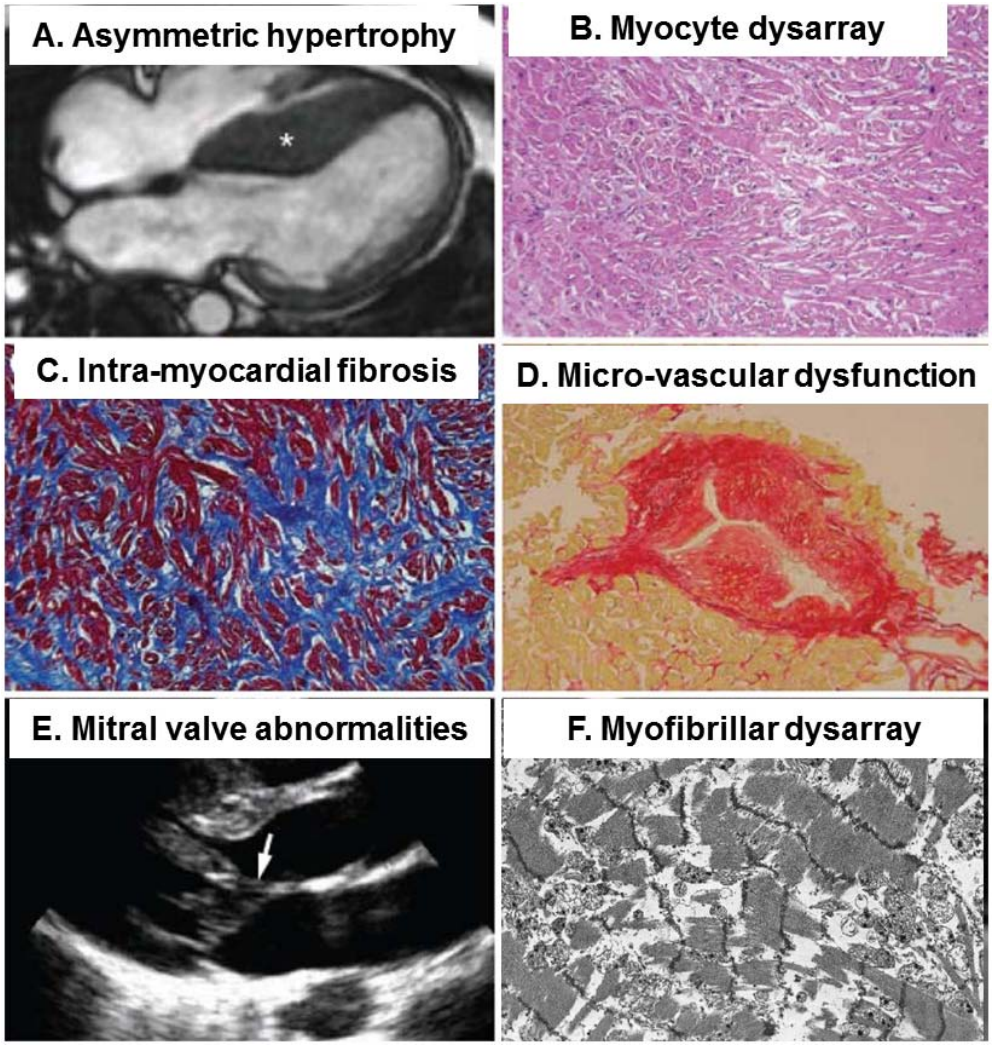

Figure 7. The FHC features . A, Asymmetric LV hypertrophy. Cardiac magnetic resonance four-chamber view showing regional hypertrophy at the ventricular septum (asterisk). B, Myocardial disarray. Surgical myectomy sample showing bizarre cardiomyocyte orientation with loss of alignment. C, Interstitial fibrosis. Marked over-representation of interstitial collagen, appearing in blue. D, micro-vascular dysfunction. Remodeling of an intra myocardial coronary arteriole, with thickening of the vessel wall due to medial hypertrophy and intimal hyperplasia, associated with decreased luminal size (picrosirius red, ×10). E, Mitral valve abnormalities. Echocardiographic parasternal long-axis view, showing elongated mitral leaflets with direct insertion of a papillary muscle onto the leaflet (arrow). F, Myofibrillar dysarray. Electron micrograph showing structural disorganization of sarcomeres. From Olivotto I et al., 2008

A notable feature of FHC is that the underlying molecular defect (present from birth) can apparently be compensated in nearly all patients until adolescence and indeed, as indicated by the finding of incomplete penetrance, in some individuals for all of their life. Some mutations have been reported with very high (close to 100%) penetrance whereas the penetrance of other mutations appears to be incomplete. For example,with mutations in TNNI3 (which encodes cardiac troponin I), it was reported that a single mutation (ΔLys183) had a high

penetrance with evidence of cardiomyopathy present in 88% by echocardiography and 96% by ECG (Kokado et al., 2000).

However, a report of 100 TNNI3 mutation carriers identified in 23 families (13 different mutations) found that disease penetrance was only 48% and that penetrance was complete in only one family (Mogensen et al., 2004). Further, there is evidence that some FHC mutation carriers can make an abrupt transition from having a structurally normal heart to one showing overt hypertrophy in later adult life (Maron B et al., 2003). These are important points, in that they give rise to the suggestion that there may be a "tipping point", beyond which pathways are activated to stimulate disease progression. The physiological and metabolic conditions that define this point may be manipulated to prevent downstream consequences and specific interventions aimed at this may modify (and potentially halt) the disease process resulting in substantial therapeutic benefit. However, no specific drug or other therapeutic measure has been shown able to prevent the development of overt disease in carrier patients, making it still a great medical need.

It will be made clear through this introduction that, although great recent advances in the understanding of the pathophysiogy of FHC brought new light into the field, no totally effective therapy is yet available that is able to substantially reduce the clinical burden of this disease.

1.10 HCM and diastolic dysfunction

Recent studies have shown that detectable diastolic abnormalities (impaired LV filling) are the first changes in myocardial function in HCM mutation carriers without hypertrophy, both in animal models and in patients (Nagueh SF, 2000; Ho CY, 2002).

The origin of diastolic dysfunction in HCM is multifactorial and complex, with changes at the cellular level (e.g. impaired sarcomeric function and Ca^{2+} handling) and also abnormalities at the tissue level (myocyte disarray, interstitial fibrosis, microvascular dysfunction). Other morphological factors, like ventricular shape and geometry, may also lead to reduced LV distensibility and alter relaxation. Additionally, Diastolic Dysfunction is the main determinant of symptoms in HCM patients: reduced exercise capacity, chest pain and discomfort, dyspnea episodes, are all associated with impaired myocardial relaxation, which leads to increased ventricular filling pressure and increased atrial pressure. Even though the possible causes of diastolic dysfunction in HCM are, at least partially, understood, no specific therapy exists that is able to improve myocardial relaxation in these patients. Other than microvascular fibrosis, also

an impaired myocardial relaxation and the subsequent increased LV tissue pressure during diastole can contribute to myocardial blood flow impairment. Reduction of diastolic dysfunction with an appropriate and specific therapy could therefore not only reduce symptoms in patients, but also prevent disease worsening and evolution to heart failure. As reported above diastolic dysfunction in HCM is an early feature, that often occurs with overall systolic ventricular function enhanced. Alterations of diastolic function are now considered the first signs of HCM even before the development of overt hypertrophy, the so called preclinical HCM.

1.11 HCM and arrhythmias and Sudden Death

Sudden Death (SD) occurs in 1-2 % of HCM patients and identifying high-risk patients remains a very challenging task. SD in HCM is arrhythmia-based due to primary ventricular tachycardia/fibrillation (VT/VF) (Maron B et al., 2007) with a relationship to patient age (Maron B, 2002). SD may occur at a wide range of ages with the highest rate during adolescence and young adulthood, most commonly less than about 25 to 30 years of age. Indeed, HCM is now recognized as the most common cause of SD in young people (Maron B, 2003). Although most patients die suddenly while sedentary or during normal/modest physical activity, an important proportion collapse associated with vigorous exertion, including young competitive athletes in organized sports. Only a small proportion of patients with HCM are at risk for SD and some major risk factors for SD have been identified (e.g. repeated episodes of syncope, left ventricular out-flow tract obstruction, family history of SD, episodes of sustained ventricular tachycardia, impaired blood-pressure response to exercise).

The link between SD and the degree of LV hypertrophy remains controversial. The genetic background may also play a significant role, since mutations in cardiac troponin T (cTnT) are often associated with mild or no ventricular hypertrophy but with a high frequency of sudden cardiac death.

Most HCM patients have abnormal ECG findings, which are non-specific but often represent the reason for diagnosis in asymptomatic patients undergoing sports, professional, or family screening. These include signs of LV strain and hypertrophy, deep Q waves in the inferior and lateral leads, diffuse T wave inversion, P wave prolongation, intraventricular conduction abnormalities, and QTc prolongation (Maron B et al., 2003; Eriksson M et al., 2002; Kitaoka H et al., 2003). About 6% of patients presenting with echocardiographic evidence of HCM have a

totally normal ECG at the time of diagnosis. In this subset, the lack of ECG abnormalities is associated with less severe phenotype and more benign outcome compared to the overall HCM population (Maron B et al., 2003).

A major goal in treatment of HCM is to limit the life-threatening consequences of arrhythmia. The greatest limitation to this however is the relative lack of knowledge about the molecular and cellular mechanisms determining HCM-related pro-arrhythmic substrate. While tissue fibrosis and microvascular dysfunction might provide a substrate for the maintenance of ventricular automaticity by favoring establishment of reentry circuits, to date no knowledge of the cellular triggers for arrhythmias initiation in HCM is present. As precise triggers for arrhythmias that produce SCD in HCM are unknown, management strategies aim to treat high risk patients with implantable cardiac defibrillators (ICD).

1.12 HCM genetic features

In 1990, the first missense mutation in a sarcomeric protein, R403Q in the β-cardiac myosin heavy chain (β-MyHC), was shown to be responsible for FHC (Geisterfer-Lowrance et al., 1990). Since then, molecular genetics has revealed that FHC is a complex molecular disease, exhibiting both gene and allele heterogeneity (multiple disease genes and multiple mutations), with as many as 10 sarcomere related genes and more than 400, predominantly missense, mutations described. Besides β-MyHC, the disease genes encode other thick filament proteins: cardiac myosin binding protein-C (cMyBP-C also named cardiac C-Protein), both regulatory (RLC) and essential (ELC) myosin light chains, thin filament proteins: α-tropomyosin (α-Tm), cardiac troponin T (cTnT), cardiac troponin I, cardiac troponin C (cTnC), actin, and the giant protein titin which spans both the thick and thin filament. Disease-causing mutations in sarcomere proteins are detected in 60-70% of HCM affected individuals and the most commonly affected genes are MYBPC3 (cMyBP-C) and MYH7 (β-MyHC). The prevalence of mutations in sarcomeric proteins has led to the designation of HCM as primarily a "*disease of the sarcomere*" (Thierfelder et al., 1994; Seidman and Seidman, 1995; Marian et al., 1999; Belus et al., 2008). This raises the question of how molecular defects in sarcomeric proteins can lead to the heterogeneous phenotypic expression that characterizes FHC. In fact asymmetric left ventricular hypertrophy, diastolic dysfunction and sudden death are only the three well known hallmarks of FHC, but the disease has a much wider spectrum of clinical faces, including the so called "pre-hypertrophic phenotype". Healthy carriers of sarcomeric mutations during the pre-hypertrophic phase often have subtle

echocardiographic abnormalities but will not necessarily develop an overt hypertrophy and/or symptoms. Atrial remodeling (e.g. increase size) and abnormalities of the mitral valve apparatus (including disproportionate mitral leaflet elongation, anomalous chordae and/or papillary muscle insertions, and papillary muscles alterations in terms of site and number) are common in FHC patients, and have been described also in patients with very mild or no hypertrophy. No treatment are now in use during the pre-hypertrophic phase to prevent the development of hypertrophy: with the wider availability of genetic screening for FHC-related mutations, the number of detected *genotype-positive* mutation carriers without cardiac hypertrophy is increasing: in the Florence cohort of FHC patients' relatives, 200 undiseased mutation carriers have been already recognized. A treatment to prevent the development of hypertrophy could therefore be applicable to such patients and the lack of an effective drug is a great unmet medical need.

Although mutations involving cardiac isoform of troponin T (TNNT2) have a reduced frequence in FHC population (Table 2), around 5-15% of total amount of patients, the interest related to the investigation on TnT mutation is due to the extremly severe phenotipe that is often manifested in the early age of patient, related to high frequence of sudden deth in particular in young people.

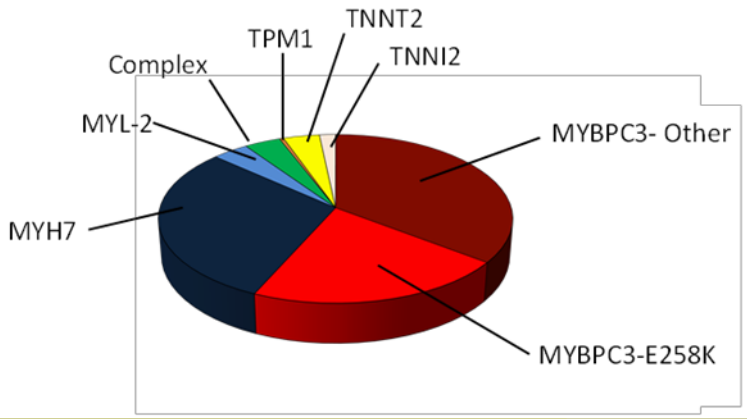

Mutational analysis	
Myofilament negative	141 (36.7%)
Myofilament positive	243 (63.3%)
Thick filament	218 (90%)
MYBPC3 (Protein C)	137 (56.4%)
MYBPC3 (E258K)	49 (20.2%)
MYH7 (Myosin Heavy Ch.)	72 (29.6%)
MYL2 (Myosin Light Ch.)	9 (3.7%)
Thin filament	17 (7%)
TNNT2 (Troponin T)	12 (4.9%)
TNNI3 (Troponin I)	2 (0.8%)
TPM1 (Tropomyosin)	2 (0.8%)
ACTC (Actin)	1 (0.4%)
Complex (multiple genes)	8 (3.2%)

Table 2. Distribution of mutations in myofilament -positive FHC population

1.13 Cardiac Troponin T

As previously introduced, the troponin complex consists of three subunits: troponin I, troponin T, and troponin C. This complex is associated with the thin filament and acts as the calcium sensor, which, together with tropomyosin (Tm), is responsible for the regulation of contraction and relaxation of striated muscle. cTnT binds the troponin complex to Tm and is involved with the positioning of the troponin complex along the actin filament (Tardiff J. C., 2011; Jin J P et al., 2010). cTnT consists of 298 aminoacids and is also named as TNNT2 from the neme of gene that encode the cardiac isoform. It is composed by two domains and a linker that connect them. The N-terminus includes a highly helical domain, TNT1, where approximatey 75% of all cTnT FHC-linked mutations occur or are adjacent to, including those discussed below. It is well

accepted that the N-tail of cTnT including TNT1 is required for cooperative activation of the thin filamnt; the C-terminal domain TNT2 is necessary for cTnT-cTnI-cTnC calcium-sensitive interactions. In addition, studies suggest that flexibility of TNT1 is important in interactions between cTn and Tm. There is a flexible linker between TNT1 and TNT2 (Figure 9). Despite the cTnT linker's role in calcium signal propagation, little is known about its structure due to its hypervariability (Manning E. P et al., 2012; Jin JP et al., 2010).

Mutations in the cTnT gene are responsible for causing 5–15% of HCM cases (Thierfelder L et al., 1994). Individuals with cTnT mutations generally exhibit mild or no ventricular hypertrophy, but have a high incidence of premature sudden death (Watkins H et al., 1995; Moolman J C et al., 1997).

Since troponin T mutations are less common in patients, and more common mutations in human patients present with a large degree of clinical heterogeneity, making genotype-phenotype correlations difficult, different transgenic mouse models have been developed to simulate and study main mutations leading to FHC in human patients.

A transgenic mouse model expressing a truncated mouse cTnT (Δ160E) allele analogous to one found in FHC patients has been described (Tardiff J et al., 1998).

Heterozygous mice expressing the truncated cTnT at low levels (<5%) developed cardiomyopathy and had significantly smaller ventricles and impaired cardiac contractility and relaxation.

A

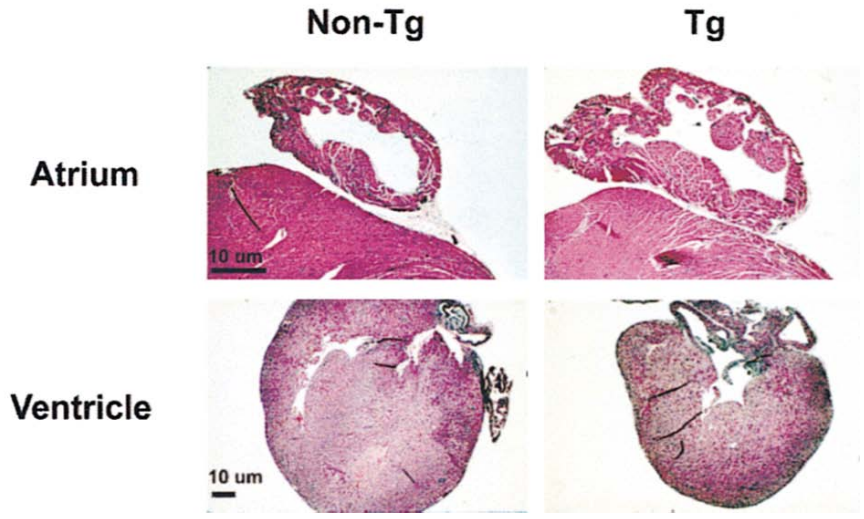

B

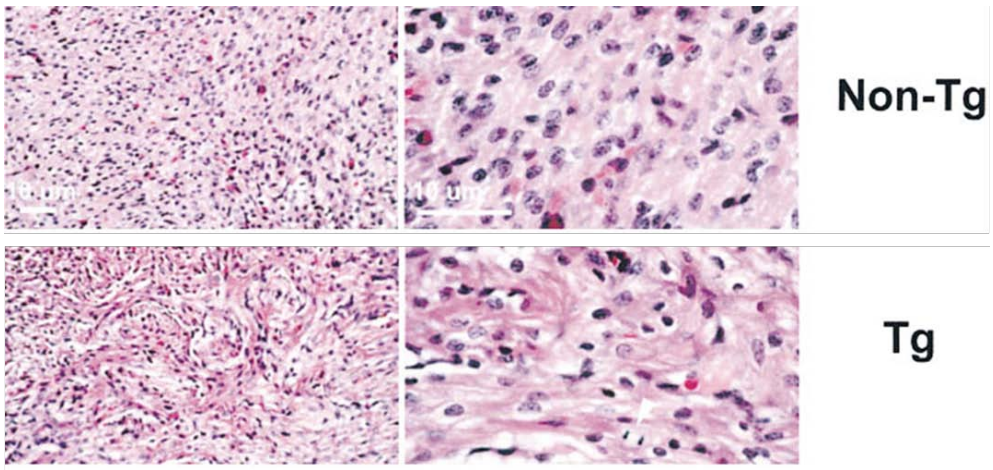

Figure 8. A, Atrial and ventricular hypertrophy in 5-mo-old heterozygous cTnT-Myc-truncation mice. Representative cross-sections from paraffin-embedded hearts stained with hematoxylin and eosin.
B, Cardiac TnT-Myc-truncation neonatal mice display myocellular disarray and degeneration similar to that found in patients with FHC (modif. from Tardiff et al., 1998)

Histopathological analysis of their hearts showed myocellular disarray and degeneration, but no fibrosis or myocyte hypertrophy (see Figure 8). The cTnT-truncation (Δ160E) mice bred to homozygosity expressed twice the amount of truncated protein (5–10%) than their heterozygous littermates and died within 24 h of birth. This demonstrates an important relationship between the quantity of mutant protein expression and severity of disease presentation. Interestingly, the same splice donor site mutation has also been generated in a transgenic rat model, which overexpresses the human truncated cTnT protein (Frey N et al., 2000). These rats display features of FHC including diastolic dysfunction and increased susceptibility to ventricular arrhythmias, particularly during exertion or stress (Luedde M et al., 2009).

A second cTnT transgenic mouse model was developed that expresses the missense mutation R92Q (Javadpour MM et al., 2003) within the Tm-binding domain of cTnT, which is known to cause FHC in humans. Similar to the truncated cTnT model, R92Q mice had small left ventricles, myocyte disarray, and lacked myocyte hypertrophy. In contrast, however, the R92Q hearts demonstrate significant interstitial fibrosis and upregulation of hypertrophic markers. Studies with isolated cardiomyocytes from R92Q mice show increased basal sarcomere activation, impaired relaxation, and shorter sarcomere lengths. Isolated working heart data are consistent, showing hypercontractility and diastolic dysfunction, both of which are common findings in patients with FHC. Moreover, both R92Q and Δ160E mice showed an increased frequency of

arrhythmias (premature ventricular contractions) upon isoproterenol administration in the living animal as well as a slightly prolonged QRS and alterations in the atrio-ventricular conduction (Jimenez J et al., 2011).

In contrast with the R92Q mutation, patients who carry of the Arg-92-Leu (R92L) troponin T mutation often exhibit ventricular hypertrophy and eventually develop cardiac failure, while the frequency of sudden death is relatively low (Ertz-Berger BR et al., 2005). R92W mutation, instead, behaves similarly compared to R92Q, albeit with heightened severity and earlier onset.

A transgenic mouse expressing mutant R92L TnT was generated and tested: accordingly, mice carrying this mutation showed a significant degree of hypertrophy with a later onset (7-10 months) and increased myocyte size, as well as slowed cardiac relaxation and residual diastolic tension. In conclusion, although troponin T mutations are less common in patients, troponin T mutant mice are able to replicate all the different clinical phenotypes of human FHC: an early onset disease with scarce hypertrophy and fibrosis but high risk of arrhythmias (Δ160E), a restrictive-like disease presentation with fibrosis and severe diastolic dysfunction (R92Q & R92W), a later-onset presentation with hypertrophy, impaired relaxation but only slight increase of arrhythmogenic risk (R92L). Available troponin T mutant mice are therefore an optimal model to study the pathophysiology of human FHC and test the efficacy of specific therapies on subjects with different disease phenotypes.

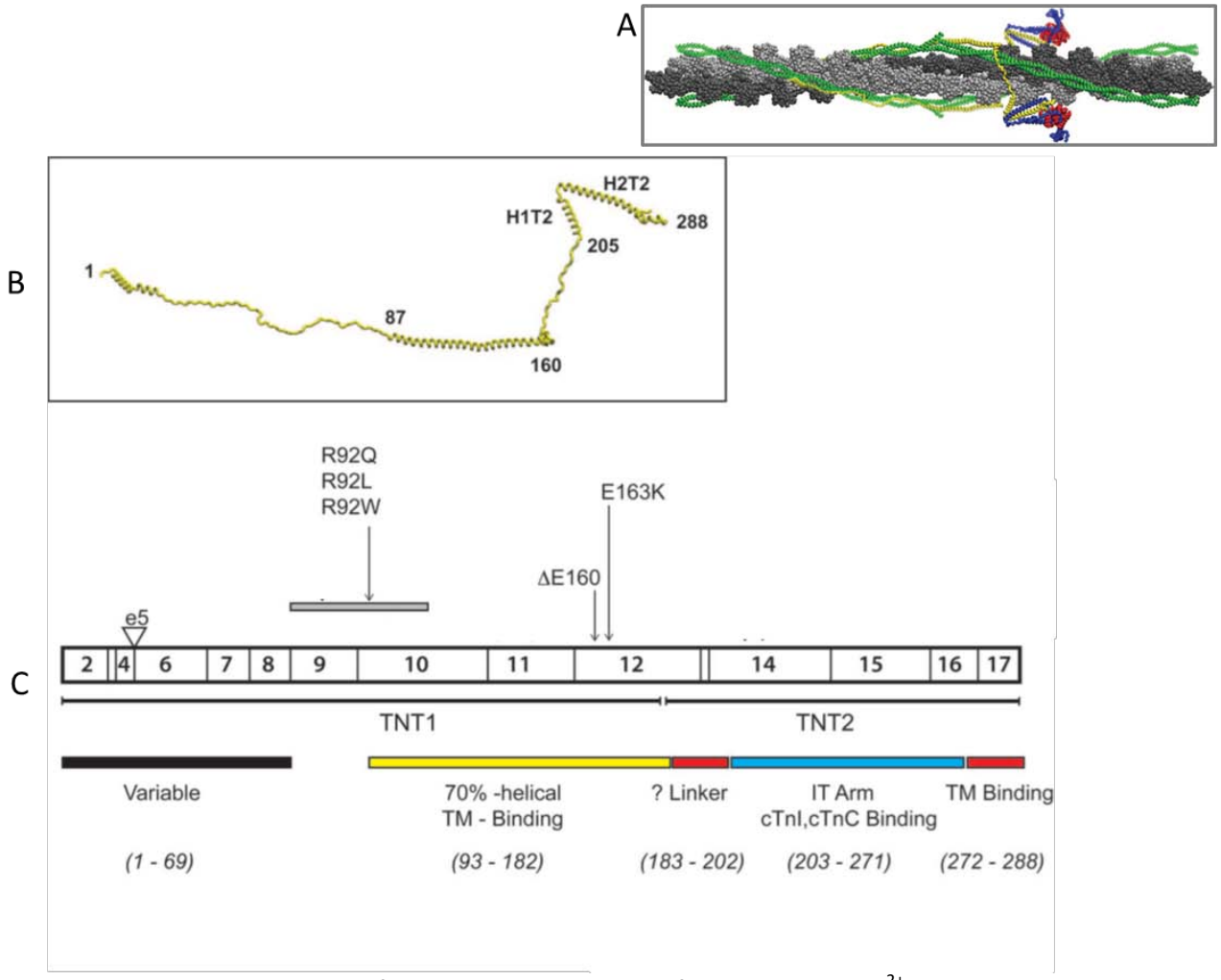

Figure 9. A, an atomistic model of the human cardiac thin filament in the Ca^{2+}-activated state. Yellow indicates cTnT; blue, cTnI; red, cTnC; green,α-TM; silver/gray, actin filament; B, predicted cTnT secondary structur; C, Human cardiac cTnT exons, structure, and functional domains. Listed mutations discussed in text. Undefined structures are red and black. (mod. Tardiff JC, 2011; Takeda S et al., 2003)

1.14 K280N TnT mutation

Until now, no animal model has been developed for the particularly rare mutation found in a young australian male patients carryng the homozyous mutation K280N. This was a particularly rare, but extremly severe condition that was manifested in the early age of patient. Only the mutant protein was found in biopsies and myectomies from septal and free wall of left ventricle. Scarce hypertrophy and fibrosis was present. Nevertheless the patient developed an end-stage progression so that cardiac transplantation had been evaluated necessary. Also in this case, there was a clear correlation between the quantity of mutant protein expression and the severity of disease presentation. Studies with isolated skinned cardiomyocytes from K280N myectomies showed reduced fibrosis compared to diferent mutation related to FHC, giustifying

the small reduction in active tension generation, present also at myofibrillar level (see Results). It has then being hypothyzed that the contractile defect associated with the presence of K280N TnT mutation in the sarcomere arises from increased sarcomere activation, due to the increased overall crossbridge turnover rate.

1.15 A skeletal congenital myopathy: nemaline myopathy

The term nemaline myopathy (NM) encompasses a heterogeneous group of disorders of primary skeletal muscle weakness of affected individuals. Disease severity is variable and unpredictable, with prognosis ranging from neonatal death to almost normal motor function. Recent advances in the identification of NM disease genes demonstrate that NM is a disease of the skeletal muscle sarcomere and, in particular, of the thin filaments. These findings are starting to alter the approach that neurologists and geneticists take to diagnosing and counseling patients with NM, and could lead to insights into specific directed therapies in the future (Sanoudou D and Beggs AH, 2001).

Nemaline myopathy (NM) is a slowly- or non-progressive neuromuscular disorder characterised by muscle weakness and the presence of rod-shaped structures, nemaline rods, in affected muscle fibers (North KN et al., 1997). NM was first described in 1963 by Conen et al. (Conen PE et al., 1963) and Shy et al. (Shy GM et al., 1963) and its name reflects the perceived thread-like appearance of the rod bodies (nema being the Greek word for thread). Although a relatively rare disease, it is the most common of the non-dystrophic congenital myopathies, occurring worldwide with an estimated incidence of 0.02 per 1000 live births (Wallgren-Pettersson C, 1990). Many cases are sporadic, but some exhibit either autosomal recessive or dominant patterns of inheritance. As with most other congenital myopathies, NM is pathologically defined on the basis of structural abnormalities of the muscle fibres, which can be visualized after staining of muscle biopsy sections by histochemical or electron microscopic methods.

To date, seven genes have been implicated in NM. Strikingly, despite a great degree of both clinical and genetic heterogeneity, six of these genes code for proteins of the skeletal muscle thin filament: alpha-tropomyosin-3 and beta-tropomyosin (TPM3 and TPM2), nebulin (NEB), actin alpha 1 (ACTA1), troponin T type 1 (TNNT1), and cofilin-2 (CFL2). The seventh implicated gene, KBTBD13, was only recently discovered and the function of its protein product is currently unknown (Kawabuchi M, 1982). With mutations in NEB likely accounting for more than 50% of NM cases (Yamaguchi M et al.,1982), NEB is the most frequently affected gene in NM. To date, 64 different mutations in NEB have been reported in NM probands (Lehtokari VL et al., 2009; Lehtokari VL et al., 2006; Pelin K et al., 1999).

1.16 Clinical an genetic basis of NM

The wide range of clinical presentations represents a continuum from neonatal-lethal forms to late onset slowly progressive weakness (Ryan MM et al., 2001) To facilitate phenotype–genotype correlation, tree different categories has been attempted, typical, moderate and severe nemaline myopathy (Wallgren-Pettersson C and Laing NG, 2000).

The typical, most common, form of NM is usually autosomal recessive and presents with congenital or infantile hypotonia, weakness and often, feeding difficulties (Shimomura C and Nonaka I,1989). In cases with profound weakness and hypotonia in the neonatal period, strength often improves with age, leading to delayed attainment of gross motor skills. Although fine motor activity is normal, gross motor activity is impaired. Proximal muscles are generally more affected than distal ones, although distal weakness, especially later in life, is not uncommon. The respiratory muscles are always involved, and nocturnal hypoxia and hypercarbia are a constant danger, even for patients with minimal skeletal muscle weakness. Joint hypermobility is commonly seen and joint deformities or contractures can occur congenitally or occasionally develop at later stages of the disease. The weakness is often static or only slowly progressive and many patients lead an active life. Respiratory problems persist throughout the patient's life, and eventual death is often associated with respiratory insufficiency (Ryan MM et al., 2001). As for all clinical forms, the central nervous system is unaffected, and intelligence and cardiac contractility are usually normal.

At the mildest end of the spectrum are patients with similar clinical and pathological findings to the typical cases, but with childhood onset of symptoms (Laing NG et al., 1992; Nowak KJ et al., 1999). These cases are also often sporadic (or possibly, autosomal recessive) but occasionally can clearly be inherited as autosomal dominant traits. At later ages, these mild cases can be indistinguishable from typical cases with age of onset the only differentiating factor. Severe NM presents at birth with hypotonia and profound muscle weakness, particularly affecting the diaphragm and intercostal muscles, which results in severe respiratory insufficiency. Patients have few spontaneous movements with difficulties swallowing and sucking. Occasionally, multiple contractures are prominent features. Despite intensive neonatal care and ventilatory support, death from respiratory insufficiency or pneumonia often occurs in the first months of life. These cases can present significant prognostic dilemmas as some patients with these apparently severe initial presentations go on to survive with only minimal residual disabilities and retrospectively become classified in the progressive weakness is associated with

inflammatory changes on muscle biopsy, suggesting that these cases might represent a distinctly different pathophysiological mechanism (Gyure KA et al., 1997). Others present with cardiomyopathy and only minimal skeletal muscle weakness (Meier C et al., 1984).

1.17 Muscle pathology in NM

Standard haematoxylin and eosin stained sections of skeletal muscle from patients with NM can appear normal, or can exhibit some fiber size variation, but staining of frozen sections by the Gomori trichrome method readily reveals the nemaline rods that are the hallmark of this disorder (Figure 10A). The rods vary from 1–7 μm in length and from 0.3–2 μm in width and stain dark red or purple contrasting with the pale blue-green myofibrils. They tend to cluster under the sarcolemmal membrane or around nuclei, and rarely can be intranuclear (Paulus W et al., 1988; Goebel HH et al., 1997). Although there has been some speculation that intranuclear rods might indicate a poor prognosis (Rifai Z et al., 1993) there is a report of adult-onset NM with nuclear rods (Paulus W et al., 1988). Moreover, the majority of severe cases do not contain intranuclear rods. The proportion of fibers containing rods can vary from less than 1% to virtually all fibers and does not correlate with the degree of muscle weakness, although more active muscles, such as diaphragm, can have greater numbers of rod-containing fibers. Histochemical stains for myosin ATPase reaction at different pH levels reveals the other common myopathic change in these muscles. Fiber type proportions and sizes can vary widely from the normal ratio of 1:1:1 of equal sized type 1:2a:2b fibers. Often, NM biopsies exhibit fiber type 1 predominance, and in extreme cases, fiber typing by the ATPase reaction is impossible owing to uniform reactivity of a pure population of type 1 fibers. Rods can be found equally in all fiber types or preferentially in either type 1 or type 2 fibers. Often, but not always, the rod-containing fibers are hypotrophic. Areas with extensive rod formation exhibit significant disruption and disorganization of sarcomeric structure, probably accounting for some degree of the associated weakness. Occasionally, muscle fibers are replaced by fat or fibrous tissue, but fiber necrosis and regeneration is rare. None of the variable pathological findings described above have been correlated with any particular clinical or genetic category of NM. Electron microscopy reveals the definitive ultrastructure of the rods and can be used as an objective means to define these bodies (Figure 10B). The rods are electron dense and appear similar in composition to the Z lines from which they emanate (Dubowitz V, 1985). They can appear as enlarged Z lines or elongated structures replacing thin filaments in a disorganized

mass of sarcomeric components. Thickening and streaming of the Z lines is also sometimes seen, but these are not diagnostic features by themselves. Consistent with their appearance as extensions of Z lines, the rods are largely made up of α-actinin as well as several other Z line proteins (Valle G et al., 1997; Takada F et al., 2001; Jennekens FG et al., 1983). Digestion with Ca^{2+}-activated protease removes the α-actinin, revealing an actin-containing thin filament backbone. A three-dimensionaln reconstruction of rods has revealed adjacent actin filaments of opposite polarity cross-linked by probably α-actinin dimers (Morris EP et al., 1990), suggesting that rod formation might involve an inability to terminate or 'cap' the thin filament ends at Z lines. It is important to note that nemaline rods are not pathognomonic for NM as they can be reproducibly induced to form in tenotomized rat muscle (Karpati G et al., 1972) or neostigmine myopathy and are also rarely found in small numbers in normal or non-NM myopathic muscles as well as in HIV-associated myopathy (Gherardi RK, 1994). In particular, they are also found in a subset of patients with central core disease caused by certain ryanodine receptor gene mutations (Monnier N et al., 2000; Scacheri PC et al., 2000). Thus, rod formation probably represents a common pathophysiological response of skeletal muscle to certain pathological situations. Understanding the mechanisms of (secondary) rod formation in these situations will probably provide important insights into the 'primary' or 'pure' nemaline myopathies.

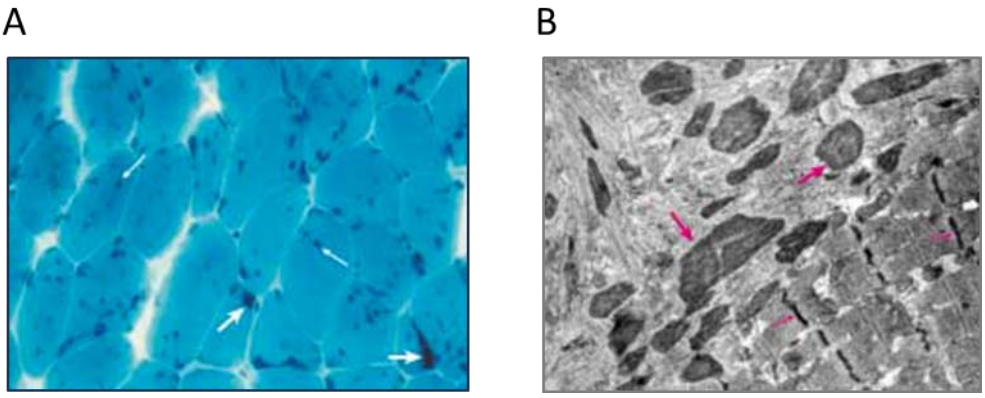

Figure 10. A, Gomori trichrome-stained transverse section of skeletal muscle from a nemaline myopathy (NM) patient. Nemaline rods appear in virtually all fibers as darkly staining bodies distributed throughout the cytoplasm (small arrows) and as larger subsarcolemmal accumulations in occasional fibers (large arrows). Note that NM pathology is variable as biopsies from other cases do not necessarily have rods in all fibers, and rod-containing fibers can sometimes be significantly smaller than fibers

without rods. B, Electron micrograph illustrating typical nemaline rods and disorganized myofibrillar apparatus in a patient with nemaline myopathy. An area of relatively normal muscle structure with

normal Z lines (small arrows, bottom right) is seen next to a structurally disorganized region with multiple nemaline rods (large arrows) and disorganized thin filaments (top left).

1.18 Nebulin

More than 50% of NM cases are associated with mutation of Nebulin (Pelin K et al., 1999). Nebulin is a giant sarcomeric protein (~800 kDa); its C-terminus is anchored in the Z-disk and its N-terminus is located close to the thin filament pointed end thus, a single nebulin molecule spans nearly the entire length of the thin filament (Figure 5, Giant structural proteins; Labeit S and Kolmerer B, 1995). Nebulin plays important roles in sarcomeric structure and contractile performance. It stabilizes the thin filament and specifies its minimal length (Bang ML et al., 2006; Castillo A et al., 2009; Pappas CT et al., 2010; Witt CC et al., 2006). Recent evidence also suggests that nebulin modulates both the kinetics of actomyosin interaction (Bang ML et al., 2009; Chandra M et al., 2009) and the calcium sensitivity of force generation (Chandra M et al., 2009). Skeletal muscle fibers of NM patients with NEB mutations might develop muscle weakness due to loss of these functions of nebulin; their myofibers contain shorter thin filaments (Ottenheijm CA et al., 2009), have altered crossbridge cycling kinetics (Lawlor MW et al., 2011; Ottenheijm CA et al., 2010), and their calcium-sensitivity of force generation is reduced (Ottenheijm CA et al., 2010). However, studies on muscle fibers from patients are limited due to, for example, the small size of diagnostic muscle biopsies and the heterogeneity of the study populations. Consequently, our understanding of the mechanisms underlying muscle weakness in NM patients with nebulin mutations remains incomplete. To improve this understanding requires the development of mouse models that harbor mutations in neb that are found in patients. To date, such models were not available.

Recently, Granzier and coworkers generated a mouse model in which exon 55 of the nebulin gene is deleted using an in-frame deletion known to frequently occur and to cause autosomal recessive NM (Anderson SL et al., 2004; Lehtokari VL et al., 2009; Lehtokari VL et al., 2006). This model (*Neb*ΔExon55) allowed, for the first time, for a detailed and comprehensive investigation of the disease mechanisms caused by a nebulin mutation and for the evaluation of potential treatments (Ottenheijm et al., in prep). Findings related to that new model reveal that homozygous mice have a phenotype that recapitulates that observed in NM patients with

deletion of *NEB* exon 55, including severe muscle weakness, and that muscle strength can be restored by a novel fast skeletal troponin activator that augments the response of the thin filament to calcium.

1.19 Generation of NebulinΔEx55 mice

NebulinΔEx55 mice were designed to mimic the 2,502-bp deletion that has previously been found to cause nemaline myopathy in humans (Anderson SL et al., 2004). The construct replaced exon 55 and parts of introns 54 and 55 with an FRT flanked neomyosin cassette. No difference in phenotype was found when the neomyosin cassette was removed with a FLP deleter strain (B6;SJL-Tg(ACTFLPe)9205Dym/J- purchased from Jackson). Animals were maintained on a C57/BL6 background. All experiments were approved by IACUC and followed the NIH Guidelines "Using Animals in Intramural Research" for animal use. A targeting construct was assembled by cloning arms of homology from genomic DNA into a pCKOB vector. The vector was introduced into C57BL/6J- *Tyr*$^{c-2J}$/J ES cells by electroporation. The deletion was introduced by homologous recombination and selected by negative selection against thymidine kinase (using Ganciclovir) and positive selection for neomyosin resistance (G418). The surviving ES cell clones were verified by long PCR and used to produce *Neb*ΔEx55 mice by injection into C57/BL6 blastocyst.

Mice heterozygous for the targeted allele (HET) are viable and fertile and survive into adulthood with no obvious clinical or contractile phenotype. Homozygous offspring (NebΔExon55 KO) are produced at expected Mendelian genetic ratios (~1/4 of total number of pups using heterozygous breedings), with a weight at birth that is not different from that of HET and WT littermates. However, NebΔExon55 KO mice show severe growth retardation after birth (Figure 11) and typically do not survive past the first week.

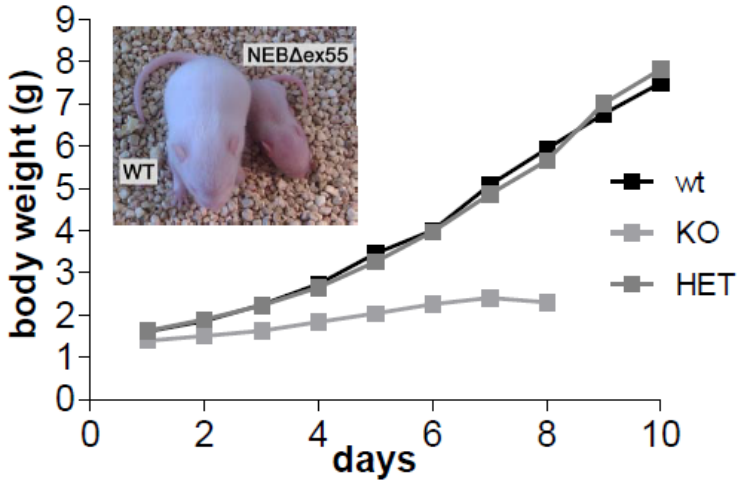

Figure 11. Body weight of *Neb*ΔExon55 KO mice at birth is not different from that of HET and wt littermates. *Neb*ΔExon55 KO mice show severe growth retardation after birth.

As previously reported, nemaline myopathy in humans is characterized by the presence of nemaline bodies, which is often accompanied by myofiber hypotrophy. Sections of quadriceps muscle from 6d old WT and NebΔExon55 KO mice stained with hematoxylin and eosin (H&E) or Gomori trichrome reveal smaller muscle fibers in NebΔExon55KO mice. Moreover, discrete populations of large and small fibers were not observed in NebΔExon55 KO mouse muscle. Nemaline bodies were not visible at the light microscopic level on Gomori trichrome stain (Figure 12A, lower panel) of quadriceps muscle, but electron microscopy revealed electron-dense nemaline bodies at the location of the Z-band (arrows, Figure 12B, in the Tibialis Cranialis (TC) muscles of NebΔExon55 KO mice). These nemaline bodies displayed electron density equivalent to normal Z-bands, which differentiates them from the Z-band streaming that can be found in a variety of muscle disorders. Nemaline bodies were not seen in WT mouse muscle. Thus, NebΔExon55 KO mice display a histological phenotype that resembles NM, including the presence of nemaline bodies and hypotrophic fibers.

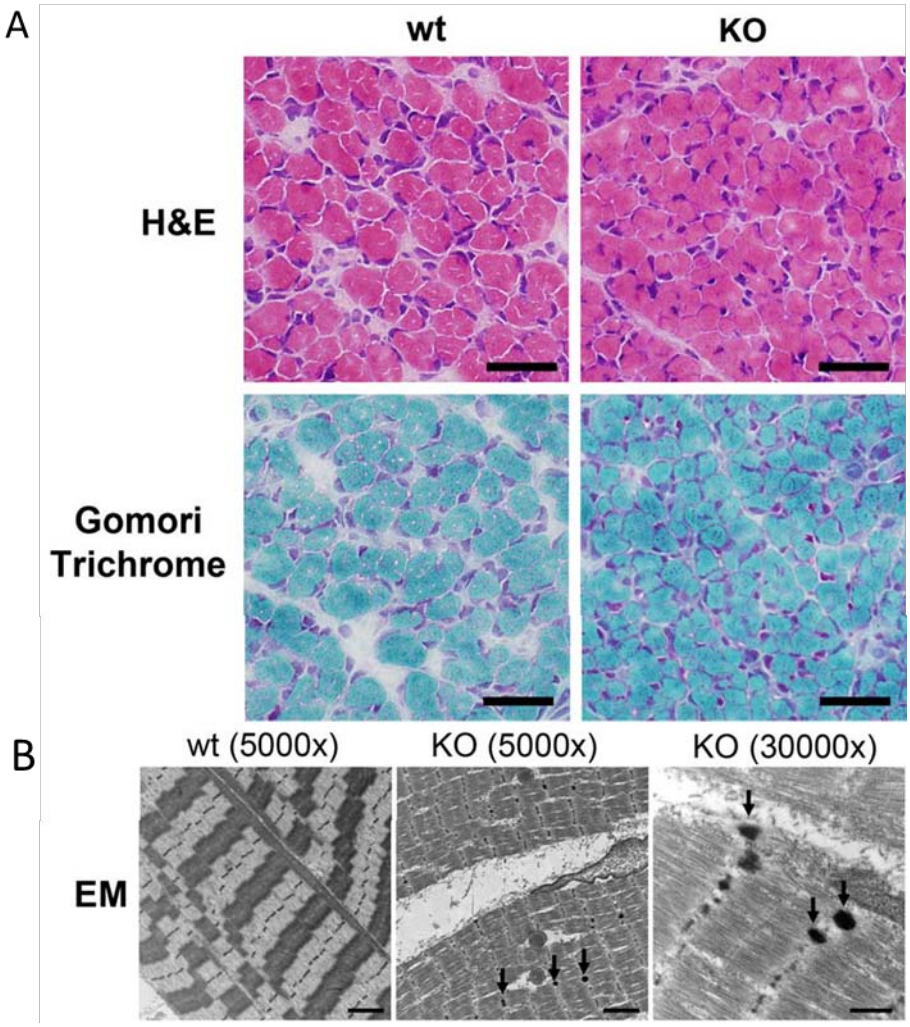

Figure 12. Histological findings in 6d old WT and NebΔExon55 KO mice. A, Hematoxylin and Eosin (H&E) stained sections of quadriceps muscle from wild type (WT) and NebΔExon55 KO (KO) mice reveal smaller muscle fibers in NebΔExon55 KO mice. Nemaline rods were not visible at the light microscopic level on Gomori trichrome stain, but electron-dense nemaline bodies (arrows) were seen on electron microscopy (EM) in the Tibialis Cranialis (TC) muscle from all NebΔExon55 KO mice. Nemaline bodies were not seen in WT mouse muscle (B). Bar = 40 µm for H&E and Gomori trichrome pictures, 2 µm for 5000x EM pictures, and 500 nm for the 30000x EM picture.

1.20 Deletion of exon 55 results in severely reduced nebulin protein levels

NEB exon 55 encodes thirty-five amino acids and represents ~4 kDa at the protein level. As deletion of exon 55 maintains the reading frame 3' of exon 55, it could be expected the NebΔExon55 KO mice to express a nebulin isoform that is ~4 kDa smaller than WT nebulin. However in 5 day old NebΔExon55 KO mice, nebulin proteins levels were severely reduced in all muscle types tested, as well as protein level evalueted at embrionic stage and at one day after birth, confirming a severe reduction of nebuline in KO mice compared tp WT. Moreover, molecular investigation at level of DNA transcription and of mRNA translation, showed that, in

addition to the expected reduction of exon 55 mRNA, transcription of nearly all nebulin exons was significantly reduced in NebΔExon55 KO muscle suggesting that the low nebulin protein levels in NebΔExon55 KO mice are not caused by defects in the translation of nebulin mRNA into protein but rather by changes in transcription of the mutant nebulin gene or in the stability of the mutant nebulin mRNA.

1.21 NebΔExon55 KO mice have shorter thin filament lengths

Nebulin plays an important role in specifying thin filament length, and shorter thin filaments clearly contribute to reduced sarcomeric force generation in human nebulin-deficient NM (Ottenheijm et al., 2009). In NebΔExon55 KO muscle fibers thin filament length has been measured using immunofluorescence confocal scanning laser microscopy by determining the location of tropomodulin (a thin filament pointed end capping protein) relative to the Z-disk and then measuring the width of the band obtained using the fluorescently labeled actin-binding protein phalloidin. Figure 13, shows that the staining pattern of fluorescently labeled phalloidin differed between myofibrils from NebΔExon55 KO and WT TC muscle; WT myofibrils showed broad actin labeling with uniform intensity (except for the Z-disk area where actin filaments overlap), whereas in NebΔExon55 KO myofibrils the labelling was narrower, and intensity gradually decreased from the Z-disk towards the middle of the sarcomere. Densitometric analysis revealed that the width at half-maximal intensity was 2.25 ± 0.03 µm for WT and 1.75 ± 0.01 µm for NebΔExon55 KO myofibrils (Figure 13, right).

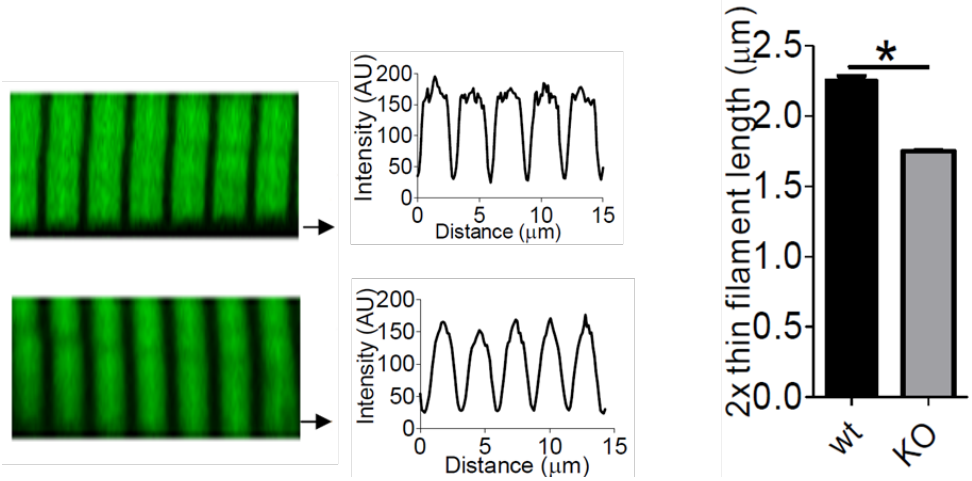

Figure 13. Left: Actin staining with phalloidin-AlexaFluor 488 in 6d TC myofibrils from *Neb*ΔExon55 KO and WT mice shows broad staining in WT myofibrils (top), whereas this staining is narrowed in *Neb*ΔExon55 KO myofibrils (bottom) Right: Analysis of phalloidin line scan intensities revealed significantly reduced average thin filament lengths in *Neb*ΔExon55 KO myofibrils.

Tropomodulin staining in WT myofibrils showed a distinct doublet in the middle of the sarcomere, 2.03 ± 0.03 µm apart, measured across the Z-disk, whereas in myofibrils from NebΔExon55 KO mice this value was only 1.67 ± 0.03 µm. These findings supported the results from the phalloidin experiments and suggested that thin filament lengths were reduced from ~1.0 µm in WT myofibrils to ~0.85 µm in NebΔExon55 KO myofibrils.

The experiments with fluorescently labelled tropomodulin revealed that thin filaments were shorter in NebΔExon55 KO myofibrils (as found in previus works, Bang ML et al., 2006; Gokhin DS et al., 2009) and suggesteded that capping at the thin filament pointed end by tropomodulin remained intact in these myofibrils. Immunofluorescence experiments on CapZ (a thin filament barbed end capping protein) showed that capping at the barbed end also remained intact in NebΔExon55 KO myofibrils.

1.22 NebΔExon55 KO mice display severe muscle weakness

Because sarcomeres generate force in proportion to thick and thin filament overlap, a well-defined thin filament length is an important determinant of muscle function. This is illustrated by the force-sarcomere length relationship, which is characterized by a force plateau at optimal filament overlap, followed by a descending limb at higher sarcomere lengths as filament overlap decreases. Shortened thin filaments will reduce thick and thin filament overlap and impair the sarcomere's force generating capacity, which is reflected by a leftward shift of the force-sarcomere length relationship. Hence to study whether the reduced thin filament length in NebΔExon55 KO myofibrils affects the force generating capacity of muscle, Granzier and coworkers determined the force-sarcomere-length relationship in permeabilized fiber preparations. Fibers from WT muscle showed a characteristic force plateau up to a sarcomere length of ~2.6 µm, followed by a linear descending limb (Figure 14A). Note that the descending limb of WT fibers intercepts the x-axis at ~3.6 µm. Assuming that thick filaments are constant at ~1.6 µm, this would suggest that thin filament length is ~1.0 µm, which is in line with thin filament lengths as determined by our confocal microscopy studies. Importantly, fibers from NebΔExon55 KO muscle showed a leftward-shift of the force-sarcomere length relationship, indicating shorter thin filament lengths (Figure 14A). The descending limb of NebΔExon55 KO fibers intercepts the x-axis at a sarcomere length of ~3.4 µm, a length that is consistent with thin filament lengths of ~0.9 µm, which is close to the length as determined by the confocal microscopy studies (0.85 µm).

Considering that thin filament length is an important determinant of a muscle's force generating capacity, authors also plotted tension (force normalized to fiber cross-sectional area) versus sarcomere length (Figure 14B, upper panel). Importantly, at a sarcomere length of 2.4 µm - a length on the plateau of the Force- SL relation of both genotypes, absolute maximal tension was reduced in fibers from NebΔExon55 KO muscle to ~38% of WT values (Figure 14B, lower panel). To study whether the reduced maximal tension of NebΔExon55 KO fibers is caused by a reduction in myofibrillar fractional area or rather by changes in myofibrillar function, the contractile force of single myofibrils isolated from NebΔExon55 KO and WT muscle fibers was also determined. As described in Chapter 3, the maximal tension generated by NebΔExon55 KO myofibrils was reduced to ~36% of WT values, a reduction that is similar in magnitude to that observed in NebΔExon55 KO fibers. Thus, these findings indicate that muscle from NebΔExon55 KO mice is significantly weakened, that this weakening is primarily caused by changes in myofibrillar function, and that reduction of thin filament length contributes to weakness especially at longer sarcomere lengths.

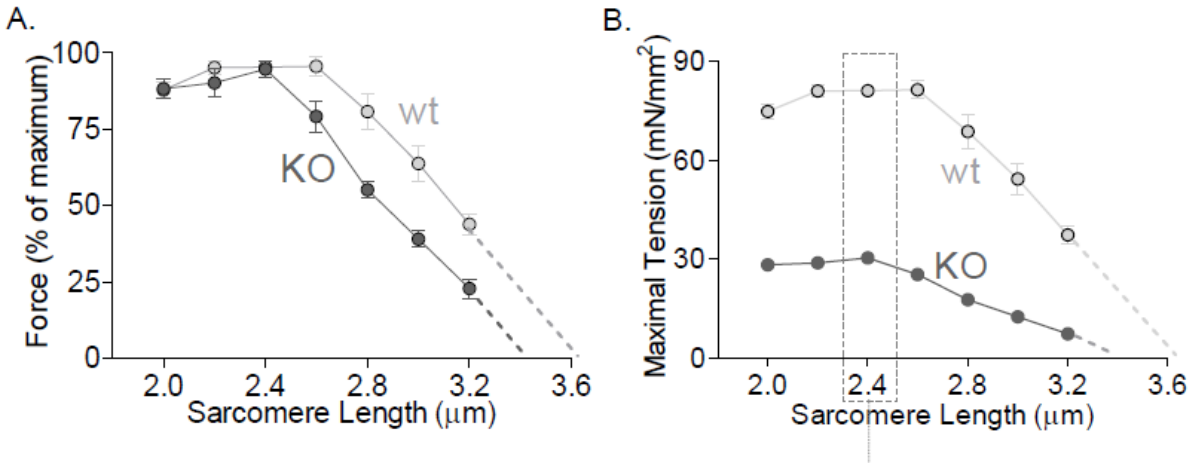

Figure 14. A, The force-sarcomere length relation of TC fibers from 6d old *Neb*ΔExon55 KO and WT mice, with force normalized to maximal force at the optimal length: the relation is shifted leftward in *Neb*ΔExon55 KO fibers suggesting shorter thin filaments in KO fibers. B, Upper panel: the maximal tension-sarcomere length relation of *Neb*ΔExon55 KO and WT fibers, illustrating that KO fibers develop at all sarcomere lengths a reduced level of force. This indicates that other factors, in addition to shorter thin filaments, contribute to the weakness of KO muscle; lower panel: at a sarcomere length of 2.4 µm, maximal tension is reduced in fibers from *Neb*ΔExon55 KO muscle to ~38% of WT values.

Aim of the thesis

Aim of this Thesis is to gain better insight in the physiology or pathophysiology of different kind of myopathies, spanning from cardac inherited disease to skeletal congenital pathologies. An additional aim is also to caracterize a donor, unaffected sample, of human cardiac tissue harboring a homozigous mutation of TnT.

To this aims it is required not only the investigation of changes in morphology, biochemical and genetic profiles but also the biophysical characterization of the function of the molecular motor and of its regulation. In this thesis this biophysical approach has been used to investigate the mechanisms that determine direct contractile alterations in very different pathologies like familial hypertrophyc cardiomyopathy and nemalin myopathy. These myopathies involve unrelated *apparati*, cardiac and skeletal, and different protein mutations. In this thesis, the focus was on a mutation of cardiac troponin T associated to cardiomyopathy and on mutation of nebuline, associated to nemaline myopathy. The main experimental approach used for this work has been the fast solution switching tecnique for the activation of contraction of myofibril preparations (Colomo F et al., 1998) from both skeletal and cardiac muscle. This technique allows the acccurate analysis mechanical and kinetic properties at subcellurar level as well as the characterization of the calcium dependent activation of contraction. This approach was also used to support, integrate and validate machanical, energetic and structural results obtained with different tecnique in research unit that collaborated with our laboratory (Jolanda van der Velden, VU-Amsterdam; Henk Granzier, TU, Arizona).

Chapter 2: Methods

1 Experimental models

Myofibrils isolated from skeletal and cardiac muscle (both animal and human) were used to investigate mechanics of muscle contraction.

1.1 Skeletal preparations

Thin bundles of skeletal myofibrils were obtained from flash frozen dryed or glycerinated *tibialis cranialis* of neonatal mouse (days 4-11) from a novel NEM2 mouse model developed in Dr. H Granzier laboratory (University of Arizona, Tucson, USA). The in-frame deletion of nebulin's exon 55 (NEBΔex55) mimics a deletion in the nebulin gene found in a large group of patients affected by Nemalin Myopathy (NM). NEBΔex55 heterozigous (HET) KO and WT myofibrils were used to investigate and compare biophysical properties of contraction in the different experimental models.

1.2 Human cardiac preparation

Myofibrils were isolated from frozen (-80°C or liquid nitrogen) myectomy (inter ventricular septum, IVS, or left ventricule free wall, LV) from patients affected by various cardiac pathologies.
Myectomies were collected from Azienda Ospedaliero Universitaria Careggi in Florence and from other clinical and research units in Europe and in Australia that share collaborations with our research unit.

The first part of this study focused on an interesting sample of a young patient (20 yrs, male) affected by a particular severe form of familial hypertrophic cardiomyopathy (FHC) due to an homozygous mutation of cTnT K280N on TNNT2 gene. The contractile behavior of myofibrils obtained from this sample (left ventricle free wall and IVS tissue samples from heart transplantation surgery collected in cardioplegic solution, flash frozen in liquid nitrogen and stored at -80 °C) was compared with that of myofibrils obtained from myectomies from patients affected by various other cardiac pathology or control. This in order to understand the molecular basis of the contractile alteration associated with cTnT K280N mutation. Control myofibrils were obtained from frozen left ventricular samples of explanted hearts from donor patients that had not been used for transplantation (**Control donor**).

Following previously reported data (Piroddi et al., 2007) and recent unpublished results from our group, we used as controls also myofibrils obtained from non-failing, non-hypertrophic left ventricular samples of patients undergoing corrective cardiac surgery (**Control patients**).
Myectomies from mutation negative HCM patients (MN_{HCM}) were also used as control group. Patients belonging to this group had septal hypertrophy but no sarcomeric mutation was found with the routine screening of HCM patients **(Mutation negative HCM patients)**.
A third group of myofibrils used as control was obtained from Secondary Hypertrophy patients biopsies. IVS was collected by patients with aortic stenosis undergone to aortic valve surgery (**Secondary hypertophy patients)**.
Experiments involving the use of human samples had been approved by the Local Ethical Committee (Azienda Ospedaliero Universitaria Careggi; prot. n. 2006/0024713– 28/06/2006). The study followed rules for investigation of human subjects as defined in the Declaration of Helsinki.

1.3 Myofibril preparation

Single myofibrils and small bundles of myofibrils were isolated from frozen striated muscle samples (human cardiac biopsies or mouse skeletal muscle *tibialis cranialis*). Muscle specimens were placed in small container bottom-covered with Sylgard, cut into thin strips and pinned down under a stereomicroscope in ice-cold rigor solution containing (mM) NaCl 132, KCl 5, MgCl2 1, Tris 10, EGTA 5 (pH 7.1) (Linke et al., 1993). The strips were incubated for 3 h (4°C) in the same solution added with 1% Triton-X 100 or, alternatively, overnight with 0,5% Triton-X 100. After skinning the strips were rinsed to remove Triton with fresh ice-cold rigor solution containing (mM) Tris 50, KCl 100, MgCl2 2, EGTA 1 (pH 7.0)(Linke et al., 1993). All solutions to which the samples and myofibrils were exposed contained a cocktail of protease inhibitors including NaN3 (500 µM), pepstatin (5 µM), PMSF (200 µM), DTE (0.5 mM) and E64 + leupeptin (10 µM). The demembranated sample was then ready to be mechanically homogenized. Two or three pieces were transferred to a plastic centrifuge tube containing 1.5 ml ice-cold rigor solution added with a cocktail of protease inhibitors and homogenized using a tissue tearor (Biospec Products inc., USA, mod. 985-370) at medium speed for 15 seconds. A second homogenization was performed to refine the quality of suspension.

All experimental solutions were made using double-distilled water (18 MΩ·cm) purified using the Milli Q system (Millipore Corporation, MA, USA). All experimental solutions were gauged with CRISON GLP 21 pH-meter (Crison, Barcellona, UE).

1.4 Experimental solutions

All experimental solutions, contained 5mM MgATP, an excess of magnesium over ATP so to give a free magnesium concentration of 1 mM and a re-phosphorilating system made of creatin kinase (200u/ml) and creatine phosphate (10 mM). Sodium sulphate and sodium propionate were added to adjust the ionic strength to 200 mM. All solutions had 10 mM MOPS and pH 7. EGTA concentration in the experimental chamber was 10mM, to keep the free Ca^{2+} low in between activation cycles. EGTA concentration was 1mM in relaxing and activating solutions used for the experiment. Measurements were performed at 15°C.

pCa	Stock sol.	9
MgProp	**0.1M**	6.078
NaEGTA	**0.1M**	10
KProp	**1M**	5.42
Na_2SO_4	**0.1M**	17.68
MOPS	**1M**	1
ATP		0.2996 g
Creatin Phosphate		0.3272 g
ml/ 100ml		

Table 1. Chamber solution (pH 7). Solution used to fill the experimental chamber in which myofibrils were rinsed before the experiment

pCa	Stock sol.	4.5	8	9
$CaCl_2$	**0.1M**	1.084	0.0188	0
MgProp	**0.1M**	5.998	6.0028	6.002
NaEGTA	**0.1M**	1	1	1
KProp	**1M**	5.22	5.42	5.42
Na_2SO_4	**0.1M**	26.61	26.69	26.68
MOPS	**1M**	1	1	1
ATP		0.3036 g	0.2996 g	0.2996 g
Creatin Phosphate		0.3272 g	0.3272 g	0.3272 g
ml/ 100ml				

Table 2. Relaxing and activating solutions (pH 7). Experimental solutions used during the fast solution switching protocol of myofibrilsactivation-relaxation (Colomo F et al., 1998)

1.5 Experimental apparatus

The experimental apparatus was centered around an inverted microscope (OLYMPUS IX70, Japan) placed on an air suspension table (Ealing System, Massachusetts, USA) and equipped with conventional bright-field and phase-contrast optics

The microscope stand was equipped with a temperature controlled experimental chamber, where myofibrils were transferred and mounted, hydraulically controlled micromanipulators, tension transducer system, myofibril length-control motor (see below) and a rapid perfusion solution switching system (Colomo F et al., 1998).

1.6 Preparation of glass microtools and myofibril attachment

The microtools used to mount myofibrils in between length and force transducers were pulled from 1 mm external diameter capillaries of borosilicate glass (Clark Electromedical Instruments, UK) using a conventional horizontal puller (P-87, Sutter, U.S.A.). The pipette end was cut to produce tips with an outer diameter of 10-30 µm. Next, pipettes were fire-polished by microforge (MF-79, Narishige, Japan) to obtain tips with a rounded shape and a size that fit their specific use. Micropipettes used as force probes were bent at 90° at 1-3 mm starting from the tip. The end region had an outer diameter of around 10-15 µm; and the tip of the force probe was blackened with micropigment ink in order to increase the sensitivity of the photodiode used as photosensors.

The same capillaries of borosilicate glass were used to produce the other glass microtool, the stretcher, connected to the shaft of the length-control motor. The capillary was pulled, cut and fire-polished to obtain a straight-shape pipette with an outer diameter of 20-30 µm.

Theta borosilicate glass capillary tubes (Warner Instrument Corp., USA; outside diameter 2.0mm) were used to produce the injection pipette.

The capillaries were pulled and the tip cut with a diamond-tip pencil. Dimension of tip was subsequently adjusted using a specific stone to file and polish to a rounded shape the edge of the pipette. Small polyethylene tube (Warner Instrument, USA; 0.61 OD x 0.28ID) were inserted up to the tip in both the separated channel of the theta pipette and sealed with epoxy-glue so to connect the injection pipette to the perfusion system.

1.7 Force probe and tension detecting

The apparatus for tension recording from myofibrils consisted of a force probe microtool, the inverted microscope, a white light source and a photosensor.

The force probe was the glass microtool acting as a cantilever. The tension generated by the mounted myofibril was measured by recording the elastic deflection of the tip of the probe that was proportional to the force developed and the compliance of the force probe. The compliance of the force probe was carefully measured by determining the force/deflection relation of each force probe with a calibrator obtained from a modified microamperometer (Minns, 1971; Cecchi et al., 1993). The force/deflection relation (the compliance) of each force probe was determined under the microscope by touching the tip of the force calibrator pointer with the tip of the force probe and measuring the amount of deflection produced by a given current through the calibrator coil. For this study we used force probes with compliances ranging from 3 to 9 μm/μN. Highly compliant and very sensitive probes were used in experiments in which the force produced by a myofibril was expected to be small; stiffer and less sensitive probes were used when the force measured was expected to be larger. In any given experiment, force probes were selected for compliance so that myofibril shortening during maximal force production was limited to less than 3 % of the slack myofibril length.

The white light was generated by an halogen display-optic lamp (OSRAM, EU, 12V, 100W) mounted on the lamp housing of the inverted microscope. The light beam passing through the microscope condenser was focused to on the blackened tip of the force probe. The image of the spot with the force probe in its center was projected (optical magnification 90X) onto the photosensor through the 40 x objective. The photosensor was made up of a photodiode, a silicate detector split in two part by a septum. The photodiode was mounted on a piece of fibreglass circuit board which was mounted in a micropositioner on the frontal port of the microscope.

The sensitivity of the force transducer was measured by an indirect method. During the experiment, any deflection of the force probe, caused by the tension generated by the myofibril, resulted in an increase in either the light area of one part of photodiode or the shadow area of the other one, and, in turn, in a change of the photosensor output current which was converted to voltage by means of an current-to-voltage (I-V) converter. This change of output current was electronically converted to voltage proportional to the tension generated by the preparation and the compliance of the force probe.

In each experiment the sensitivity of the transducer system was measured by varying the position of the photosensor relative to the force-probe image and measuring the photodiode output. The mean output value obtained by applying 2 μm steps was used to establish the

sensitivity of the transducer system in mV/µm. Usually, the sensitivity was between 250 mV/µm and 500 mV/µm. The tension developed by a myofibril was converted into nN on the basis of the actual compliance of the force probe used.

1.8 Length control motor

The length of the preparations was controlled by a piezomotor that could produce rapid (less than 1 ms) length changes. The device was a piezoelectric motor guided by a PZT-Servo controller (Physik Instrumente (PI) GmbH & Co, EU). Stainless steel connection was mounted on the motor to connect the stretcher glass microtool.

1.9 Injection pipet motor

The motor that controlled the movement of the injection pipette was a stepper motor device (Haydon Switch and Instrument, USA) and the controller of the motor was a Perfusion Fast Step SF-77B (Warner Instrument Corporation, USA) able to perform fast movement in less than 10 ms in a range of 100-800 µm. The injection pipette (see 1.11) was connected to perfusion system by small tubing coming from single valve system. Upstream each valve was connected to a specific syringe by small tubs. The valve system was controlled by VC-6 six channel valve controller (Warner Instrument Corporation) permitting the simultaneous use of more than two different solutions. In our conditions, this was manually activated during each experimental activation protocol.

1.10 Data acquisition

Force and length analogic signals were continuously monitored throughout the experiment using commercial software and programs readjust and modified to our use (National InstrumentsTM, LabVIEWTm). The same signals were also recorded during experimental protocols and later used for data analysis. Data measurements were made directly with an homemade LabVIEW Analysis program converting analogic signal to numeric values and commercial software (OriginTM, SigmaPlot®).

1.11 Experimental protocol

A small volume of myofibril suspension was transferred to a temperature controlled chamber filled with relaxing solution on the inverted microscope. Temperature control was achieved by means of a continuous flow of constant temperature water (SBF7, FALC INSTRUMNS, EU) inside

a channel system dug in the chamber walls so that temperature could be stable at 15°C. The chamber bottom was made by a cover slip. Selected preparations (single myofibrils or bundles of few myofibrils, 25-80 μm long, 1-4 μm wide) were mounted horizontally between two glass microtools.

Firstly, one of myofibril ends was attached to the stretcher and raised vertically, leaving the other end still attached to the glass. This was then attached to the force probe, picking up the myofibril. Myofibrils were mounted taking advantage of the great spontaneous adhesiveness of myofibrils to glass, likely due to electrostatic attractions. The attachment of myofibrils to glass microtools was usually very strong and resisted maximal tension development during the contraction.

As previously described (1.7), force was measured from the elastic deflection of the force probe, by projecting its image on a split photodiode. Average sarcomere length and myofibril diameter were measured from video images using Image J, a Java-based image processing program developed at the National Institutes of Health, USA. The initial sarcomere length l_0 of myofibrils was set around 2-2.2 μm. Myofibrils were activated and relaxed by rapid solution switching. A Selected myofibril was continuously perfused by one of two parallel streams of solutions (relaxing pCa 9.0 or activating pCa 4.5) delivered by the theta glass pipette positioned at right angle with the preparation. Myofibril was initially perfused by relaxing-low Ca^{2+} solution. Following rapid displacement of the injection pipette, myofibrils was then perfused by maximal activating solution allowing the development of isometric active tension. A second displacement of the pipette back to the initial position restored relaxing conditions: myofibrils was perfused again by fully relaxing low Ca^{2+} solution and tension relaxation transient could be recorded. The solution change took place with a time constant of 2-3 ms and was complete in less then 5ms.

1.12 Measured parameters

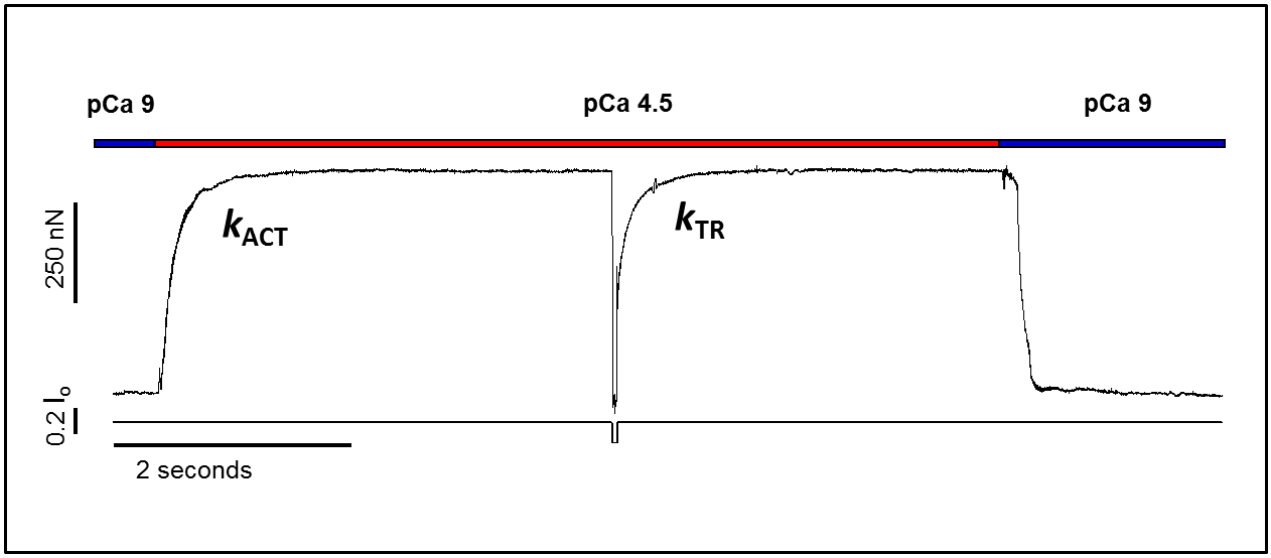

Figure 1. Illustrative trace of force rise, characterized by constant rate k_{ACT}, in response to maximal activation (pCa 4.5), followed by release-restretch maneuver and redevelopement of tension, described by constant rate k_{TR}, and final relaxation phase after removal of Ca^{2+} (pCa9)

When a myofibril, mounted in the experimental apparatus and held in the solution stream of pCa9, was exposed to the activating solution (pCa4.5) by switching the position of the perfusion pipette, force rapidly raised to a maximum that was steadily maintained as long as the perfusion pipette is hold in the 'activating' position. Maximal isometric tension (mN/mm2) was calculated as maximum force developed (mN) normalized for the cross sectional area (mm2) of the preparation. The cross-sectional area of myofibrils was calculated by assuming a circular shape and using as diameter the mean of the largest and the smallest width values along the preparation.

The raise of isometric active tension to the plateau was approximately mono-exponential with rate constant k_{ACT} . As this rate constant could be influenced by the time course of solution change, we also measure the rate of tension generation under steady state Ca^{2+} activation using "Brenner maneuver" (Brenner, 1988) i.e. from the rate of tension redevelopment (k_{TR}) following a rapid mechanical perturbation. k_{TR} is known to reflect solely turnover kinetics of cross-bridges (CB). In our conditions, k_{ACT} is usually found equal to k_{TR} (Poggesi et al., 2005). Different values between k_{ACT} and k_{TR} could also suggest alteration in regulation and activation of thin filament.

Switching back the position of the perfusing pipette, myofibril was perfused again by fully relaxing low Ca^{2+} solution and tension relaxation was recorded.

In all types of striated muscles tested so far, the time course of force relaxation was biphasic (Tesi et al., 2002), starting with a slow linear force decay followed, after a 'shoulder', by a fast exponential relaxation phase. We measured the apparent rate constants of the slow linear and the fast exponential force decay (slow k_{REL} and fast k_{REL}; s^{-1}) and the duration of the slow phase of relaxation (ms). It has been shown that the slow linear force decay occurs under isometric conditions of sarcomeres and in the absence of Ca^{2+}. Slow k_{REL} is predominantly the apparent rate with which attached cross bridges leave force-generating states under isometric conditions. The fast exponential phase fast k_{REL} follows the 'give' of a few sarcomeres and is dominated by inter-sarcomere dynamics (Stehle et al., 2002).

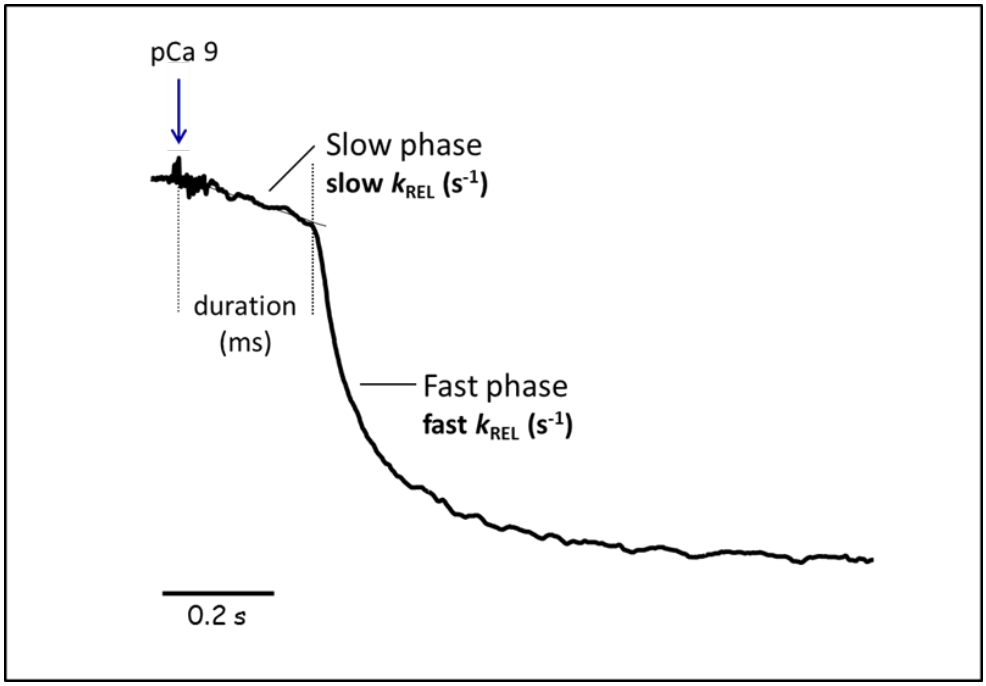

Figure 2. Relaxation following Ca^{2+} removal by fast solution switching was described by a slow linear phase that occurred under isometric conditions and a fast exponential phase reflecting inter sarcomere dynamics

1.13 Troponin replacement in myofibrils

Tn complex replacement is a relatively easy technique that permit the extraction of the endogenous Tn and the introduction of an exogenous, recombinant Tn in the myofibrillar protein structure.

Tn complex replacement in myofibrils suspension is obtained by mass-action, therefore the success of the method is strictly related to the concentration of protein used for the replacement as well as to the quality of the sample from which myofibrils were isolated.

1.14 Recombinant WT troponin complex

cTn complex we used was made by Pieter de Tombe's group (University of Illinois at Chicago, USA). As described previously by Sumandea et al. (2003), recombinant troponin subunits were cloned into pET-17b vector, expressed in BL21 (DE3) pLysS E. Coli, purified by column chromatography, and lyophilized. The Tn complex was formed by reconstitution of the Tn subunits in 6 mol/liter Urea, followed by multiple dialysis steps at increasing lower strength, the final step of which was against rigor exchange solution.

1.15 Exchange protocol

After the skinning and the homogenization of the selected sample in rigor solution as previously described (1.3), a part of the suspension was used as control to check quality and properties of the sample. The rest of suspension was used for the replacement method, divided in two parts, one used for the exchange with recombinant Tn (treated exchanged samples) and the other one as treated contol to check for potential alterations occurring with protein replacement method. Both batches were treated in parallel.

To remove the rigor solution used for myofibril isolation, 1ml of sample was centrifuged for 10 min at 4000 rpm at 4°C. Then the supernatant was removed, 1ml of exchange solution was added to the pellet and after resuspension of myofibrils in the new solution the samples was again centrifuged (10 min, 4000 rpm, 4°C).

The supernatant was removed and in the treated control 500µm of exchange solution was used to resuspend myofibrils. In the exchanged samples, exchange solution and solution with Tn complex were added on the pellet reaching the final volume of 500 µm. Protein concentration was around 0.5 mg/ml. Samples were resuspended and stored overnight at 4°C on ice.

After incubation, samples were centrifuged to remove exchange solution and the proteins, then the supernatant was removed. Rigor with high EGTA was used to rinse the pellet and to remove Ca^{2+} in excess from exchange solution. Last centrifugation was done to replace the high calcium with the low calcium rigor solution, commonly used for myofibrils preparation and storage.

1.16 Solutions for the exchange protocol

Myofibrils were isolated according to the protocol previously described in rigor solution with protease inhibitors. The solution that allowed the replacement of exogenous Tn complex was an exchange solution, that corresponded to a rigor solution modified, in particular characterized by high level of $CaCl_2$. Therefor after the incubation the sample was rinsed with a specific rigor solution with high EGTA concentration to cage Ca^{2+} contaminant. Solutions were added with a cocktail of protease inhibitors (NaN3 (500 µM), pepstatin (5 µM), PMSF (200 µM), DTE (0.5 mM) and E64 + leupeptin (10 µM).

Imidazolo	**10 mM**
NaCl	**170 mM**
$MgCl_2$	**5 mM**
EGTA	**2.5 mM**
$CaCl_2$	**100 mM**

Table 3. Exchange solution (pH 6.9). Solution used to performed recombinant Tn complex replacement

Tris	**50 mM**
KCl	**100 mM**
$MgCl_2$	**2 mM**
EGTA	**10 mM**

Table 4. High EGTA rigor (pH 7). Solution used to rinse myofibrils after overnight Tn complex replacement

1.17 1D SDS-polyacrylamide gel electrophoresis

SDS-polyacrylamide gel electrophoresis was used to assess the extent of the exchange in all suspensions of myofibrils.

Each sample was washed to remove excess of exogenous protein and then placed in Laemmli sample buffer (Laemmli, 1970). Endogenous proteins were then denatured by heat in a Laemmli buffer containing sodium dodecyl sulfate (SDS) and a thiol reducing agent (2-βmercaptoethanol; β-ME). The resultant polypeptides take on a uniform charge-to-mass ratio proportional to their molecular weight. The protein content from myofibrils suspension was analyzed by sodium dodecyl sulfate-polyacrylamide gel electrophoresis (SDS-PAGE).

A 12 % SDS-PAGE (acrylamide to bis-acrylamide ratio 200:1; pH 9.3) (Giulian et al. 1983) was used to evaluate the exchange of cTn. The stacking gel contained 3.5% total acrylamide (acrylamide to bis-acrylamide ratio 20:1; pH 6.8).

The Mini-PROTEAN 3 system (Bio-Rad) and a home-made cell electrode device were used to run hand cast gels. Gels were run for 4 hours at 20° C and subsequently stained with Coomassie Brilliant Blue R-250 to reveal the resolved protein bands. To determine the amount and the relative distribution of the various isoform of TnT, Coomassie stained gels were scanned with a densitometer.

1.18 ATPase experiments

Complementary experiments on the same samples used for mechanical measurements on myofibrils were done on skinned tissue in Jolanda van der Velden group in Amsterdam using a technic for the measurement of ATPase activities (Glyn & Sleep; 1985). In these experiments, skinned trabeculae or strips were mounted in a set up designed to simultaneously measure Force development and ATPase rate, using a fluorimetric enzyme coupled assay (see below). This experimental approach, using different methods of analysis, potentially permit to associate mechanical disfunctions to energetic alterations, giving a broad overview of pathologies at the level of 'molecular device'.

1.19 Multicellular skinned preparations

Skinned trabeculae or thin skinned bundles of cardiac tissue from IVS or free wall LV were used for ATPase activities measurements. In order to obtain good estimations of ATP consumption, preparations should have small diameters and linear cellular, not easily observed in fibrotic HCM cardiac tissue. The preparations were left in a 1% Triron X 100 relaxing solution for 2 h to allow solubilization of all membranous structures.

The composition of standard relaxing solution used for these experiments was: (mM): Na_2ATP 7.3, $MgCl_2$ 10.6, EGTA 20, phosphocreatine (PCr) 10, Bes 100; pH=7.1, adjusted with KOH, ionic strength 200mM (adjusted with KCl).

1.20 Solutions

Tree different solution were used during the experimental protocol: relaxing, preactivating and activating solution. The sample was left for tree minutes in each, starting from the relaxing one. The preparation was then mounted between a motor and a force probe in relaxing solution containing high concentration of EGTA (5mM). The preactivating solution was used to prepare the skinned sample to the complete activation. In this solution EGTA concentration was reduced and in part replaced with HDTA, which is a milder calcium chelator than EGTA. Activating solution had a maximally activating Ca^{2+} concentration.

Na_2ATP	5.73mM
EGTA	5.00mM
MgCl	7.40mM
Kprop	86.50mM
BES	60.0mM
PEP	10.0mM
Na-azide	5.0mM

Table 5. Activating solution (ionic strength 200, pH 7.1, 20°C)

Na_2ATP	5.83mM
MgCl	7.33mM
Kprop	96.96mM
BES	60.0mM
EGTA	0.50mM
HDTA	4.50mM
PEP	10.0mM
Na-azide	5.0mM

Table 6. Preactivating solution (ionic strength 200, pH 7.1, 20°C)

Na_2ATP	5.83mM
MgCl	7.46mM
Kprop	92.72mM
BES	60.0mM
EGTA	5.0mM
PEP	10.0mM
Na-azide	5.0mM

Table 7. Relaxing solution (ionic strength 200, pH 7.1, 20°C)

1.21 Apparatus for ATPase measurement

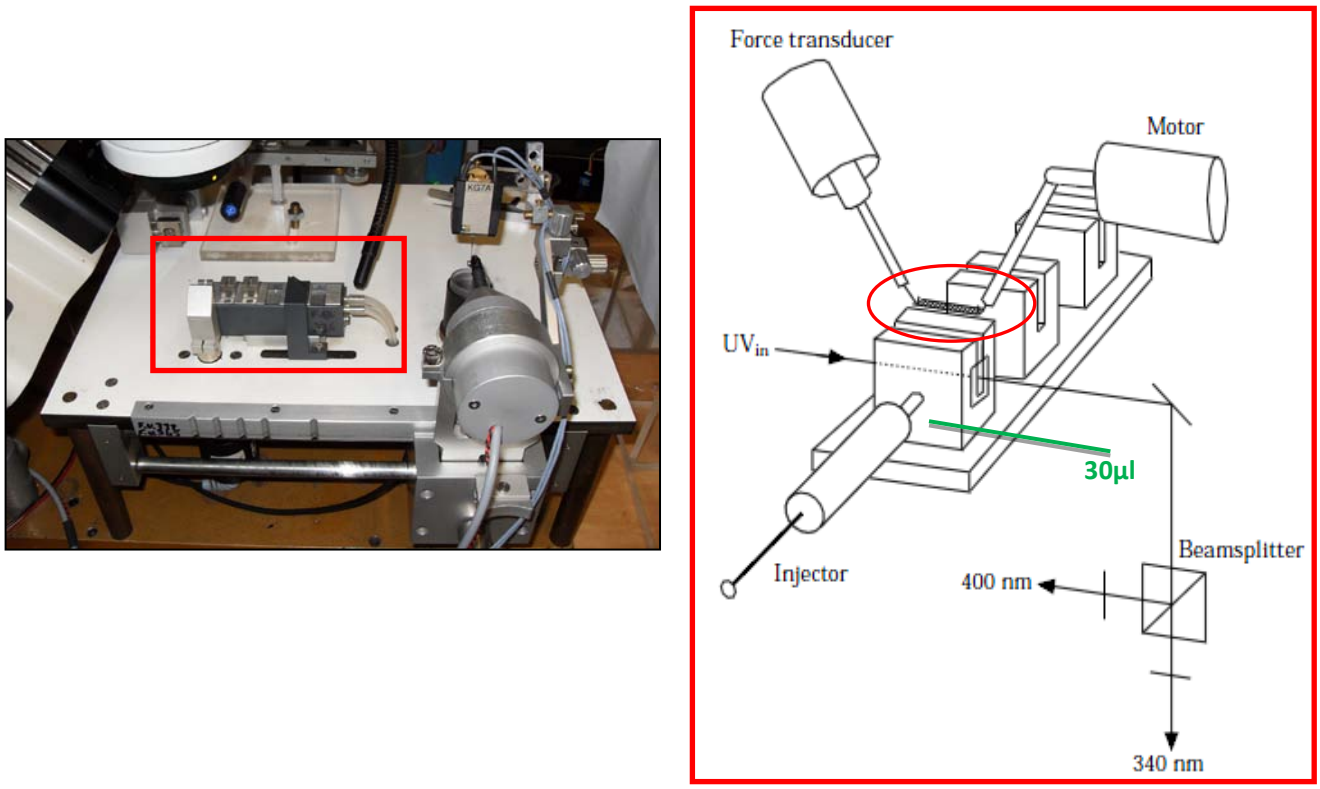

Figure 3. Picture of set-up for measurement of ATP-ase activity. Inset in red: chambers for pre-activation and activation of skinned preparation, mounted between a force transducer and a length control device.

The ATPase apparatus, firstly described by Glyn & Sleep (1985) and then by de Tombe & Stienen (1995) was composed by different functional parts. First, skinned trabeculae were placed in a bath container and then attached to a motor and a force probe. The motor permitted to apply rapid release-restretch steps to the skinned trabecula (20% muscle length; 5-20 ms), so to measure the apparent muscle stiffness and the rate of tension redevelopment (k_{TR}). The force probe allowed active tension generation recordings so that ATP consumption could be normalized for the tension generation relative to each samples. Preparation was mounted in relaxing solution with the support of a mobile stereomicroscope.

Near the UV-light emission spot (see Figure 3, red inset) three small baths were placed side by side, containing respectively relaxing, preactivating and activating solutions. The sample was left for tree minutes in each one starting to the relaxing one. The last bath, containing the activating solution, was used for the measurement of ATPase activities. This bath had a quartz end allowing transmission of near-UV light for the measurement of NADH absorbance and then of ATPase. The volume of this bath was 30 µl and was continuously stirred by motor-driven

vibration of a membrane positioned at the bottom of the bath. Sarcomere length of the preparation was measured in relaxing solution by means of a He-Ne laser. A separate pump was used to perform micro injections of an ADP solution 10mM to calibrate the signal immediately before the acquisition of signal.

1.22 Experimental Protocol and Calibration

The ATPase activity of skinned trabeculae were measured on-line by means of an enzyme-coupled assayas previously described (Glyn & Sleep, 1985; de Tombe & Stienen, 1995). Formation of ADP by the muscle was stoichiometrically coupled first to the synthesis of pyruvate and ATP from phosphoenolpyruvate, a reaction that is catalysed by the enzymepyruvate kinase, and subsequently to synthesis of lactate, a reaction that is catalysed by the enzyme lactate dehydrogenase and during which NADH is oxidized to NAD+. The breakdown of NADH was determined photometrically by measuring the absorbance of 340 nm near-UV light obtained from a 75W xenon lamp that was projected through the bath just beneath the preparation. The first time derivative of this signal, which is proportional to the rate of ATP consumption in the assay bath, was determined off-line by linear regression of the sampled data using custom-designed software. A small decline in the absorbance signal in the absence of the muscle fibre in the bath, caused by an ATPase contamination in the LDH enzyme preparation and by photo bleaching of NADH, was subtracted off-line from the absorbance data throughout the recording period. After each recording in the assay bath, the NADH absorbance signal was calibrated by multiple injections of 0.50 nmol ADP (0.050 µl of 10mM ADP solution) using a stepper motor controlled calibration pipette. Using this method, the standard error of the first time derivative of the NADH absorbance signal, determined during a period of 20 s, corresponded to about 0.1 pmol s-1. Since the isometric ATPase activity during contractions at saturating calcium concentrations typically amounted to 25 pmol s-1 (20∘C), this translates to a signal-to-noise ratio of about 250 under these conditions. During contractions at submaximal activation or at 15∘C, where the ATPase activity of the skinned trabecula was lower, a signal-to-noise ratio of at least 25 was achieved by appropriately increasing the time the preparation was activated so as to allow linear regression to be performed over a longer time period. Likewise, contractions that were performed at 25∘C were performed over a shorter time period. Ca^{2+}-activated ATPase activity was obtained by

subtracting the basal ATPase rate (measured in relaxing solution, pCa 9) from the rate measured in activating solution.

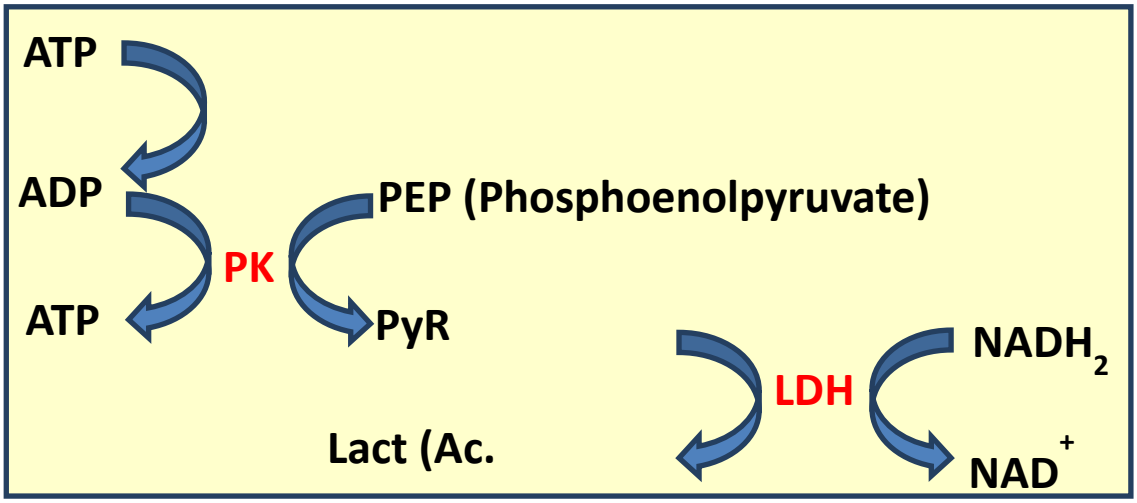

Figure 4. Scheme of enzyme-coupled assay

1.23 Statistical analysis

For each measured parameters, values were reported as means ± S.E.M. Differences between means were analyzed statistically with one−way or two-way ANOVA as appropriate. $P<0.05$ was considered significant.

Data from myofibrils and skinned muscles were expressed as mean±SEM. Statistical analysis, taking into account non-Gaussian distribution, inequality of variances and within-subject correlation, was performed as detailed in the Appendix. For categorical data, we used the Fisher exact test. For numerical variables, the P-values were calculated using linear-mixed models. $P<0.05$ was considered statistically significant.

Chapter 3: Results

3.1 Myofibrils mechanics: modification of the energetics of contraction in presence of homozygous K280N cTnT mutant in cardiac sarcomeres

3.1.1 Maximal active tension development in homozygous K280N cTnT mutant

Maximal active isometric tension of myofibrils isolated from IVS of K280N TnT mutant sample or from control samples (four healthy donor hearts and seven aortic stenosis patiens) was recorded and compared. Figure 1A shows representative traces of tension generation following maximal Ca^{2+} activation by fast solution switching tecnique, for both TnT mutant (upper trace) and control donor (lower trace) myofibrils. Average values of maximal isometric tension for TnT K280N myofibril and control groups are shown in Fig 1A and in Table 1. Values reported in donor or aortic stenosis samples represent pooled data from these experimental sets and previous studies from our group of secondary hypertrophy myofibrils and left ventricular samples of control (non-failing, non-hypertrophic) patients (Piroddi et al. 2007 and unpublished data). Control data from the age-matched donor heart were undistinguishable from the previously reported controls; as already reported (Piroddi et al.,2007). In spite of some variability, myofibril mechanical parameters did not differ significantly among myofibril populations taken from different control samples. Maximal tension in K280N TnT mutant myofibrils was significantly decreased compared with donors but was not significantly different from that of secondary hypertrophy samples.

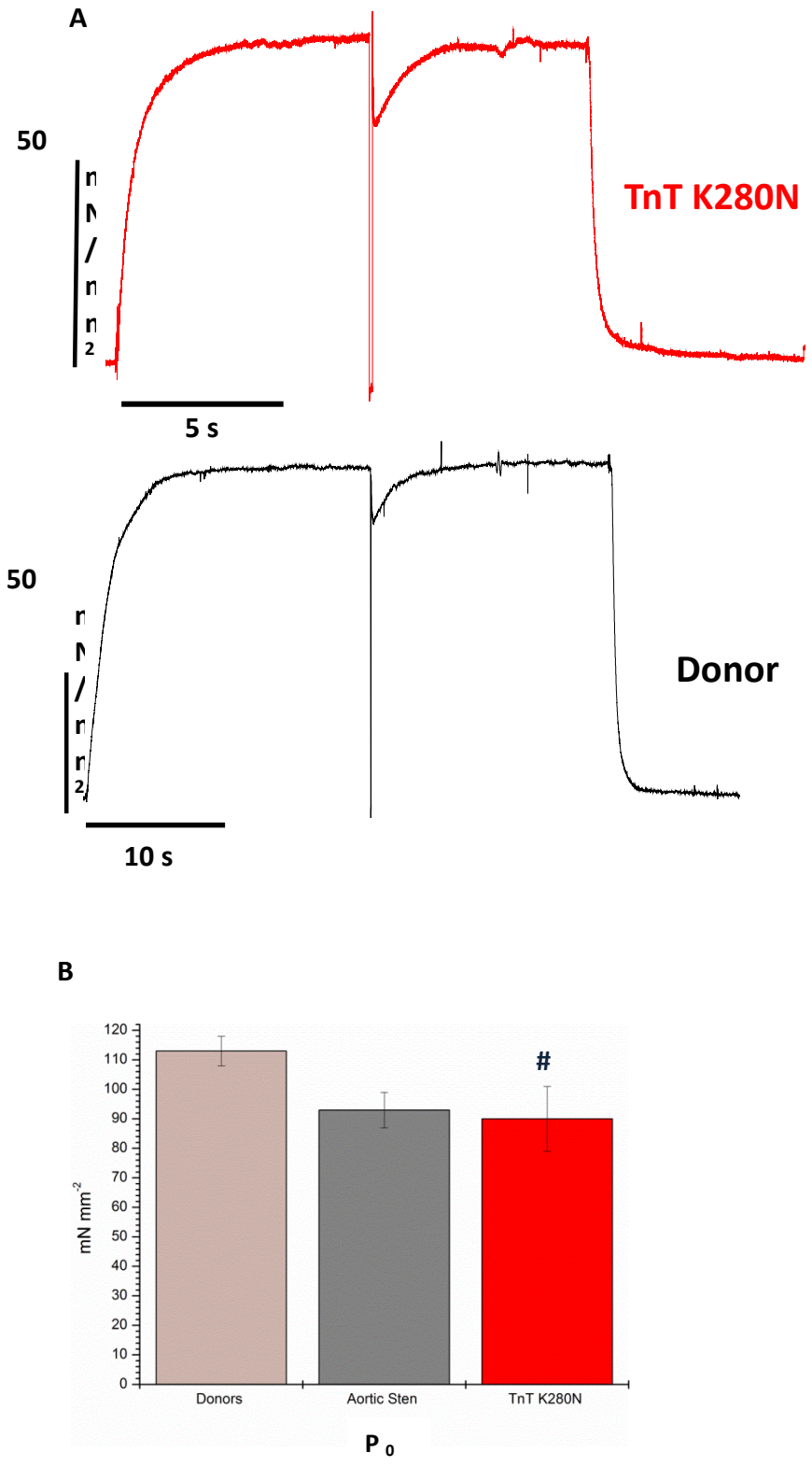

Figure 1. Isometric active tension in K280N TnT mut and control donor heart myofibrils. A, representative tension responses of K280N TnT mutant and donor myofibrils maximally activated and fully relaxed by fast solution switching technique. Temperatute 15°C. B, mean values of maximal active tension (P_0, expressed in mN mm^{-2}) for donors (dusty pink), aortic stenosis (gray) and K280N TnT mutant (red). P_0 for the Donors 113±5, for Aortic Sten 93±6 and 90±11 for TnT mutant. P_0 was significantly reduced for TnT mutant compared to Donors (#P < 0.05). Bars above columns are S.E.M.

3.1.2 Kinetics of force generation in homozygous cTnT mutant

The kinetics of tension developement following rapid maximal calcium activation by fast solution switching (k_{ACT}, s^{-1}), as well as tension redevelopment following a release-restretch protocol (k_{TR}, s^{-1}), were measured in K280N TnT mutant and control myofibrils. As shown in Figure 2 and Table 2, both k_{ACT} and k_{TR} were markedly faster in mutant myofibrils compared to both control groups, indicative of faster cross-bridge tournover rate. In all myofibril populations the time course of Ca^{2+}-activated tension developement was monoexponential. The rate constants k_{ACT} and k_{TR} were the same in both control groups as well as in TnT K280N myofibrils, with a tendence in this last case of k_{TR} to be slower than k_{ACT} but remaining always significantly increased compared to both control group values. (Table 2)

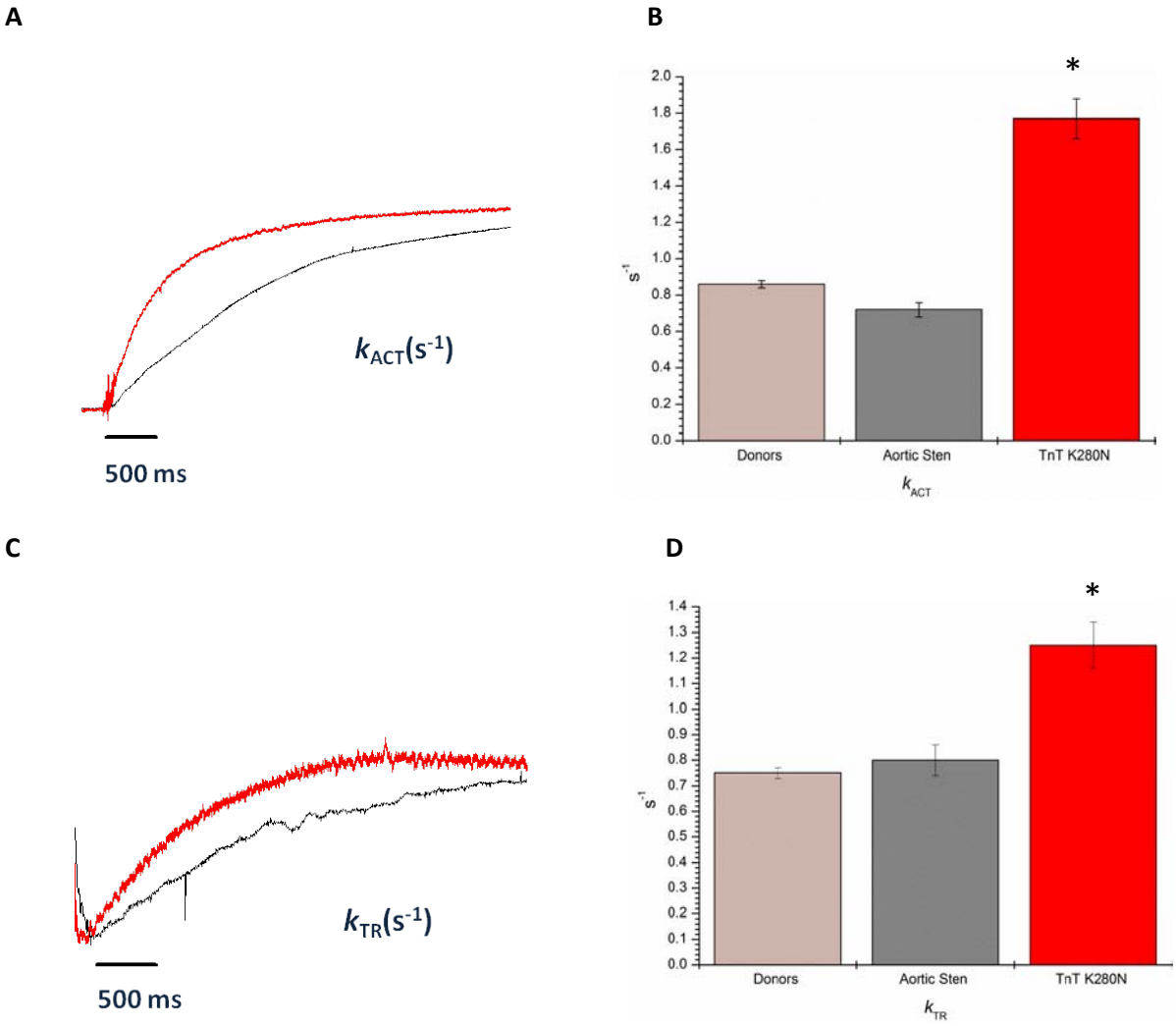

Figure 2. Kinetics of force generation in homozigous K280N TnT mutant and control groups**.** A,the time course of tension activation following sudden Ca^{2+} increase of K280N TnT myofibril and donors myofibril after normalization for maximal tension. Trace in red K280N TnT mutant, in black donors. B, mean values of k_{ACT} (s^{-1}) for K280N TnT myofibrils, donors and aortic senosis. k_{ACT} was significantly increased in TnT mutant compared to both control groups (*P < 0.01). C, time course of tension redevelopement following a quick mechanical perturbation (Brenner maneuver , Brenner, 1988) of K280N TnT myofibril and donors myofibril after normalization for maximal tension. In red K280N TnT mutant, in black donors. D, mean values of k_{TR} (s^{-1}) for K280N TnT myofibrils, donors and aortic senosis. k_{TR} was significantly increased in TnT mutant compared to both control groups (*P < 0.01).

MYOFIBRIL SAMPLES	ACTIVE TENSION GENERATION		
	P_0 (mN mm^{-2})	k_{ACT} (s^{-1})	k_{TR} (s^{-1})
Donors (4 pts)	113 ± 5 (104)	0.86 ± 0.02 (107)	0.75 ± 0.02 (86)
Aortic Sten (7 pts)	93 ± 6 (58)	0.72 ± 0.04 (64)	0.80 ± 0.06 (61)
Tnt K280N (1 pts)	90 ± 11 (39)	1.77 ± 0.11 (38)*	1.25 ± 0.09 (33)*

Table 1. Active tension generation parameters: means (± S.E.M.) of P_0, k_{ACT}, k_{TR} in K280N TnT, donors and aortic stenosis myofibrils. * P< 0.01 K280N TnT mut *versus* donors and aortic sten. (estimated by Student t test; number of myofibrils in parenthesis). Experimental conditions: 15°C, pCa relaxing and activating solutions, 9.0 and 4.5 respectively; [MgATP] 5 mM; [P_i] < 5µM.

3.1.3 Tension relaxation parameters in K280N cTnT mut

Tension relaxation parameters in K280N TnT mutant and in control donors and aortic stenosis control myofibril groups are shown on a faster time scale in Fig. 3.a. As previously described in Chapther 2, the time course of force relaxation in human cardiac myofibrils was biphasic (Piroddi et al. 2007), starting with a slow, linear force decay, described by two different parameters, duration of slow phase (ms) and its rate slow k_{REL} (s^{-1}). The second phase is a fast, exponential relaxation phase, fast k_{REL} (s^{-1}), that followed the slow phase after a 'shoulder'. As shown in Fig. 3.B and table 2, the slow phase of of relaxation was markedly accelerated in K280N TnT myofibrils compared to both control groups: slow k_{REL} was about two time faster than in both controls groups, indicative of a faser crossbridge detachment under isometric conditions (Tesi et al., 2002). The trend was the same for fast k_{REL} which was significantly increased in TnT mutant compared with aortic stenosis patients myofibrils, but not significantly different in donor patients (See Table 2). Regarding the duration of the slow phase of relaxation, this was rather variable: in K280N TnT myofibrils it was significantly increased compared to donors but similar to values found in aortic stenosis myofibrils (See Table 2).

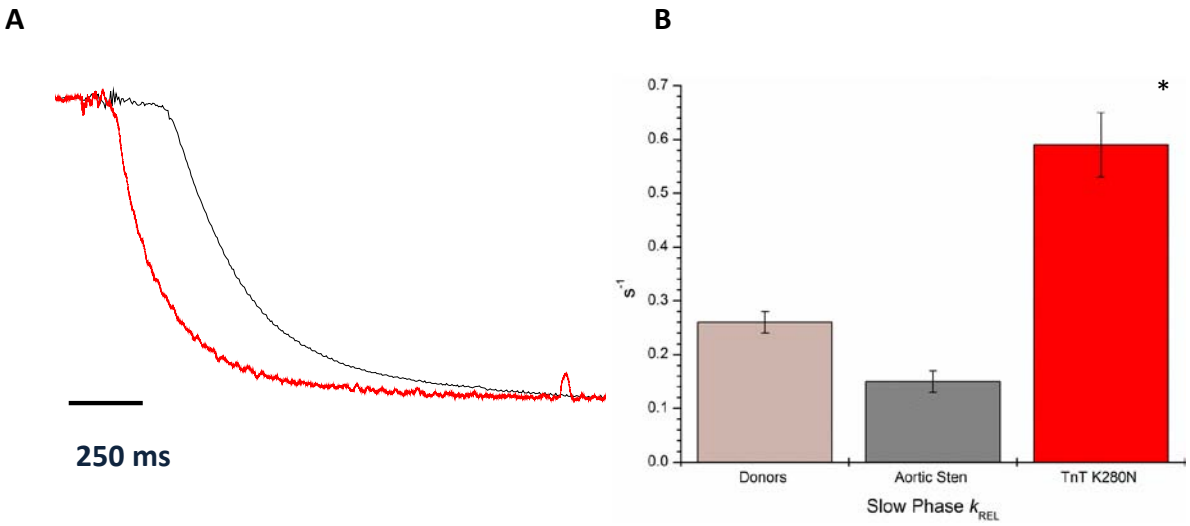

Figure 3. Tension relaxation kinetics following sudden Ca^{2+} removal. A, TnT mutant (red) and Donor(black) traces superimposed on a faster time base after normalization for maximal tension. The rate constant of the early slow force decline (slow k_{REL}) is estimated from the slope of the regression line fitted to the tension trace normalized to the entire amplitude of the tension relaxation transient. The rate constant for the fast phase of tension decline (fast k_{REL}) is estimated from mono-exponential fit. B, mean values (s^{-1})of slow k_{REL} for the donors (0.26±0.02), aortic stenosis (0.15±0.02), and TnT k280N (0.59±0.06) myofibrils. Bars above columns are S.E.M., *P<0.001.

MYOFIBRIL SAMPLES	TENSION RELAXATION	
	Slow Phase	Fast Phase
	Duration (ms)	k_{REL} (s^{-1})	k_{REL} (s^{-1})
Donors (4 pts)	194 ± 7 (66)	0.26 ± 0.02 (62)	3.70 ± 0.16 (66)
Aortic Sten (7 pts)	258 ± 15 (37)	0.15 ± 0.02 (37)	2.75 ± 0.20 (37)
Tnt K280N (1 pts)	248 ± 20 (14)	0.59 ± 0.06 (14)*	3.44 ± 0.28 (14)

Table 2. Tension relaxation parameters: means (± S.E.M.) of relaxation in K280N TnT, donors and aortic stenosis myofibrils. * P< 0.01 K280N TnT mut *versus* donors and aortic sten. (estimated by Student t test; number of myofibrils in parenthesis). Experimental conditions: 15°C, pCa relaxing and activating solutions, 9.0 and 4.5 respectively; [MgATP] 5 mM; [P_i] < 5µM.

3.1.4 Recombinant WT Tn complex exchange

To test whether the observed changes could be directly related to the TnT mutation, Tn-exchange experiments were performed as previously described in Chapter 2 and WT cTn was replaced into K280N myofibrils. Human WT recombinant cardiac troponin complex (gift from University of Illinois, P. de Tombe laboratory) had a Myc tag that on TnT(Myc-TnT) that allowed exogenous TnT to be distinguished from the endogenous protein on SDS gels and the extent of Tn replacementto be estimated.

3.1.5 Human WT cTn replacement into K280N myofibrils

Human WT cTn complex exchange experiments were performed to test whether alterations of sarcomeric function in K280N myofibrils could be rescued by replacing the human cardiac mutant protein with recombinant WT protein.

3.1.6 Human WT cTn replacement into DONOR myofibrils

The same human cTn WT complex was replaced into donor myofibrils to check for potential alterations occurring with protein replacement method. Previous experiments demostrated that the replacement tecnique of troponin complex did not alter kinetic properties, also if maximal active tension was slightly reduced, as well as resting tension tendentially increased. Donor myofibrils used for these replacement experiments were obtained from one of donor samples used in experiments described above.

MYOFIBRIL SAMPLES	ACTIVE TENSION GENERATION		
	P_0 (mN mm^{-2})	k_{ACT} (s^{-1})	k_{TR} (s^{-1})
Donor	125 ± 5 (104)	0.86 ± 0.04 (22)	0.66 ± 0.04 (20)
Donor WT TnExch	116 ± 11 (34)	0.87 ± 0.03 (34)	0.69 ± 0.03 (25)
TnT K280N	82 ± 7 (12)	1.69 ± 0.08 (12)	1.07 ± 0.13 (9)
TnT K280N WT TnExch	81 ± 6 (14)	1.02 ± 0.10 (16)	0.82 ± 0.06 (16)

Table 3. Active tension generation parameters: means (± S.E.M.) of P_0, k_{ACT}, k_{TR} Donor, Donor WT TnExch (Donor after replacement with WT troponin complex), K280N TnT, and K280N WT TnExch (K280N mutant after replacement with WT troponin complex. Experimental conditions: 15°C, pCa relaxing and activating solutions, 9.0 and 4.5 respectively; [MgATP] 5 mM; [P_i] < 5µM.

MYOFIBRIL SAMPLES	TENSION RELAXATION		
	Slow Phase		Fast Phase
	Duration (ms)	k_{REL} (s^{-1})	k_{REL} (s^{-1})
Donor	126 ± 12 (7)	0.34 ± 0.11 (5)	4.43 ± 0.24 (7)
Donor WT TnExch	130 ± 14 (14)	0.35 ± 0.04 (14)	4.01 ± 0.22 (37)
TnT K280N	224 ± 20 (5)	0.65 ± 0.06 (5)	3.86 ± 0.28 (5)
TnT k280N WT TnTExch	289 ± 29 (7)	0.39 ± 0.08 (7)	2.91 ± 0.24 (7)

Table 4. Tension relaxation parameters: means (± S.E.M.) of relaxation in Donor, Donor WT TnExch (Donor after replacement with WT troponin complex), K280N TnT, and K280N WT TnExch (K280N mutant after replacement with WT troponin complex). Experimental conditions: 15°C, pCa relaxing and activating solutions, 9.0 and 4.5 respectively; [MgATP] 5 mM; [P_i] < 5µM.

3.1.7 15% SDS-PAGE gel of suspensions of human cardiac myofibrils undergone Tn replacement

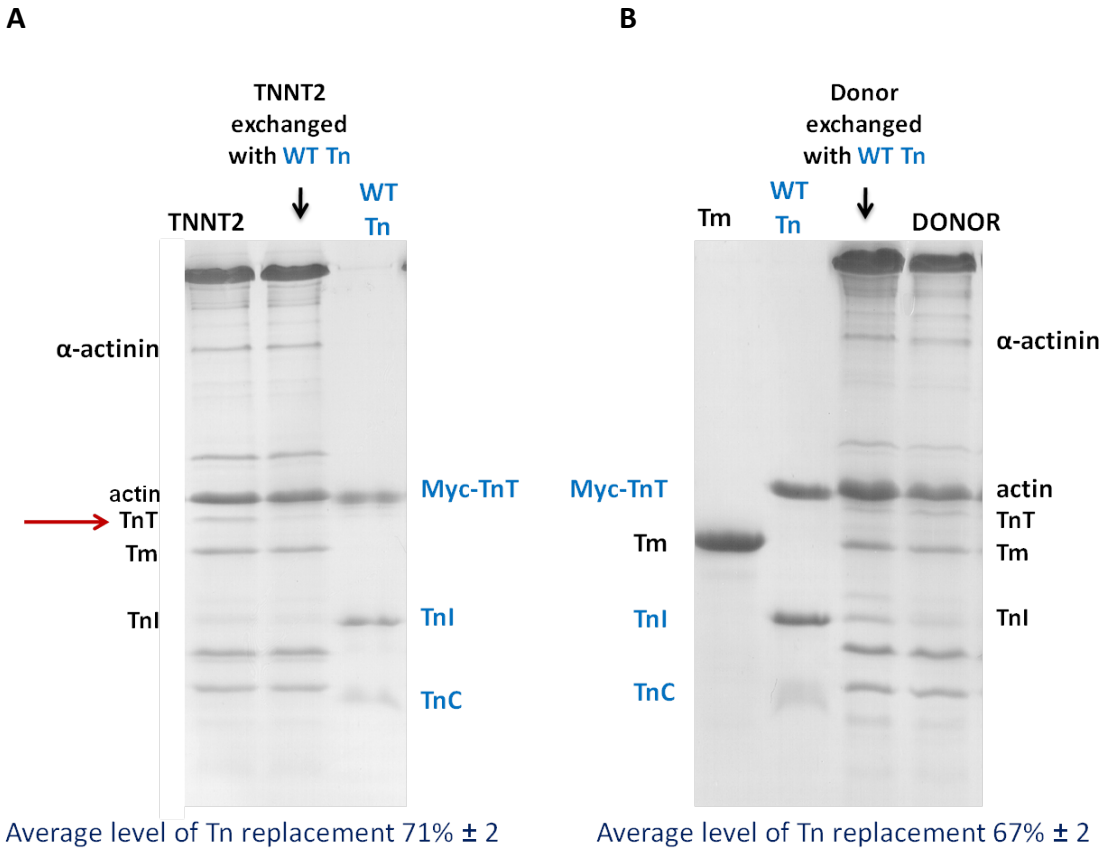

Figure 4. SDS-PAGE gels from hWT cTn replacement into K280N myofibrils (A) and hWT cTn replacement into DONOR myofibrils (B). Average level of Tn replacement in mutant myofirils was 71% ± 2 and in donor myofibrils was 67% ± 2. The extent of Tn replacement was determined by the intensity ratio endogenousTnT/α-actinin in each lane. Mean was ± s.e.m, $n_{of\ gels} = 3$

3.1.8 Tension generation and kinetic properties of force generation after hWT cTn complex replacement

Maximal active tension of control and treated myofibrils of both groups (K280N and donor groups) were not significantly different (see Table 3 and Table 4). Kinetics of force generation in K280N myofibrils are slowed down following Tn-exchange with the WT protein. As shown in Figure 5A, 5B and Table 3, both k_{ACT} and k_{TR} of K280N myofibrils become close to control myofibrils, which were unaffected by Tn replacement.

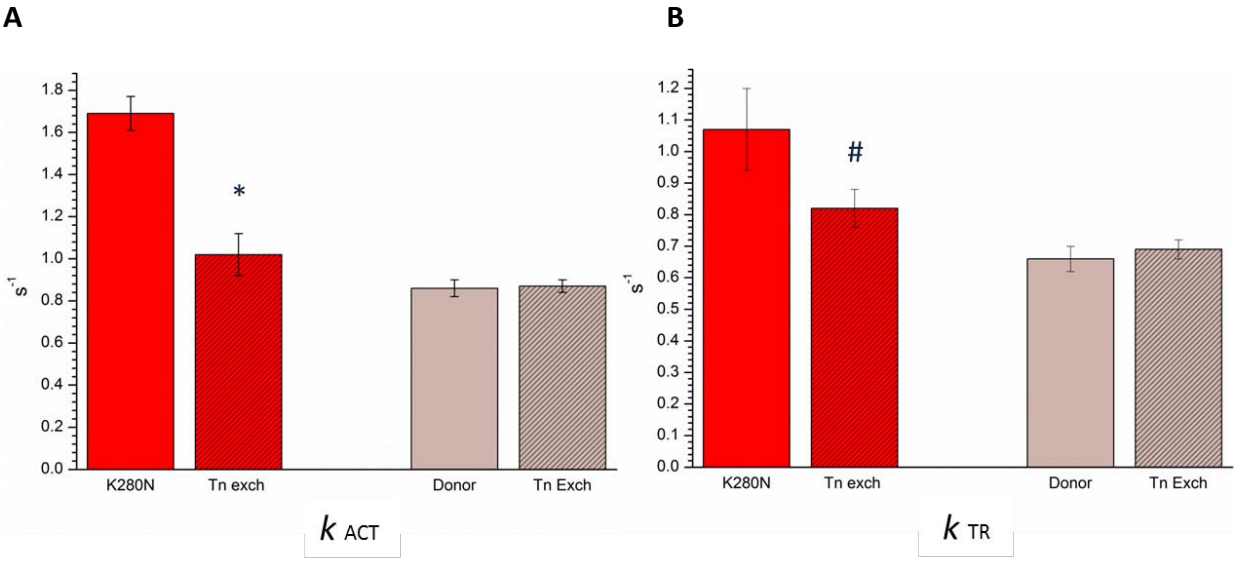

Figure 5. Kinetic properties of force generation after WT Tn complex replacement in mutant and donor myofibrils. A, the rate constant of tension generation (k_{ACT}, s^{-1}) following fast Ca^{2+} activation was significantly reduced in exchanged K280N myofibrils (1.02±0.10) compared to control K280N mutant myofibrils (1.69±0.08), (*P<0.001), restoring values close to those of donor myofibrils. k_{ACT} in donor myofibrils resulted unaffected by Tn replacement (0.86±0.04 vs 0.87±0.03 after exchange; values in s^{-1}). B, same behavior was observed for k_{TR}. In exchanged K280N myofibrils k_{TR} was significantly reduced (0.82±0.06) compared to control K280N mutant myofibrils (1.07±0.13), ($^{\#}$P<0.05). Donor myofibrils values: 0.66±0.04 and 0.69±0.03 (control and treated myofibrils, data in s^{-1}).

3.1.9 Tension relaxation parameters after hWT cTn complex replacement

All relaxation parameters (slow phase duration, slow k_{REL}, fast k_{REL}) are slowed down in K280N myofibrils following hWT cTn complex exchange whereas in donor myofibrils relaxation kinetics remained the same after Tn exchange experiment (See Fig. 6 and Table 3). K280N exchanged myofibrils, slow k_{REL} was reduced and became close to that of control myofibrils (unaffected by Tn replacement).

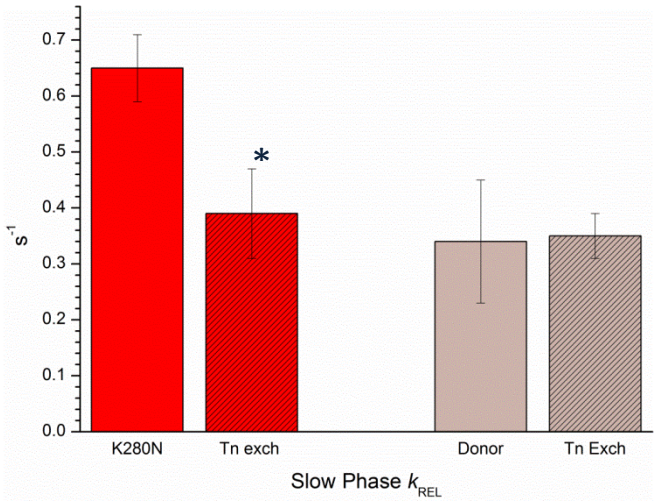

Figure 6. Slow k_{REL} was affected after WT Tn complex replacement in mutant but not in donor myofibrils. Mean values of slowk_{REL} for K280N mutant (red and red..) and for donor (gray and gray..) myofibrils before and after WT Tn complex replacement. Exchanged K280N myofibrils restored slow k_{REL} values close to that of donor, resulting in a significantly reduction of this relaxation kinetic parameter: K280N mutant 0.65±0.06, K280N exchanged 0.39±0.08, donor 0.34±0.11, donor exchanged 0.35±0.04. Bars above columns are S.E.M., *P< 0.001; number of myofibrils is given in Table 3.

3.1.10 Calcium sensitivity of force

The calcium sensitivity of force generation was also measured on TnTK280N, donor and secondary hypertrophy preparations to analyse the response of force to submaximal activation levels, that tipically caracterize muscle *in vivo*. To determine the calcium sensitivity of force, myofibrils from each sample were exposed to incremental calcium concentrations and the force response was recorded. As shown in Figure 9, the Force-pCa curve of TnTK280N myofibrils, as well as, of secondary hypertrophy, tended to be shifted leftward,so that pCa_{50} was higher in TnT mut compared to donor myofibrils (PCa50 6.03 ± 0.08 TnT mut, 6.03 ± 0.03 SAO, 5.8 ± 0.03 in donors). This indicated that the calcium sensitivity of force tended to be increased in hypertrophyc samples compared to those from donor patients. The cooperativity of activation (n_H) of TnT mutant was decreased compared to both donors and aortic stenosis groups, which were similar. nH values were: 1.37 ± 0.11 for TnT mut, 2.74 ± 0.61 for SAO, 2.30 ± 0.21 for donors. This is an indication of a lower cooperativity of activation in presence of TnT K280N mutant

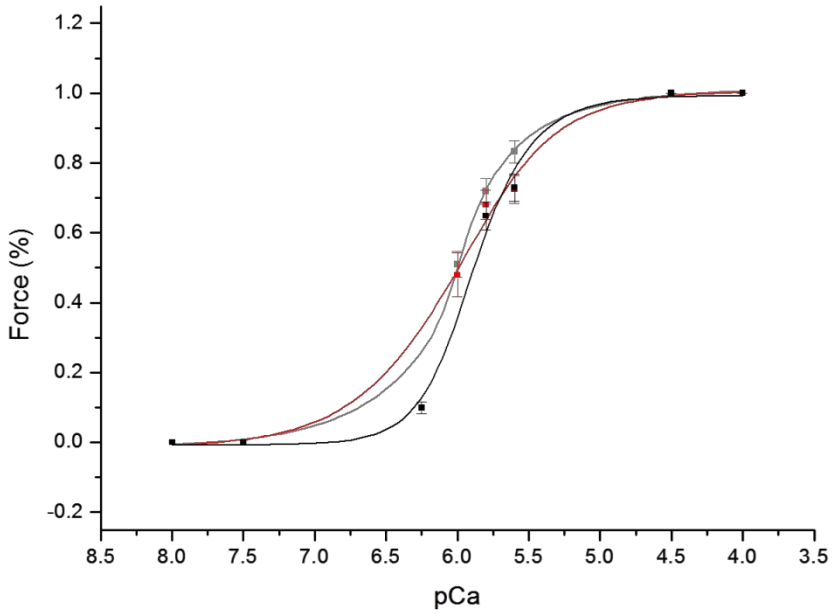

Figure 9. Calcium sensitivity of force. Mean values for K280N TnT mutant (red), aortic stenosis (grey) and donor myofibrils (black).

3.1.11 Isometric tension and ATP consumption in skinned trabecolae

Measurements of ATPase activity were performed in Jolanda van der Velden research unit (VU Medical Center, Amsterdam, NL), on the same K280N TnT homozygous sample used in our laboratory. As controls, we used two samples from patients affected by aortic stenosis and 5 samples from sarcomeric mutation negative familial hypertrophyc cardiomiopathy patients FHC_{smn} (See Methods). As previously described (See Methods), all the experiments were performed on skinned strips of tissue. Tension cost was determined by the simultaneous direct measurements of isometric force (kN m^{-2}) during contraction and ATPase from NADH breakdown with NADH levels enzymatically coupled to ATP utilization (see Methods). The slope of the [NADH] vs. time curve was normalized by the fiber volume to obtain ATP consumption rates (µmol l-1 s-1). These values could be compared in differently sized muscle preparations. By normalizing ATP consumption rates to the tension generated and fiber volume, the tension cost could be determined.

3.1.12 Direct measurements

Isometric tension in K280N TnT mutant was markedly reduced compared to FHC_{smn} control group ($P<0.001$). Force in TnT mutant skinned trabeculae was signignificantly different ($P<0.05$) also compared to aortic stenosis preparations (Fig.7A). This reproduced the same trend observed in isometric active tension measured in myofibrils were P_0 was significantly reduced vs Donor but not vs aortic stenosis (for myofibrils data see Results 3.1.1, Table1). A parallel behavior was reproduced in ATP consumption measurements (Fig 7B). ATP consumption was significantly reduced in cardiac TnT mutant compared both control groups ($P<0.05$).

Skinned trabeculae	Force	ATP consumption	Tension cost
TNNT2 IVS(mut)	9.075 ± 1.026	23.266 ± 3.402	2.859 ± 0.499
FHC smn	25.65 ± 1.803	40.683 ± 3.017	1.636 ± 0.105
LVH ao	18.107 ± 1.896	31.474 ± 4.012	1.737 ± 0.091

Table 5. Force (expressed in kN m^{-2}), ATP consumption (in µmol/Ls) and tension cost (µmol L^{-1} s^{-1}/ kN m^{-2}) data from skinned trabeculae of inter ventricular septum of K280N TnT mutant (TNNT2 IVS(mut)), hypertrophyc cardiomyopathy of sarcomeric mutant negative (FHC smn) and aortic stenosis (LVH ao) patients.

3.1.13 Tension cost

As previously described, tension cost was evaluated normalizing ATP consumption rates to tension generated and fiber volume. ATP consumption was markedly increased in K280NTnT mutant compared to FHC_{smn} and aortic stenosis skinned trabeculae ($P<0.05$; see Fig. 8).

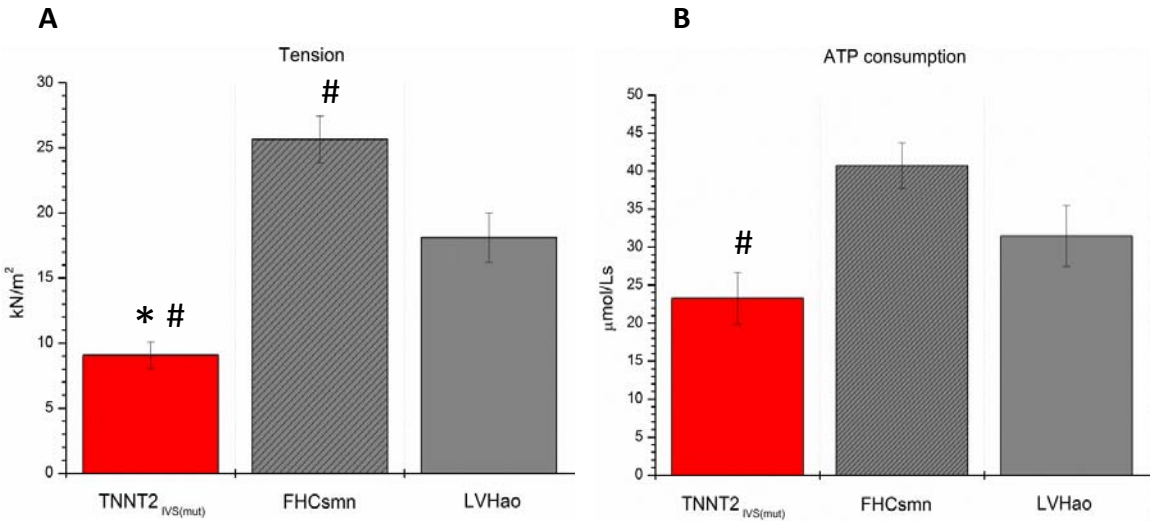

Figure 7. Isometric tension and ATP consumption rate in K280N mutant, FHC_{smn} and aortic stenosis controls. Mean values for tension and ATP consumption of K280N TnT mutant, FHC_{smn} and aortic stenosis of skinned muscle preparations. Bars above columns are S.E.M., *P< 0.001; # P<0.05. A, K280N preparation isometric force was significantly reduced compared to FHC_{smn} and aortic stenosis groups (*P<0.001 vs FHC_{smn}; #P<0.05vs LVHas). B, ATP consumption rate in K280N TnT mutant was significantly reduced compared to FHC_{smn} but not compared to aortic stenosis (#P<0.05vs FHC_{smn}).

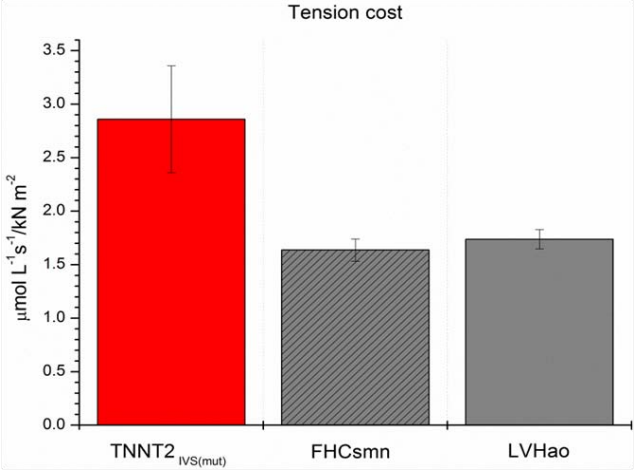

Figure 8. Tension cost of tension generation. Mean values for tension cost in K280N TnT mutant, FHC_{smn} and aortic stenosis of skinned muscle preparations. Tension cost in K280N TnT mutant was significantly increased compared both control groups (*P<0.001?? anche #??).

3.2 Deleting exon 55 from the nebulin gene induces severe muscle weakness in a mouse model for nemaline myopathy

This study was done on a new transgenic mouse model of nebuline exon 55 delection developed in Henk Granzier laboratory, (Tucson, University of ArizonaSimoulaneously with our laboratory, an accurate analysis of the mechanical and biophysical properties of the model was done on skinned muscle fiber (Tucson) and on myofibril preparations (Florence). This study involved also the molecular investigations and the caracterization of the phenotipe stability of the model.

3.2.1 Mice in which *neb* exon 55 is deleted display a phenotype that resembles NM

Using homologous recombination, exon 55 was removed from the nebulin gene. Mice heterozygous for the targeted allele (HET) were viable and fertile and survived into adulthood. Homozygous offspring (*Neb*ΔExon55 KO) were produced at expected Mendelian genetic ratios (~1/4 of total number of pups using heterozygous breedings), with a weight at birth that was not different from that of HET and WT littermates. However, *Neb*ΔExon55 KO mice showed severe growth retardation after birth (Fig. 10A) and typically did not survive past the first week (Fig. 10B).

A B

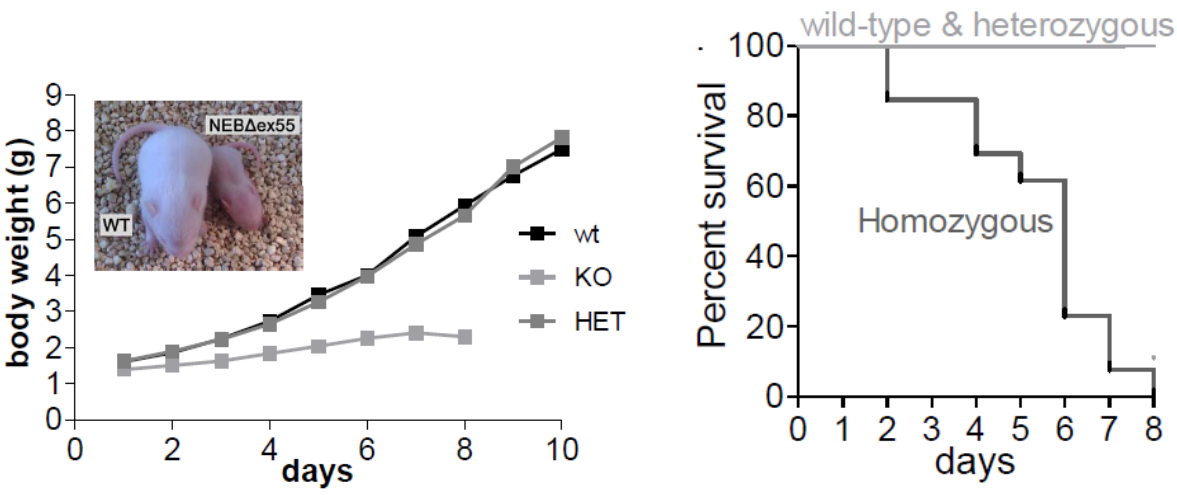

Figure 10. A, body weight of *Neb*ΔExon55 KO mice at birth was not different from that of HET and WT littermates. *Neb*ΔExon55 KO mice show severe growth retardation after birth, and (B) typically did not survive past the first week (survival curve based on 57 pups). Inset: photograph of a *Neb*ΔExon55 KO (HOM) and a WT littermate mouse illustrating the growth retardation in KO mice.

Nemaline myopathy in humans is characterized by the presence of nemaline bodies (often called nemaline rods when they were rod-shaped), which is often accompanied by myofiber hypotrophy. To test whether these histological characteristics of NM were present in *Neb*ΔExon55 KO mice, first sections of quadriceps muscle were evaluate stained with hematoxylin and eosin (H&E) or Gomori trichrome. As shown in Figure 11 A (upper panel), the H&E stained sections from WT and *Neb*ΔExon55 KO mice revealed smaller muscle fibers in *Neb*ΔExon55KO mice. Quantitative analysis revealed that where average fiber minFeret diameter was 13.0±0.4 µm in WT mice, this was significantly reduced to 10.1±0.3 µm in *Neb*ΔExon55 KO mice ($p<0.01$). Discrete populations of large and small fibers were not observed in *Neb*ΔExon55 KO mouse muscle. The number of central nuclei was <1% in both WT and *Neb*ΔExon55 KO muscle, and *Neb*ΔExon55 KO muscle showed no signs of fibrosis. Nemaline bodies were not visible at the light microscopic level on Gomori trichrome stain (Figure 11 A, lower panel) of quadriceps muscle, but electron microscopy revealed electron-dense nemaline bodies at the location of the Z-band (arrows, Fig. 11 B) in the *tibialis cranialis* (TC) muscles of *Neb*ΔExon55 KO mice. These nemaline bodies displayed electron density equivalent to normal z-bands, which differentiated them from the Z-band streaming that coud be found in a variety of muscle disorders. Nemaline bodies were not seen in WT mouse muscle. Thus, *Neb*ΔExon55 KO mice displayed a histological phenotype that resembles NM, including the presence of nemaline bodies and hypotrophic fibers.

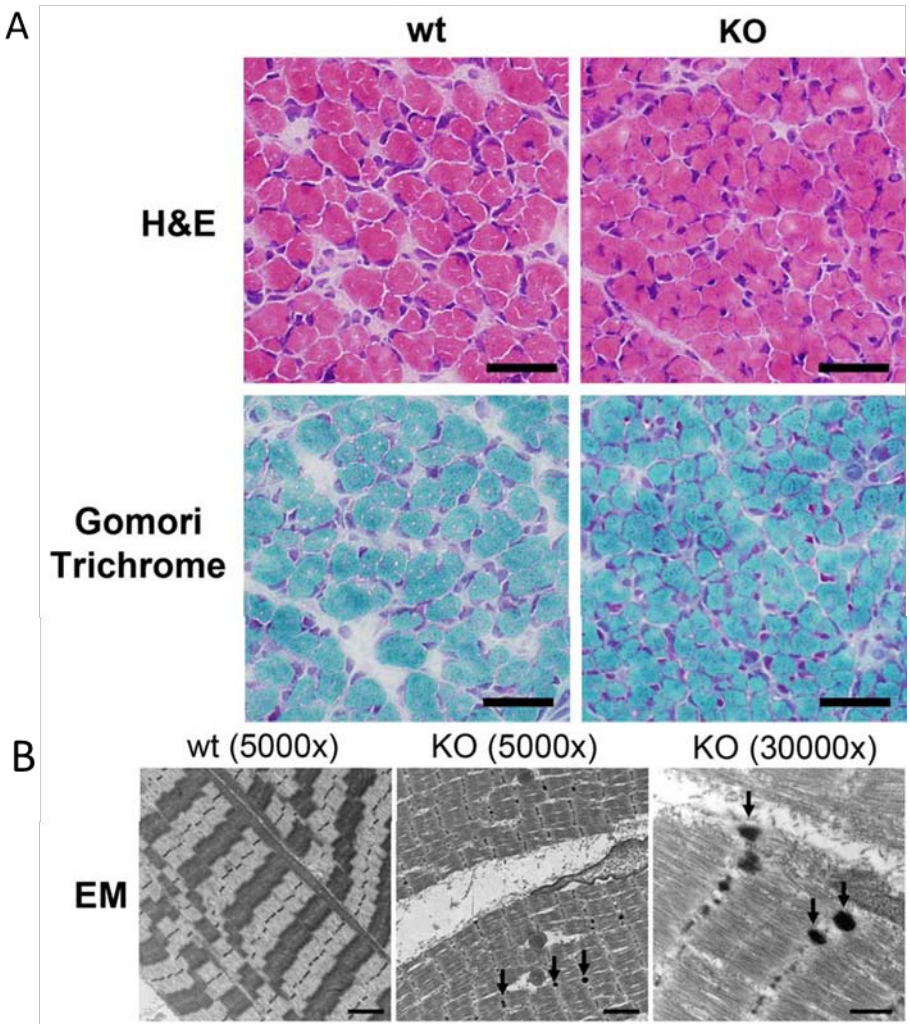

Figure 11. Histological findings in 6d old WT and NebΔExon55 KO mice. A, Hematoxylin and Eosin (H&E) stained sections of quadriceps muscle from wild type (wt) and NebΔExon55 KO (KO) mice revealed smaller muscle fibers in NebΔExon55 KO mice. Nemaline rods were not visible at the light microscopic level on Gomori trichrome stain, but electron-dense nemaline bodies (arrows) were seen on electron microscopy (EM) in the Tibialis Cranialis (TC) muscle from all NebΔExon55 KO mice. Nemaline bodies were not seen in WT mouse muscle (B). Bar = 40 µm for H&E and Gomori trichrome pictures, 2 µm for 5000x EM pictures, and 500 nm for the 30000x EM picture.

3.2.2 Deletion of exon 55 results in severely reduced nebulin protein levels

NEB exon 55 encoded thirty-five amino acids and represented ~4 kDa at the protein level. As deletion of exon 55 maintained the reading frame 3' of exon 55, it was expected the *Neb*ΔExon55 KO mice to express a nebulin isoform that was ~4 kDa smaller than WT nebulin. However, SDS-agarose gel analysis showed that, in 6 day old *Neb*ΔExon55 KO mice, nebulin was nearly absent from all muscle types tested (Fig. 12 A). Western blot experiments using an antibody directed against nebulin's N-terminus confirmed these findings (Fig. 12 B, left panel) and revealed that nebulin levels in *Neb*ΔExon55 KO quadriceps muscle (normalized to myosin heavy chain) were reduced to less than 2% of WT values . To evaluate whether the low nebulin protein levels at day 6 after birth were preceded by a gradual decrease from normal levels at birth, also nebulin levels at day 1 after birth were evaluated (Fig. 12 C) and at embryonic day 19 (Fig. 12 D). These experiments showed that nebulin protein levels were severely reduced to near absence in *Neb*ΔExon55 KO muscle at both time points. Thus, deletion of exon 55 resulted in almost complete loss of nebulin protein. To evaluate whether the reduced nebulin protein levels were caused by alterations at the level of DNA transcription or of mRNA translation, a home-made nebulin exon microarray was used to study the expression of all 166 murine nebulin exons. In addition to the expected reduction of exon 55 mRNA, expression of nearly all nebulin exons was significantly reduced in *Neb*ΔExon55 KO muscle. Thus, these results suggest that the low nebulin protein levels in *Neb*ΔExon55 KO mice were not caused by defects in the translation of nebulin mRNA into protein but rather by changes in transcription of the mutant nebulin gene or in the stability of the mutant nebulin mRNA .

A

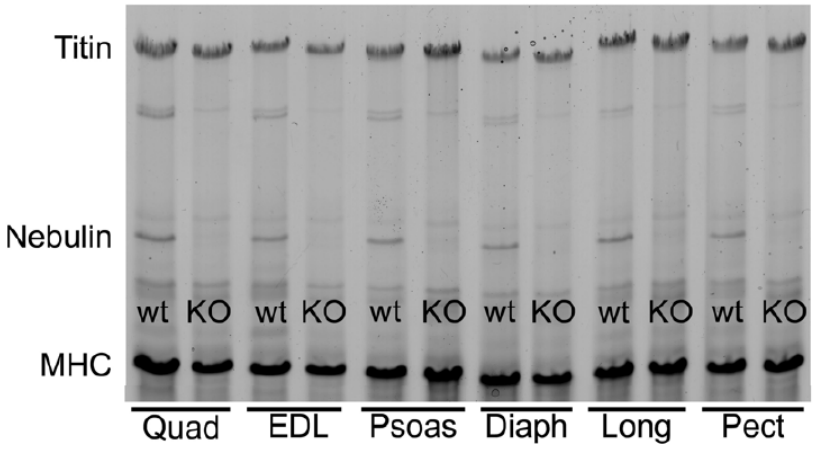

B

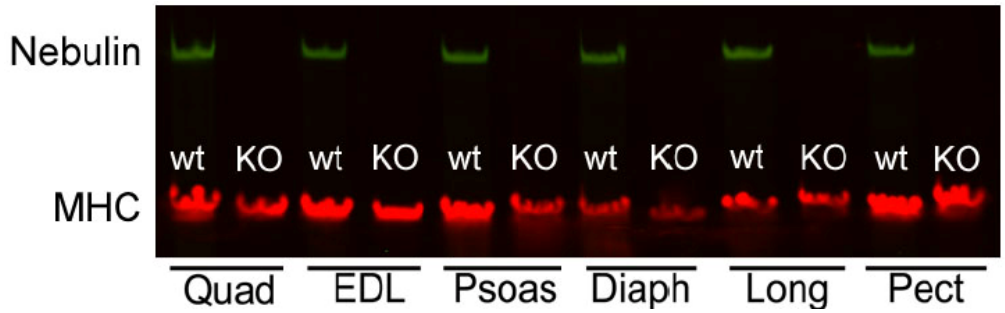

C

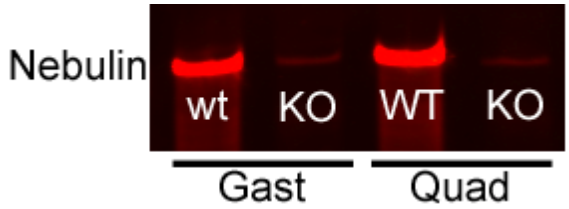

D

Figure 12. A) SDS-agarose gel electrophoresis revealed severely reduced nebulin protein levels in *Neb*ΔExon55 KO mice in all skeletal muscle types tested, whereas myosin heavy chain (MHC) and titin levels were unaltered. Muscles were obtained from 5d old mice. Quad: m. quadriceps; EDL: extensor digitorum longus; Psoas: m. psoas major; Diaph: m. diaphragm; Long: m longissimus dorsi; Pect: m. pectoralis major. (B) Quantitive Western blotting studies with an antibody against nebulin's N-terminus showed that nebulin protein levels were ~2% of WT levels. Western blotting studies with the same antibody on muscle from 1d (p1) old mice (C) and from embryonic E19 mice (D) show that nebulin protein is 10% of WT values at E19 and 8% of wt values at d1. Gast: m. gastrocnemius. *: $p<0.05$.

3.2.3 *Neb*ΔExon55 KO mice have shorter thin filament lengths

Nebulin plays an important role in specifying thin filament length, a length that is crucial for optimal force generation by sarcomeres. Therefore, thin filament length was measured in *Neb*ΔExon55 KO muscle fibers. Using immunofluorescence confocal scanning laser microscopy, we determined the location of tropomodulin (a thin filament pointed end capping protein) relative to the Z-disk was measured as well as the width of the band obtained using the fluorescently labeled actin-binding protein phalloidin. Figure 13 A, shows that the staining pattern of fluorescently labeled phalloidin differed between myofibrils from *Neb*ΔExon55 KO and WT *tibialis cranialis* muscle; WT myofibrils showed broad actin labeling with uniform intensity (except for the Z-disk area where actin filaments overlap), whereas in *Neb*ΔExon55 KO myofibrils the labelling was narrower, and intensity gradually decreased from the Z-disk towards the middle of the sarcomere. Densitometric analysis revealed that the width at half-maximal intensity was 2.25 ± 0.03 µm for WT and 1.75 ± 0.01 µm for *Neb*ΔExon55 KO myofibrils (Fig. 13 A, right). Tropomodulin staining in WT myofibrils showed a distinct doublet in the middle of the sarcomere, 2.03 ± 0.03 µm apart, measured across the Z-disk, whereas in myofibrils from *Neb*ΔExon55 KO mice this value was only 1.67 ± 0.03 µm. These findings supported the results from the phalloidin experiments, suggesting that thin filament lengths were reduced from ~1.0 µm in WT myofibrils to ~0.85 µm in *Neb*ΔExon55 KO myofibrils.

The experiments with fluorescently labelled tropomodulin revealed that thin filaments were shorter in *Neb*ΔExon55 KO myofibrils and suggested that capping at the thin filament pointed end by tropomodulin remained intact in these myofibrils. Immunofluorescence experiments on CapZ (a thin filament barbed end capping protein) showed that capping at the barbed end also remained intact in *Neb*ΔExon55 KO myofibrils.

A

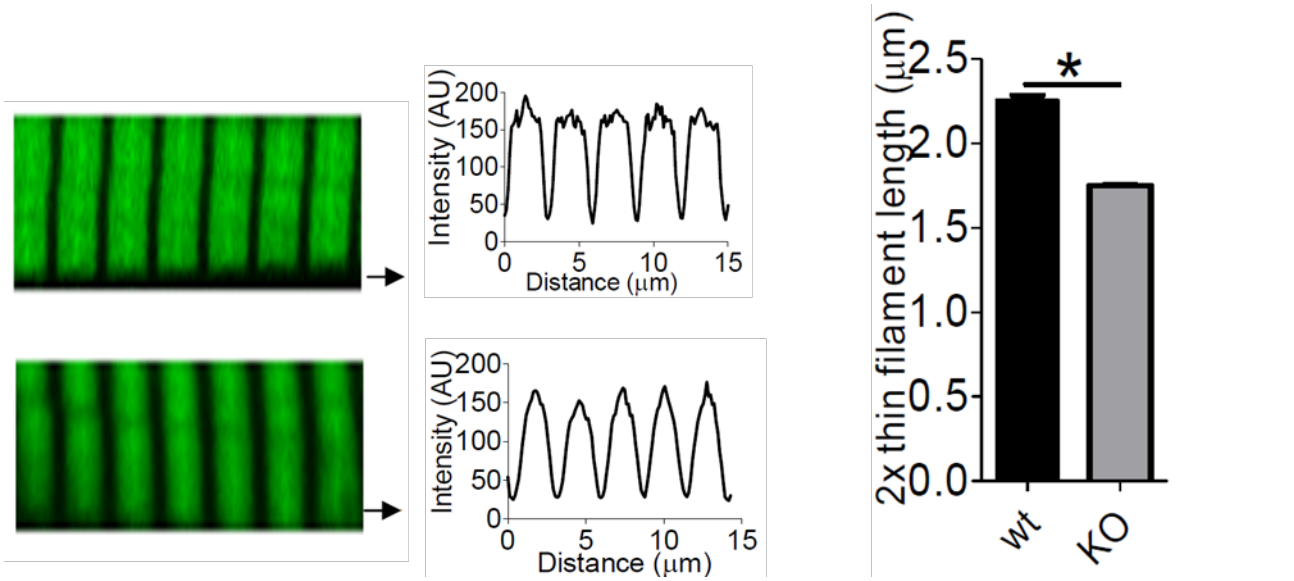

B

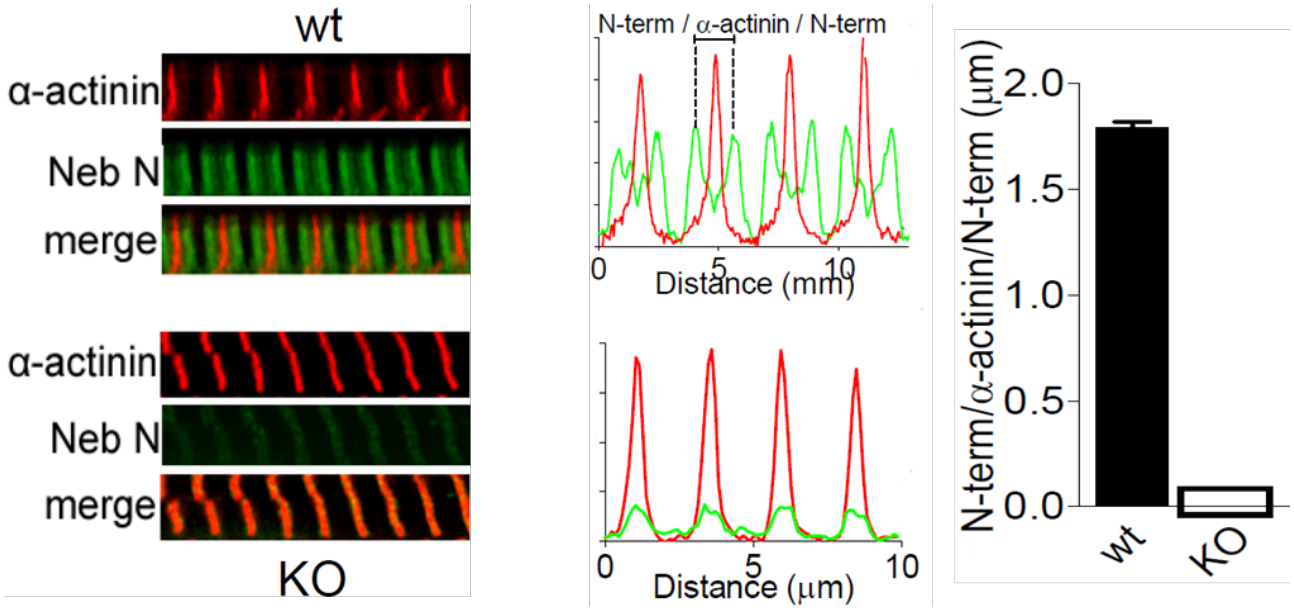

Figure 13. A) Left: Actin staining with phalloidin-AlexaFluor 488 in 6d TC myofibrils from *Neb*ΔExon55 KO and WT mice showed broad staining in WT myofibrils (top), whereas this staining was narrowed in *Neb*ΔExon55 KO myofibrils (bottom). Right: Analysis of phalloidin line scan intensities revealed significantly reduced average thin filament lengths in *Neb*ΔExon55 KO myofibrils. B) Left: *Neb*ΔExon55 KO and WT myofibrils stained for α-actinin and nebuln's N-terminus (Neb N). Right: analysis of line scan intensities. Note that Neb N staining was nearly absent in *Neb*ΔExon55 KO myofibrils. *: $p<0.05$.

Finally, the data in Figure 13 B, in which an antibody against nebulin's N-terminus was used, showed that nebulin was nearly absent from *Neb*ΔExon55 KO myofibrils, thereby confirming the Western blot experiments (Fig. 12). Thus, immunofluorescence confocal microscopy experiments showed that in *Neb*ΔExon55 KO muscle thin filament capping was intact but that thin filament length was significantly reduced.

Recent work has led to the notion that nebulin was important for the tuning of cross bridge cycling kinetics to maximize force generation (23). To determine whether changes in cross bridge cycling kinetics contributed to the weakness that caracterize *Neb*ΔExon55 KO phenotipe, mechanical, kinetic and biochemical parameter were investigated on fibers and myofibrils preparations.

3.2.4 Mechanics on single myofibrils : active tension in NEBΔexon55 KO mutant vs WT

The mechanical behavior of single myofibrils isolated from NEBΔexon 55 KO and WT muscle fibers was determined by measuring maximal tension development and the kinetics of force development and of force relaxation.

Active isometric tension of myofibrils isolated from frozen skinned or glycerinated *tibialis cranialis* of neonatal mice muscle of NEBΔexon 55 KO mutant were compared to myofibrils from WT mice. Figure 14 shows, for both WT and KO myofibrils, representative traces of tension generation to maximal Ca^{2+} activation by fast solution switching. Average data for all activation parameters related to KO an WT myofibrils were illustrated in Table 6. Maximal myofibril tension was significantly decreased, more than 2 times, in KO myofibrils compared with WT (see below, Table 6).

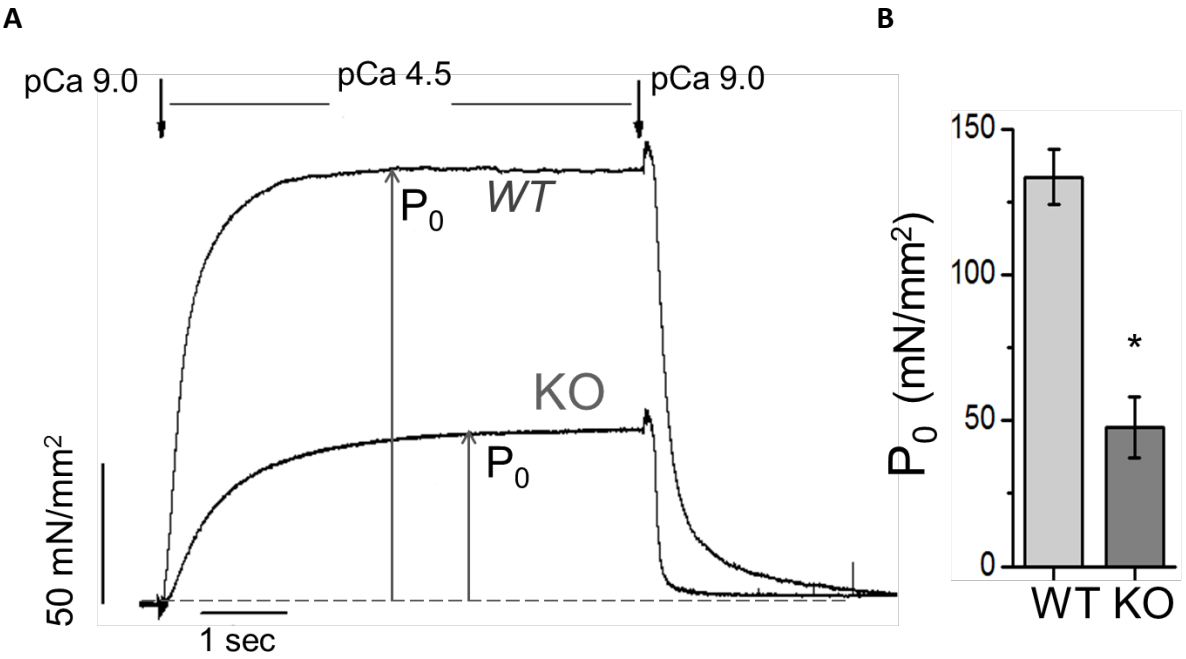

Figure 14. Isometric active tensionin NEBΔexon 55 KO and WT *tibialis cranialis* myofibrils from neonatal mice. A, representative tension responses of NEBΔexon 55 KO and WT myofibrils maximally activated and fully relaxed by fast solution switching thecnique (pCa changes at arrows as indicated). NEBΔexon 55 KO myofibrils developed 40% of WT tension. Experimental teperature 15°C. B, mean values of maximal active tension (P_0, expressed in mN mm^{-2}) WT (light gray) and KO (gray). P_0 for the WT 133.4±9.5 and for KO 49.7±10.6. P_0 was significantly reduced for KO compared to WT (*P < 0.01). Bars above columns are S.E.M.

3.2.5 Kinetics of force generation in NEBΔexon 55 KO and WT *tibialis cranialis* myofibrils

The kinetics of tension developement (k_{ACT}, s^{-1}), as well as the kinetics of tension redevelopement k_{TR} (See Table 14), were markedly slower compared to WT (see Figure 15). In all myofibril populations the time course of Ca^{2+}-activated tension developement was monoexponential . The activation rate constant k_{ACT} tended to be the same as k_{TR} in both groups WT and KO although k_{TR} tended to be slower than k_{ACT}. However the rate of tension redevelopement k_{TR} of KO was significantly decreased compared to k_{TR} in WT. Note that the magnitude of k_{TR} reduction in myofibrils was in the same order as observed in NEBΔexon 55 KO fibers. (See Table 6).

	WT	NEBΔexon 55 KO	
P_0(mN mm^{-2})	133 ± 9.5 (19)	49.7 ± 10.6 (11)	P<0.01
k_{ACT} (s^{-1})	2.89 ± 0.21 (18)	1.46 ± 0.07 (10)	P<0.01
k_{TR} (s^{-1})	3.29 ± 0.25 (13)	2.27 ± 0.16 (7)	P<0.01

Table 6. Active tension generation parameters: means (± S.E.M.) of isometric active tension P_0, activation rate k_{ACT}, costant rate of tension redevelopement k_{TR} in NEBΔexon 55 KO and WT *tibialis cranialis* myofibrils. P< 0.01 for all parameters of KO *versus* WT (estimated by Student t test; number of myofibrils in parenthesis). Experimental conditions: 15°C, pCa relaxing and activating solutions, 9.0 and 4.5 respectively; [MgATP] 5 mM; [P_i] < 5µM.

3.2.6 Tension relaxation parameters in NEBΔexon 55 KO myofibrils

Force relaxation kinetics in the NEBΔexon 55 KO myofibrils were significantly faster than in WT myofibrils. Interestingly, the magnitude of increase in slow k_{REL} in KO myofibrils was close to that of the increase in tension cost in fibers observed by Ottenhheijm (Ottenheijm; Amsterdam - paper in prep.; see Discussion).

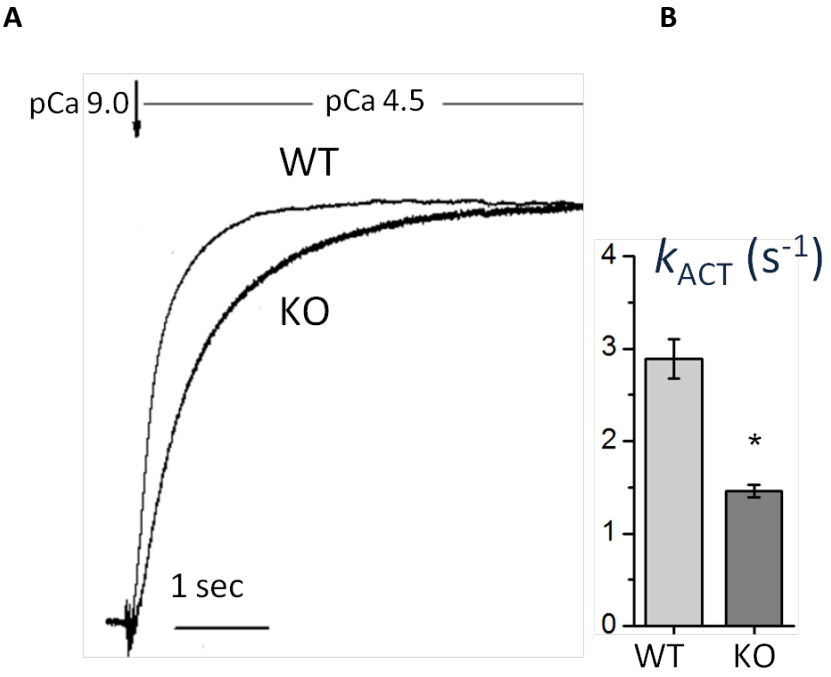

Figure 15. Kinetics of force generation in NEBΔexon 55 KO and WT *tibialis cranialis* myofibrils. A,the time course of tension activation following sudden Ca^{2+} increase NEBΔexon 55 KO myofibril and WT myofibril after normalization for maximal tension. B, mean values of k_{ACT} (s^{-1}) for WT and KO myofibrils. See Table 1 for number of myofibrils (in parenthesis). k_{ACT} was significantly decreased in KO (1.46±0.07) compared to WT (2.89±0.21). Data in s^{-1}; bars above columns are S.E.M, *P < 0.01.

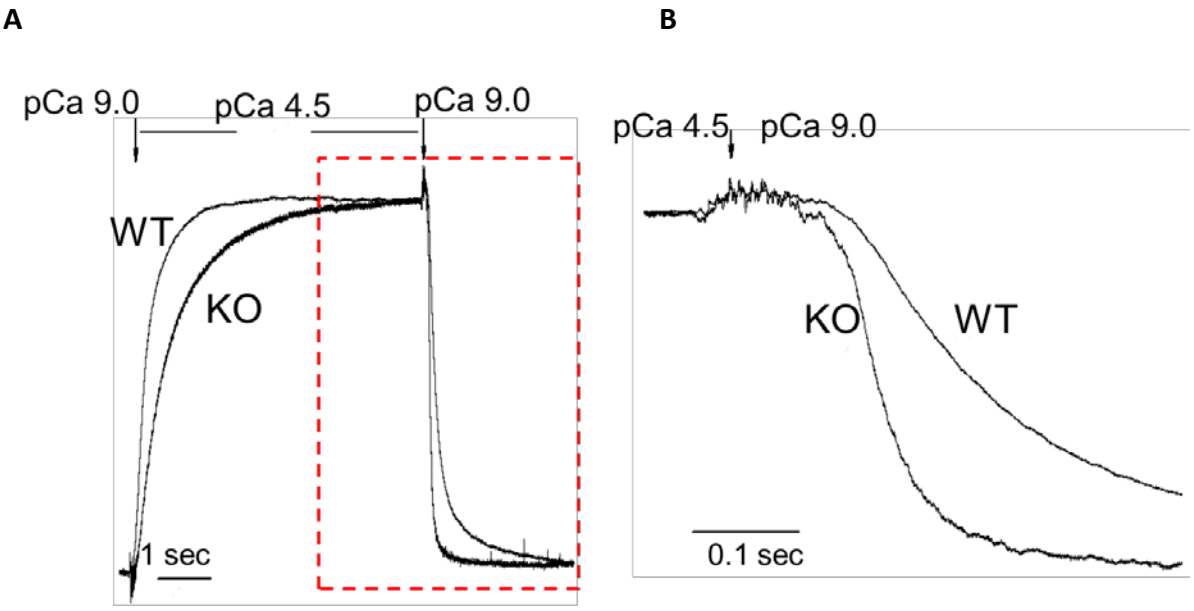

Figure 16. Representative tension relaxation traces in a NEBΔexon 55 KO and a WT *tibialis cranialis* myofibrils. Tension relaxation kinetics following sudden Ca^{2+} removal. Same traces (A,B) as in Figure 14 superimposed on a faster time base after normalization for maximal tension. B, magnification of the red-dot squarein A. Clear overview of relaxation behavior of KO myofibril caracterised by shorter and faster slow relaxation phase than WT myofibril. Also fast relaxation phase appeared faster in KO than in WT.

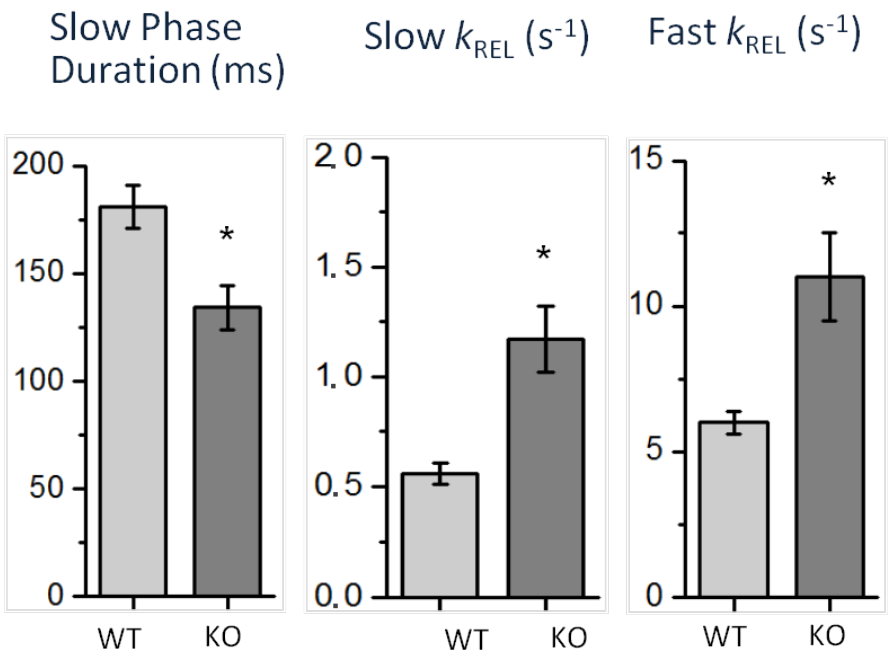

Figure 17. Kinetic parameters of relaxation and duration of slow relaxation phase in NEBΔexon 55 KO and WT *tibialis cranialis* myofibrils. The rate constant of the early slow force decline (slow k_{REL}) was estimated from the slope of the regression line fitted to the tension trace normalized to the entire amplitude of the tension relaxation transient. The rate constant for the fast phase of tension decline

(fast k_{REL}) was estimated from mono-exponential fit. Slow phase duration (ms)was significantly reduced in KO myofibrils (134±10) compared to WT (181±10). The constant rate of slow relaxation slow k_{REL} (s^{-1}) was almost doubled in KO (1.17±0.15) compared with WT myofibrils (0.56±0.05) as well as constant rate of fast relaxation phase k_{REL} (s^{-1}) (11.0±1.5 for KO vs. 6.0±0.4 for WT). Bars above columns are S.E.M, *P < 0.01.

	WT	NEBΔexon 55 KO	
D_{slow} (ms)	181 ± 10 (18)	134 ± 10 (10)	P<0.01
slow k_{REL} (s^{-1})	0.56 ± 0.05 (18)	1.17 ± 0.15 (9)	P<0.01
fast k_{REL} (s^{-1})	6.0 ± 0.4 (17)	11.0 ± 1.5 (11)	P<0.01

Table 7. Tension relaxation parameters: means (± S.E.M.) of relaxation in NEBΔexon 55 KO and WT *tibialis cranialis* myofibrils. Both kinetic parameters (slowk_{REL}; fastk_{REL}) of relaxation were strongly accelerated in KO myofibrils compared to WT. The duration of slow phase of relaxation resulted significantly reduced in KO mice. * P< 0.01 KO *versus* WT for all parameters (estimated by Student t test; number of myofibrils in parenthesis). Experimental conditions: 15°C, pCa relaxing and activating solutions, 9.0 and 4.5 respectively; [MgATP] 5 mM; [P_i] < 5µM.

3.2.7 Cross bridge cycling kinetics in skinned muscle fibers

The tension cost and the rate constant of force redevelopment, k_{TR}, were measured in fibers from *Neb*ΔExon55 KO muscle and results compared to those from WT muscle (data from H.Granzier laboratory, Tucson, University of Arizona). To determine k_{TR}, fibers were first isometrically activated at pCa 4.5 and when a steady force was reached, cross bridges were disengaged by performing a quick release, a brief period of unloaded shortening, and then a rapid restretch to the original length. Following restretch, force rebuilded with a time course that could be fit to a monoexponential with rate constant k_{TR}, (see Fig. 18A, left panel, for a typical force response). As shown in Figure 18A, k_{TR}, was significantly lower in the *Neb*ΔExon55 KO fibers than in the WT fibers (4.3 ± 0.5 vs. 5.9 ± 0.3 s^{-1}, KO vs. WT respectively). Tension cost was determined by the simultaneous measurement of the breakdown of NADH and force during contraction, with NADH levels enzymatically coupled to ATP utilization (de Tombe and Stienen, 1995; see Methods). An example of a maximally-activated *Neb*ΔExon55 KO fiber preparation with [NADH] falling linearly during the tension plateau was shown in Figure 8B, left panels. The slope of the [NADH] vs. time curve was normalized by the fiber volume to obtain ATP consumption rates that can be compared for differently sized muscle preparations. By normalizing ATP consumption rates to the tension generated and fiber volume, the tension

cost could be determined. As shown in Figure 18B, the tension cost was significantly higher in *Neb*ΔExon55 KO fibers compared to WT fibers (10.4 ± 1.1 vs. 6.4 ± 0.4 pmol/mN/mm/s, *Neb*ΔExon55 KO vs. WT respectively).

A

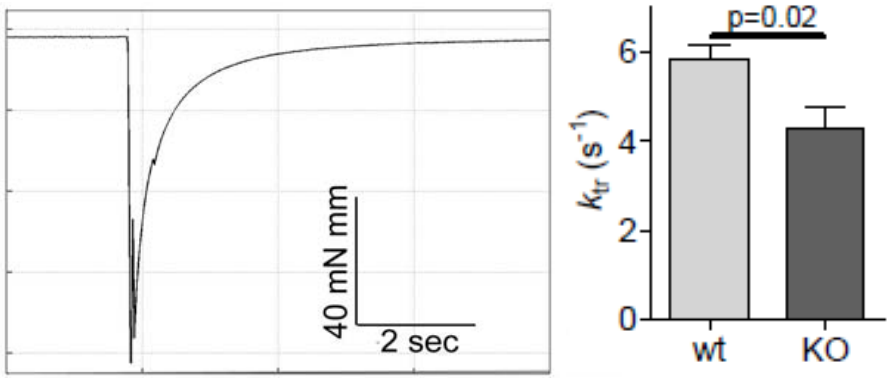

B

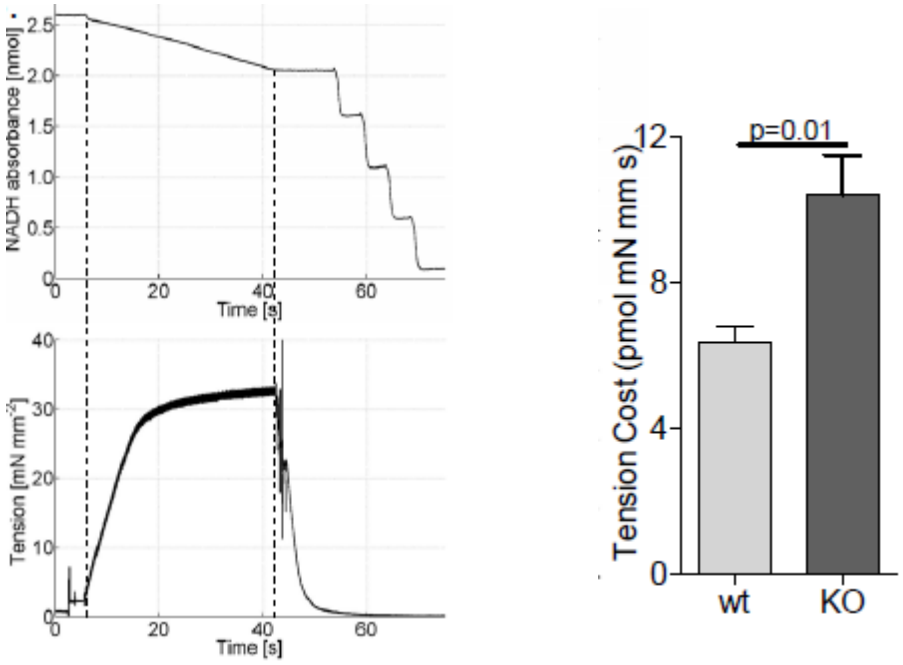

Figure 18. A, k_{TR} measurements in 6d old *Neb*ΔExon55 KO and WT fibers. Left panel: example of a k_{TR} protocol in a KO fiber preparation; right panel: k_{TR} was significantly lower in *Neb*ΔExon55 KO compared to WT fibers. B, Tension cost measurements in *Neb*ΔExon55 KO and WT fibers. Left panel: example of maximally activated *Neb*ΔExon55 KO fibers with developed force at the bottom and [ATP] at the top. The slope of the [ATP] vs time trace was divided by fiber volume (in mm^3) to determine ATP consumption rate. ATP consumption rate was normalized to tension to determine the tension cost (Brenner and Eisenberg, 1986). Right panel: tension cost was significantly higher in *Neb*ΔExon55 KO compared to WT fibers.

3.2.8 Calcium sensitivity of force

The calcium sensitivity of force generation was also an important parameter of muscle function, reflecting the response of force to submaximal activation levels at which muscle typically operates *in vivo*. To determine the calcium sensitivity of force, skinned fibers from *tibialis cranialis* (TC) muscle were exposed to incremental calcium concentrations and the force response was recorded. As shown in Figure 19, the force-pCa curve of *Neb*ΔExon55 KO fibers was shifted rightward (reflected by a lower pCa_{50} in KO fibers: 6.22 ± 0.02 vs. 6.34 ± 0.01, *Neb*ΔExon55 KO vs. WT respectively), indicating that the calcium sensitivity of force was significantly reduced in fibers from *Neb*ΔExon55 KO mice compared to those from WT mice. The cooperativity of activation (n_H) was not different between groups. Thus, the calcium sensitivity of force was reduced in *Neb*ΔExon55 KO muscle.

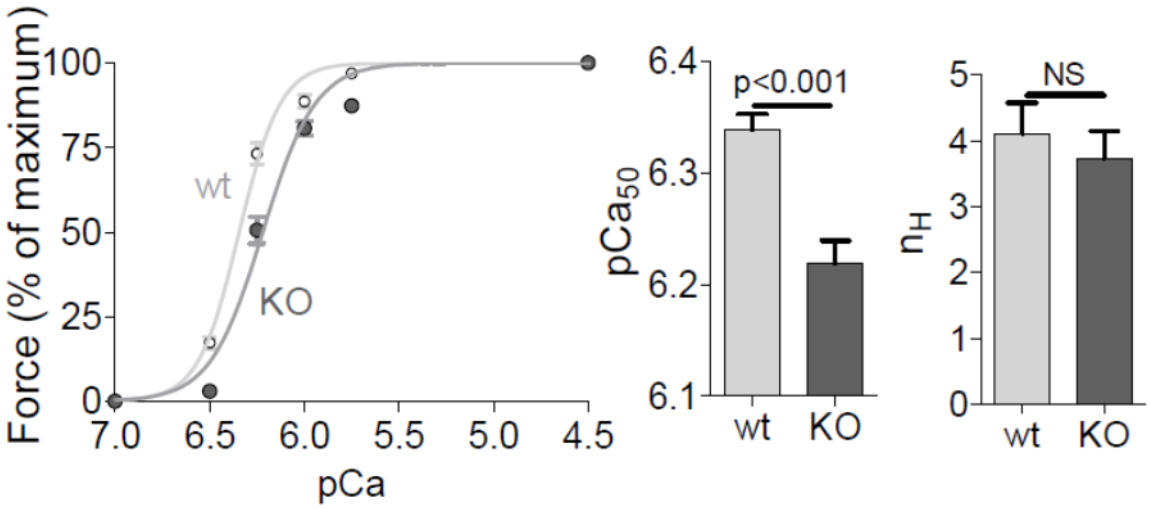

Figure 19. Force-Ca^{2+} characteristics of TC fibers from 5d old *Neb*ΔExon55 KO and WT mice; Left panel: note the rightward shift of the force-pCa relationship in *Neb*ΔExon55 KO compared to WT fibers; Middle panel, the Ca^{2+} concentration needed for 50% of maximal force generation was significantly higher (i.e., lower pCa_{50}) in *Neb*ΔExon55 KO vs. WT fibers, whereas no difference was found in the Hill coefficient (nH, right panel).

Chapter 4: Discussion

4.1 Crossbridge alteration in the presence of cTnT mutant and energy deficiency hypothesis in FHC

Although some mutations of TnT associated to cardiomyopathy could have pathological consequences related to secondary effects (i.e. alterations of flexibility or orientation of specific portion of TnT molecule, affecting the protein complex and then also the function of the thin filament, Manning et al. 2012), some mutations on the other hand seem to be directly responsible of primary effects. This means that the presence of the mutated TnT alters the cross bridge cycling kinetics by regulating the interaction between myosin-based cross bridges and the thin filament (see Results).

The specific TnT mutant that we studied, K280N mutation, seems to be a clear example of that.

According to a simple 2-state model of acto-myosin interactions (Brenner 1988) (Figure 1), the formation of force-generating crossbridges occures via an apparent rate constant f_{app}, crossbridge detachment occurs with apparent rate constant g_{app}, the overall crossbridge turnover rate is given by $f_{app}+ g_{app}$, tension is proportional to $f_{app}/(f_{app}+ g_{app})$, and the energy cost of tension generation (ATPase/tension ratio) is proportional to g_{app} (Brenner 1988; deTombe & Stienen 2007).

Figure 1: 2-state crossbridge scheme. $AM_{no\ force}$ represents all weak binding states (mostly detached) and AM_{force} all strong binding states. The transition frem the non-force-generating states to the force-generating states has an apparent rate constant f_{app} whereas g_{app} describes the return to the non-force-generating states by means of ADP release and ATP binding. The apparent rate constant for the reverse transition f'_{app} that depends on [Pi] can be neglected under the conditions of the study.

When this 2-state model of acto-myosin is used to explain our results, it provids evidence that the apparent rate with which force-generating crossbridges detach under isometric conditions (g_{app}) as well as the overall crossbridge turnover rate (given by $f_{app}+ g_{app}$) are significantly increased.

As $k_{REL} \sim g_{app}$ (0.26 ± 0.02 s^{-1} and 0.59 ± 0.06 s^{-1} in donors and K280N mutant myofibrils respectively; see Results; Table 1 and 2) and $k_{ACT} \sim f_{app}+ g_{app}$ (0.86 ± 0.02 s^{-1} and 1.77 ± 0.11 s^{-1}

in control donor and K280N mutant myofibrils respectively), the presence of TnT mutant in the sarcomere determines a more than two-fold e increase in g_{app} of, when compared to donors, together with an increase in f_{app}. This could explain the relative small reduction of P_0 associated with the K280N TnT mutation. Moreover, the 3-fold increase of slow k_{REL} (directly proportional to g_{app} and to the ATPase activity) support the hypothesys of a 3-fold increase in the energy cost of tension generation in K280N sarcomeres. Direct measurements of ATPase activity (data from Jolanda van der Velden group, VU, Amsterdam; Figure 7 and 8; Table 5; Chapter 3: Results) definitely confirm this conclusion, strongly supporting the idea that the K280N mutation, like many in FHC, could lead to inefficient ATP utilization for tension generation.

Furthermore, after the WT troponin complex replacement into mutant K280N myofibrils (see Results, Figure 5 and 6), the kinetics of force generation (k_{ACT}) and relaxation (in particolar slow k_{REL}) in K280N myofibrils were clearly slowed down, restoring values close to those of donors. This suggests the direct correlation of thatmutation to the mechanical and energetic effects observed.

It has been proposed that sarcomere mutations related to FHC may lead to increased cost of force production through inefficient or excessive ATP usage and that this ultimately results in an energy deficiency that contributes to the pathogenesis of the disease (Ferrantini et al., 2009). The “energy depletion hypothesis” for HCM is strengthened by the finding that HCM-like phenotypes have been reported in a variety of diseases that limit myocardial energy production (Ashrafian et al., 2009).

Energy depletion in critical compartments of the cardiomyocyte could lead to failure to maintain free energy levels sufficient for contraction and critical homeostatic functions, such as Ca^{2+} re-uptake by cardiac SERCA pump (Sarco-Endoplasmic Reticulum Calcium ATPase) or also compromise the ion transporter function needed for normal electrophysiological activity. This will lead to heterogeneity of membrane potentials and will increase the vulnerability of the myocardium to arrhythmias, which is often the cause of sudden cardiac death in HCM. Moreover, the enhanced activation of other signaling patways like AMP-activated protein kinase (AMPK) could lead to progressive mitochondrial dysfunction, and production of reactive oxygen species, together with chronic energy depletion. This will ensue myocyte disfunction and elevation of cytosolic Ca^{2+}, exacerbating the energetic compromise (Ashrafian et al., 2007).

The investigation of the modification of the calcium activation of contraction in the presence of the K280N TnT mutant lead to other interesting observations. Force development at submaximal calcium activation was measured, simulating *in vivo* conditions (cardiac muscle typically is submaximally activated). Myofibrils from mutant, donor and aortic stenosis (SAO) patients were exposed to various calcium concentrations (pCa 4.5, 5.6, 5.8, 6) and the force level was determined. We found that the calcium sensitivity of force generation tended to be increased in both hypertrophic samples compared to donor myofibrils, suggesting that the increase in calcium sensitivity could be a secondary effect directly related to hypertrophic remodeling pathways. Cooperativity of calcium activation resulted reduced in mutant myofibrils compared to donors and, similarly, to SAO. This effect could be directly related to the K280N mutation as it is located in a position flanking the interaction region of Tm. Tm is generally regarded as the protein transmitting the activation signal of calcium binding to TnC along the regulatory units of the thin filament. So we could speculate that cardiac K280N mutation could alter TnT flexibility and interaction with Tm, reducing the propagation of the signal along the thin filament and then the cooperativity of calcium activation.

4.2 Crossbridge alteration in *Neb*ΔExon55 KO mice

Functional findings on the new mouse model for nebulin-based nemaline myopathy by targeted deletion of *Neb* exon 55 showed that muscle from *Neb*ΔExon55 KO mice was severely weakened and contained nemaline rods, both hallmark features of NM. Following different studies, the muscle weakness in *Neb*ΔExon55 KO mice was due to several causes, atrophy of muscle fibers, shorter thin filaments, reduced calcium sensitivity of force generation and changes in cross bridge cycling kinetics. As previously described (Introduction), nebulin is a giant protein expressed at high levels in skeletal muscle. Most of the molecule was organized into super-repeat modules. This precise arrangement was thought to allow each nebulin module to interact with a single monomer of the actin filament (Labeit et al., 1991; Labeit et al., 1995), and each nebulin super-repeat to associate with a single tropomyosin (Tm)/troponin (Tn) complex (Jin and Wang, 1991; McElhinny et al., 2003; Ogut et al., 2003). NEB exon 55 encoded 35 amino acids that were part of a super-repeat portion of protein (See Introduction). The absence of exon 55 in the nebulin transcript did not generate a frameshift, and the transcript was predicted to encode a protein that was 35 amino acids smaller than the normal gene product. However, as two of the encoded 35 amino acid modules of nebulin were interrupted by the deletion of exon 55, this resulted in the disruption of the seven-module set of super-repeat 9 (Labeit et al., 1995). It has been proposed that this disruption caused a mismatch between nebulin and its binding sites on actin (Anderson et al.,2004), thereby preventing the incorporation of mutant nebulin molecules and leading to their degradation (Ottenheijm et al., 2009). Nebulin has been proposed to modulate myofibrillar function through three different and cooperative mechanisms: (1) by specifying thin filament length; (2) by regulating the interaction between myosin-based cross bridges and the thin filament; and (3) by tuning the response of the thin filament to calcium (Bang et al., 2009; Ottenheijm and Granzier, 2010). Simulations with the 2-state model of acto-myosin interactions before described to explain our results with TnT mutation, provided evidence that in *Neb*ΔExon55 KO mouse myofibrils the apparent rate with which force-generating crossbridges detach under isometric conditions (g_{app}) was markedly accelerated. In the absence of inorganic phosphate (Pi) as in the present experiments, crossbridges live their force generating states through transitions that led to ATP hydrolysis steps (Gordon et al., 2000; Poggesi et al., 2005). The faster cross bridge detachment rate (g_{app}) associated with *Neb* exon 55 delection, should then generate higher energy costs to produce a given tension (slow k_{REL} ~ g_{app} , proportional to ATP

consumption; higher ATPase/tension ratio) (de Tombe & Stienen, 1995). Direct measurements of ATPase activity definitely confirmed this conclusion, (H. Granzier et al. in prep.) supporting the idea that the *Neb*ΔExon55 deletion and so the MN patholoy, could lead to inefficient ATP utilization for tension generation. The increase in slow k_{REL} observed in *Neb* exon 55 sarcomeres implies that the increase in crossbridge detachment rate is a pivotal factor responsible for the lower maximal isometric tension. Moreover the overall crossbridge turnover (proportional to k_{ACT} and k_{TR}) was markedly reduced in *Neb*ΔExon55 KO mouse myofibrils, suggesting that slower isometric crossbridge turnover contributed together with increased crossbridge detachment rates, to reduce maximal isometric tension two times compared to WT myofibrils. Consequently, the fraction of force generating cross bridges was significantly reduced in *Neb*ΔExon55 KO muscle (increased g_{app}, decreased f_{app}).

A hallmark feature of patients with NM was muscle weakness, greatly affecting daily life-activities and negatively impacting the quality of life (North et al., 1997). At the structural level, NM was characterized by myofibrillar disarray originating from the Z-disk and culminating in nemaline rods, which consisted of thin filament and Z-disk proteins (Morris et al., 1990; North et al., 1997; Sanoudou and Beggs, 2001). Importantly, the number of nemaline rods in muscle biopsies did not correlate with muscle weakness in patients with NM (Ryan et al., 2003; Shimomura and Nonaka, 1989). This suggested that myofibrillar disarray and nemaline rods were a secondary phenotype and were not the sole contributors to the muscle weakness associated with NM. The new KO model had a relative paucity of rod bodies yet muscle weakness was severe, supporting the notion that muscle weakness in NM with nebulin mutations was caused primarily by changes in myofilament function. The maximal tension generated by muscle fibers from *Neb*ΔExon55 KO mice was severely reduced (see Introduction, Figure 13), and based on electron microscopy studies this reduction was unlikely due to myofibrillar disarray (see introduction, Figure 11B). This conclusion is supported by our studies on the maximal tension generation of single myofibrils (see Results): the magnitude of tension reduction in *Neb*ΔExon55 KO myofibrils was similar to that in *Neb*ΔExon55 KO fibers (62 and 64%, respectively). Thus, the weakness of muscle fibers in *Neb*ΔExon55 KO mice could be attributed to changes in myofibrillar function, rather than by myofibrillar disarray or by a reduced myofibrillar fractional area. Note that the maximal tension generated by myofibrils was higher than that by muscle fibers, both in WT and *Neb*ΔExon55 KO mice, and that this was caused by the tension in fibers being normalized to a cross sectional area that comprises

myofibrils plus non-contractile material such as mitochondria, glycogen granules, sarcoplasmic reticulum, etc. The 64% reduction in tension generation by fibers from *Neb*ΔExon55 KO muscle, combined with the reduction in fiber diameter of 23%, resulted in a total force loss of more than 75% in *Neb*ΔExon55 KO fibers when compared to WT fibers. In skeletal muscle, thin filament lengths were fine tuned at ~ 1.1-1.3 μm (depending on species and muscle type (Littlefield and Fowler, 2008)) to overlap with thick filaments and to meet the muscle's contractile requirements (Burkholder et al., 1994; Littlefield and Fowler, 2008). The extent of overlap between thick and thin filaments determined the sarcomere's force generating capacity: short thin filaments reduce overlap and impair force generation. Thus, thin filament length was a key aspect of muscle function, and recent work indicated that nebulin was involved in specifying this length (Bang et al., 2004; Witt et al., 2006). Immunofluorescence confocal microscopy studies (Granzier et al., in preparation) revealed that thin filament length was significantly reduced from 1.0 μm in WT muscle to 0.85 μm in *Neb*ΔExon55 muscle. These structural studies were corroborated by mechanical studies, which revealed a leftward shift (at sarcomere lengths of 2.4 μm and longer) of the force-sarcomere length relation in KO muscle fibers (see Introduction, Figure 13). Thus, deletion of *Neb* exon 55 resulted in shorter thin filament lengths, contributing to muscle weakness at longer sarcomere lengths. Weakness of *Neb*ΔExon55 KO fibers was also apparent at sarcomere lengths shorter than 2.4 μm (Figure 13), suggesting that the reduction of thin filament length was not the only mechanism for weakness in *Neb*ΔExon55 KO mice. Our findings showed that cross bridge cycling kinetics in *Neb*ΔExon55 KO fibers were altered, and that this contributed to muscle weakness. *Neb*ΔExon55 muscle fibers had significantly higher tension cost compared to WT fibers (see Results; Figure 18B), which indicated that the cross bridge detachment rate was higher (Stienen et al., 1996). In combination with the observation that k_{TR} was slower in *Neb*ΔExon55 KO fibers (see Results; Figure 18A), these findings led to the conclusion that the rate of cross bridge attachment was slower in *Neb*ΔExon55 KO fibers. Consequently, the fraction of force generating cross bridges was significantly reduced in *Neb*ΔExon55 KO muscle. Importantly, these findings on *Neb*ΔExon55 KO fibers were strongly supported by our results from studies on single myobrils (see Results; Figure 16 and 17). The advantages of studies on myofibrils included that due to their small size they instantly equilibrate with the bathing solution making it possible study force relaxation kinetics. Furthermore, as myofibrillar damage typically results in breakage of the myofibrils during activation, the data obtained from myofibrils reflected direct effects of

the mutated protein on cross bridge cycling kinetics without potential confounding effects of myofibrillar damage. Importantly, the magnitude of the k_{TR} changes in myofibrils were similar to that in fibers and the changes in slow k_{REL} of myofibrils were similar to that of the tension cost measured in fibers. Thus, measurement at two distinct levels of organization (myofibrils and fibers) and using distinct techniques (tension cost measurements and force relaxation kinetics) supported that alterations in cross bridge cycling kinetics greatly contributed to the observed weakness of *Neb*ΔExon55 KO muscle. The studies discussed above were carried out at a maximal activating calcium level. However, *in vivo*, skeletal muscle typically was submaximally activated. Thus, submaximal parameters of muscle function provided relevant physiological information. To test whether submaximal force generation was affected in *Neb*ΔExon55 KO fibers, permeabilized fibers were exposed to various calcium concentrations and the ensuing force level was determined. It was found (Granzier et al., paper in prep.) that the calcium sensitivity of force generation was significantly reduced in KO fibers, suggesting that in addition to maximal force generation, the capacity for submaximal force generation was greatly impaired in KO mice.

In summary, muscle of *Neb*ΔExon55 KO mice was nebulin-deficient and produced weakness by shortening thin filament lengths, reducing the fraction of cross bridges in the force generating state, and reducing the force response to submaximal calcium concentrations. Importantly, similar contractile and structural changes were observed in studies on muscle fibers from patients homozygous for deletion of *NEB* exon 55 (Ottenheijm et al., 2010; Ottenheijm et al., 2009), indicating that the phenotype of the KO model closely recapitulates that observed in patients.

Chapter 5: Conclusions

In this thesis, the effect of mutations of two different sarcomeric proteins, cardiac troponin T (cTnT) and skeletal nebuline on biophysical properties of crossbridge cicle on myofibrils were investigated. Although the sistems analysed were totally different, we used a human cardiac myectomy of a young patient affected by familial hypertrophyc cardiomyopathy (FHC) related to K280N mutation of cTnT and a novel mouse model that reproduce a delection often found in patient affcted by nemaline myopathy (NM), we investigated mechanical and kinetic properties of myofibrils from both group, finding connections that could be explained using the same 2-state model of acto-myosin interaction proposed by Brenner in 1988, previously described in Discussion (Chapter 4). This method permitted us to interpreted non related mutation, in different proteins and distinct sistem, that however, could similarly alterate the sarcomeric function and byophysics.

Both samples were caracterized by a markedly increased in apparent rate constant g_{app}, that described the crossbridge detachment rate. This directly reflects kinetic parameter related to slow relaxation phase (slow k_{REL}) that resulted increased in both human mutant and transgenc mouse samples. The apparent rate constant g_{app} was directly proportional to tension cost, so an increas of g_{app} cuold be correlated also to a rise in tension cost, confirmed by direct experiment on the skinned fiber. As previously reported (), increased energy cost of tension generation could lead to energetic deficit and myocyte energy impairment underlining the central role in FHC desease and opening a new overview to understand severe contraction deficit in Nemaline Myopathy.

The active tension developed under experimental condition was reduce for both samples. In cardiac K280N mutant the tension was only slightly reduced compered the controls group that we used, effect due to the contribution of the apparent rate constant f_{app}, despite the increase of g_{app} (as previously described tension was proportional to $f_{app}/(f_{app}+ g_{app})$).

Differently appened in nebuline knock out model, where tension was dramatically reduced. This was due to reduced f_{app} that was translated in a reduction of overall crossbridge turnover rate was given by $f_{app}+ g_{app}$.

Moreover, since the small size of troponin and the relatively easy thecnique of extraction of this protein complex, replacement of transgenic WT troponin complex in cardiac K280N mutant myofibrils was performed, restored kinetic parameters to values similar to that of controls,

indicating and supporting the evidence that alteration related to this sample was a primary effect of the mutation. Future analysis should focus on the effect of replacement of a recombinant mutant troponin carring the K280N mutation on troponin T subunit, to further validate the directly implications in altering the biophysical properties of the sample.

Calcium sensibility and cooperativity were investigated directly on human cardiac mutant myofibrils. Calcium sensitivity of force generation tended to be increased in K280N sample as well as in the sample of secondary hypertrophy (SAO), suggesting that the increase in calcium sensitivity could be a secondary effect directly related to hypertrophic remodeling pathways. Differently, cooperativity of calcium activation resulted reduced in mutant myofibrils compared to donors and SAO, in which was similar; it leave speculate that this effect could be directly related to the K280N mutation.

Any measurement had been done jet on myofibrils of calcium affinity, this could be a future perspective to extend the study on this fild and confirm also in myofibrils the massive reduction of force response to submaximal calcium concentrations found in Granzier laboratory on permeabilized fibers, probabily due to myofiament structure disarray that cause severe muscle weakness in both the mouse model and patients.

References

Adabag AS, Maron BJ, Appelbaum E, Harrigan CJ, Buros JL, Gibson CM, Lesser JR, Hanna CA, Udelson JE, Manning WJ, Maron MS. Occurrence and frequency of arrhythmias in hypertrophic cardiomyopathy in relation to delayed enhancement on cardiovascular magnetic resonance. J Am Coll Cardiol. 2008; 51:1369-74

Anderson SL, Ekstein J, Donnelly MC, Keefe EM, Toto NR, LeVoci LA and Rubin BY. Nemaline myopathy in the Ashkenazi Jewish population is caused by a deletion in the nebulin gene. Hum Genet. 2008; 115: 185-190, 2004.

Ashrafian H, Redwood C, Blair E, Watkins H. Hypertrophic cardiomyopathy: a paradigm for myocardial energy depletion. Trends Genet. 2003; 19: 263-268.

Ashrafian H, Watkins H. Reviews of translational medicine and genomics in cardiovascular disease: new disease taxonomy and therapeutic implications. J Am Coll Cardiol. 2007; 49: 1251-1264

Bang ML, Caremani M, Brunello E, Littlefield R, Lieber RL, Chen J, Lombardi V and Linari M. Nebulin plays a direct role in promoting strong actin-myosin interactions. FASEB J. 2009; 23(12): 4117-25

Bang ML, Li X, Littlefield R, Bremner S, Thor A, Knowlton KU, Lieber RL and Chen J. Nebulin-deficient mice exhibit shorter thin filament lengths and reduced contractile function in skeletal muscle. J Cell Biol. 2006; 173: 905-916

Brenner B. Effect of Ca2+ on cross-bridge turnover kinetics in skinned single rabbit psoas fibers: implications for regulation of muscle contraction. Proc Natl Acad Sci USA. 1988; 85(9): 3265-9

Brenner B and Eisenberg E. Rate of force generation in muscle: correlation with actomyosin ATPase activity in solution. Proc Natl Acad Sci U S A. 1986; 83: 3542-3546

Basso C, Thiene G, Corrado D, Buja G, Melacini P, Nava A. Hypertrophic cardiomyopathy and sudden death in the young: pathologic evidence of myocardial ischemia. Hum Pathol. 2000; 31:988–98

Belus A, Piroddi N, Scellini B, Tesi C, Amati GD, Girolami F, Yacoub M, Cecchi F, Olivotto I and Poggesi C. The familial hypertrophic cardiomyopathy-associated myosin mutation R403Q accelerates tension generation and relaxation of human cardiac myofibrils. The Journal of physiology. 2008; 586: 3639-3644

Brandt PW, Schachat FH. Troponin C modulates the activation of thin filaments by rigor cross-bridges. Biophys J. 1997; 72(5): 2262-7

Burkholder TJ, Fingado B, Baron S and Lieber RL. Relationship between muscle fiber types and sizes and muscle architectural properties in the mouse hindlimb. J Morphol. 1994; 221: 177-190

Camici PG and Crea F. Coronary microvascular dysfunction. N Engl J Med. 2007; 356: 830-40

Castillo A, Nowak R, Littlefield KP, Fowler VM and Littlefield RS. A nebulin ruler does not dictate thin filament lengths. Biophys J. 2009; 96: 1856-1865

Cecchi G, Colomo F, Poggesi C, Tesi C. A force transducer and length-ramp generator for mechanical investigations of frog-heart myocytes. Pflugers Arch. 1993; 423: 113-20

Chandra M, Mamidi R, Ford S, Hidalgo C, Witt C, Ottenheijm C, Labeit S and Granzier HL. Nebulin alters crossbridge cycling kinetics and increases thin filament activation- a novel mechanism for increasing tension and reducing tension cost. J Biol Chem. 2009; 284(45): 30889-96

Colomo F, Nencini S, Piroddi N, Poggesi C, Tesi C. Calcium dependence of the apparent rate of force generation in single striated muscle myofibrils activated by rapid solution changes. Adv Exp Biol. 1998; 453:373-81

Conen PE,Murphy EG, Donohue WL. Light and electron microscopic studies of 'myogranules' in a child with hypotonia and muscle weakness. Can. Med. Assoc. J. 1963; 89: 983–986

de Tombe PP and Stienen GJM. Protein kinase A does not alter economy of force maintenance in skinned rat cardiac trabeculae. Circulation Res. 1995; 76: 734-741

Dubowitz V. Muscle biopsy: A Practical Approach, Bailliere Tindall (1985)

Elliott P, McKenna WJ. Hypertrophic cardiomyopathy. Lancet. 2004; 363: 1881–1891

Eriksson MJ, Sonnenberg B, Woo A. Longterm outcome in patients with apical hypertrophic cardiomyopathy. Journal of the American College of Cardiology. 2002; 39: 638–645

Ertz-Berger BR, He H, Dowell C, Factor SM, Haim TE, Nunez S, Schwartz SD, Ingwall JS, Tardiff JC. Changes in the chemical and dynamic properties of cardiac troponin T cause discrete cardiomyopathies in transgenic mice. Proc Natl Acad Sci U S A. 2005; 102(50): 18219-24.

Ferrantini C, Belus A, Piroddi N, Scellini B, Tesi C, Poggesi C. Mechanical and energetic consequences of HCM-causing mutations. J Cardiovasc Transl Res. 2009; 2: 441-51

Frey N, Franz WM, Gloeckner K, Degenhardt M, Müller M, Müller O, et al. Transgenic rat hearts expressing a human cardiac troponin T deletion reveal diastolic dysfunction and ventricular arrhythmias. Cardiovascular Research. 2000; 47: 254– 264

Geeves MA, Goody RS, Gutfreund H. Kinetics of acto-S1 interactions as a guide to a model for the crossbridge cycle. J. Mol. Cell Cardiol. 1984; 28: 217-230

Geisterfer-Lowrance AAT, Kass S, Tanigawa G, Vosberg HP, McKenna W, Seidman CE, et al. A molecular basis for familial hypertrophic cardiomyopathy: A β cardiac myosin heavy chain gene missense mutation. Cell. 1990; 62: 999–1006

Gherardi RK. Skeletal muscle involvement in HIV-infected patients. Neuropathol. Appl. Neurobiol. 1994; 20: 232–237

Giulian CG, Moss RL, Greaser ML. Improved methodology for analysis and quantitation of proteins on one-dimensional silver-stained slab gels. Anal Biochem. 1983; 129: 277-287

Glyn H, Sleep J. Dependence of adenosine triphosphatase activity of rabbit psoas muscle fibres and myofibrils on substrate concentration. J Physiol. 1985; 365: 259-276

Goebel HH, Piirsoo A, Warlo I, Schofer O, Kehr S, Gaude M. Infantile intranuclear rod myopathy. J. Child Neurol. 1997; 12: 22–30

Gokhin DS, Bang ML, Zhang J, Chen J and Lieber RL. Reduced thin filament length in nebulin-knockout skeletal muscle alters isometric contractile properties. Am J Physiol Cell. 2009; 296(5): C1123-32

Gordon AM, Homsher E, Regner M. Regulation of contraction in striated muscle. Physiol Rev. 2000; 80: 853-924

Gregorio CC, Antin PB. To the heart of myofibril assembly. Trends Cell Biol. 2000; 10:355-362

Gyure KA, Prayson RA, Estes ML. Adult-onset nemaline myopathy: a case report and review of the literature. Arch. Pathol. Lab. Med. 1997; 121: 1210–1213

Harris S, Foord SM. Transgenic gene knock-outs: functional genomics and therapeutic target selection . Pharmacogenomics. 2000; 1: 433-443

Ho CY, Sweitzer NK, McDonough B, Maron BJ, Casey S A, Seidman JG et al. Assessment of diastolic function with Doppler tissue imaging to predict genotype in preclinical hypertrophic cardiomyopathy. Circulation. 2002; 105: 2992–2997

Holmes KC, Popp D, Gebhard W, Kabsch W. Atomic model of the actin filament. Nature. 1990; 347, 44-49

Huxley AF. Muscle structure and theories of contraction. Prog Biophys Biophys Chem. 1957; 7:255-318

Huxley HE. The mechanism of muscolar contraction. Science. 1969; 164: 1356-65

Javadpour M M, Tardiff JC, Pinz I, Ingwall JS. Decreased energetics in murine hearts bearing the R92Q mutation in cardiac troponin T. Journal of Clinical Investigation. 2003; 112: 768– 775

Jennekens FG, Roord JJ, Veldman H, Willemse J, Jockusch BM. Congenital nemaline myopathy. I. Defective organization of α-actinin is restricted to muscle. Muscle Nerve. 1983; 6: 61–68

Jimenez J and Tardiff JC. Abnormal Heart Rate Regulation in Murine Hearts with Familial Hypertrophic Cardiomyopathy-related Cardiac Troponin T Mutations. Am J Physiol Heart Circ Physiol. 2011; 300(2): H627-35

Jin JP and Chong SM. Localization of the two tropomyosin-binding sites of troponin T. Arch Biochem Biophys. 2010; 500(2): 144-50

Jin JP and Wang K. Cloning, expression, and protein interaction of human nebulin fragments composed of varying numbers of sequence modules. J Biol Chem. 1991; 266: 21215-21223

Karpati G, Carpenter S, Eisen AA. Experimental core-like lesions and nemaline rods. A correlative morphological and physiological study. Arch. Neurol. 1972; 27: 237–251

Kawabuchi M. Neostigmine myopathy is a calcium ion-mediated myopathy initially affecting the motor end-plate. J. Neuropathol. Exp. Neurol. 1982; 41: 298–314

Kitaoka H, Doi Y, Casey SA, Hitomi N, Furuno T, Maron BJ. Comparison of prevalence of apical hypertrophic cardiomyopathy in Japan and the United States. American Journal of Cardiology. 2003; 92: 1183–1186

Klues HG, Schiffers A, Maron BJ. Phenotypic spectrum and patterns of left ventricular hypertrophy in hypertrophic cardiomyopathy: morphologic observations and significance as assessed by two-dimensional echocardiography in 600 patients. J Am Coll Cardiol. 1995; 26:1699-708

Kobayashi T, Solaro RJ. Calcium, thin filaments and the integrative biology of cardiac contractility. Annu. Rev. Physiol. 2005; 67: 39-67

Kokado H, Shimizu M, Yoshio H, Ino H, Okeie K, Emoto Y, Matsuyama T, Yamaguchi M, Yasuda T, Fujino N, et al. Clinical features of hypertrophic cardiomyopathy caused by a Lys183 deletion mutation in the cardiac troponin I gene. Circulation. 2000; 102: 663-669.

Kreutziger KL, Piroddi N, McMichael JT, Tesi C, Poggesi C, Regnier M. Calcium binding kinetics of troponin C strongly modulate cooperative activation and tension kinetics in cardiac muscle. J Mol Cell Cardiol. 2011; 50(1): 165-74

Kreutziger KL, Piroddi N, Scellini B, Tesi C, Poggesi C, Regnier M. Thin filament Ca2+ binding properties and regulatory unit interactions alter kinetics of tension developement and relaxation in rabbit skeletal muscle. J Physiol. 2008; 586(Pt 15): 3683-700

Labeit S, Barlow DP, Gautel M, Gibson T, Holt J, Hsieh CL, Francke U, Leonard K, Wardale J, Whiting A, et al. A regular pattern of two types of 100-residue motif in the sequence of titin. Nature. 1990; 345; 273-6

Labeit S and Kolmerer B. The complete primary structure of human nebulin and its correlation to muscle structure. J Mol Biol. 1995; 248: 308-315

Labeit S, Gibson T, Lakey A, Leonard K, Zeviani M, Knight P, Wardale J and Trinick J. Evidence that nebulin is a protein-ruler in muscle thin filaments. FEBS Lett. 1991; 282: 313-316

Laemmli UK. Cleavage of structural proteins during the assembly of the head of bacteriophageT4. Nature. 1970; 227: 680-685

Laing NG, Majda BT, Akkari PA, Layton MG, Mulley JC, Phillips H, Haan EA, White SJ, Beggs AH, Kunkel LM et al. Assignment of a gene (NEM1) for autosomal dominant nemaline myopathy to chromosome 1. Am. J. Hum. Genet. 1992; 50: 576–583

Lawlor MW, Ottenheijm CAC, Lehtokari VL, Cho K, Pelin K, Wallgren-Pettersson C, Granzier H and Beggs AH. Novel mutations in NEB cause abnormal nebulin expression and markedly impaired muscle force generation in severe nemaline myopathy. Skeletal Muscle. 2011; 1: 23

Lehman W, Vibert P, Uman P, Craig R. Steric-blocking by tropomyosin visualized in relaxed vertebrate muscle thin filaments. J Mol Biol. 1995; 251: 191-6

Lehtokari VL, Greenleaf RS, Dechene ET, Kellinsalmi M, Pelin K, Laing NG, Beggs AH and Wallgren-Pettersson C. The exon 55 deletion in the nebulin gene - One single founder mutation with world-wide occurrence. Neuromuscul Disord. 2009; 19: 179-181

Lehtokari VL, Pelin K, Sandbacka M, Ranta S, Donner K, Muntoni F, Sewry C, Angelini C, Bushby K, Van den BP, Iannaccone S, Laing NG and Wallgren-Pettersson C. Identification of 45 novel mutations in the nebulin gene associated with autosomal recessive nemaline myopathy. Hum Mutat. 2006; 27: 946-956

Le Winter MM, Wu Y, Labeit S, Granzier H. Cardiac titin: structure, functions and role in desease. Clin. Chim. Acta. 2007; 375(1-2): 1-9

Le Winter MM, Granzier H. Cardiac titin: a multifunctional giant. Circulation. 2010; 121: 2137-45

Linke WA, Bartoo ML, Pollack GH. Spontaneus sarcomeric oscillations at intermediate activation levels in single isolated cardiac myofibrils. Circ Res. 1993; 73: 724-34

Littlefield RS and Fowler VM. Thin filament length regulation in striated muscle sarcomeres: Pointed-end dynamics go beyond a nebulin ruler. Semin Cell Dev Biol. 2008; 19: 511-519

Luedde M, Flögel U, Knorr M, Grundt C, Hippe HJ, Brors B et al. Decreased contractility due to energy deprivation in a transgenic rat model of hypertrophic cardiomyopathy. Journal of Molecular Medicine. 2009; 87: 411–422

Manning EP, Tardiff JC and Schwartz SD. Molecular effects of familial hypertrophic cardiomyopathy-related mutations in the TNT1 domain of cTnT. J. Mol. Biol. 2012; 421: 54-66

Marian AJ, Wu Y, Lim DS, McCluggage M, Youker K, Yu QT et al. A transgenic rabbit model for human hypertrophic cardiomyopathy. Journal of Clinical Investigation. 1999; 104: 1683–1692

Maron BJ. Hypertrophic cardiomyopathy: a systematic review. Jama. 2002; 287: 1308-1320.

Maron BJ. Sudden death in young athletes. New England Journal of Medicine. 2003; 349: 1064–1075.

Maron BJ, Spirito P, Shen WK, Haas TS, Formisano F, Link MS et al. Implantable cardioverter-defibrillators and prevention of sudden cardiac death in hypertrophic cardiomyopathy. JAMA. 2007; 298: 405–412

Maron MS, Maron BJ, Harrigan C, Buros J, Gibson CM, Olivotto I, Biller L,Lesser JR, Udelson JE, Manning WJ, Appelbaum E Hypertrophic cardiomyopathy phenotype revisited after 50 years with cardiovascular magnetic resonance. J Am Coll Cardiol. 2009; 54:220-8

McElhinny AS, Kazmierski ST, Labeit S and Gregorio CC. Nebulin: the nebulous, multifunctional giant of striated muscle. Trends Cardiovasc Med. 2003; 13: 195-201

Meier C, Voellmy W, Gertsch M, Zimmermann A, Geissbühler J. Nemaline myopathy appearing in adults as cardiomyopathy. A clinicopathologic study. Arch. Neurol. 1984; 41: 443–445

Minns HG. A voltage-controlled force generator for calibrating sensitive transducers. J Appl Physiol. 1971; 30: 895-6

Mogensen J, Murphy RT, Kubo T, Bahl A, Moon JC, Klausen IC, Elliott PM, McKenna WJ. Frequency and clinical expression of cardiac troponin I mutations in 748 consecutive families with hypertrophic cardiomyopathy.Journal of the American College of Cardiology. 2004; 44: 2315-2325

Monnier N et al. An autosomal dominant congenital myopathy with cores and rods is associated with a neomutation in the RYR1 gene encoding the skeletal muscle ryanodine receptor. Hum. Mol. Genet. 2000; 9: 2599–2608

Moolman JC, Corfield VA, Posen B, Ngumbela K, Seidman C, Brink PA et al. Sudden death due to troponin T mutations. Journal of the American College of Cardiology. 1997; 29: 549–555

Moolman-Smook J, Flashman E, de Lange W, Li Z, Corfield V, Redwood C, Watkins H. Identification of novel interactions between domains of myosin binding protein C that are modulated by hypertrophic cardiomyopathy missense mutation. Circ. Res. 2002; 91: 704-711

Morris EP et al. The three-dimensional structure of the nemaline rod Z-band. J. Cell. Biol. 1990; 111: 2961–2978

Nagueh SF, Kopelen HA, Lim DS, Zoghbi WA, Quinones MA, Roberts R et al. Tissue Doppler imaging consistently detects myocardial contraction and relaxation abnormalities, irrespective of cardiac

hypertrophy, in a transgenic rabbit model of human hypertrophic cardiomyopathy. Circulation. 2000; 102: 1346–1350

Nistri S, Olivotto I, Betocchi S, Losi MA, Valsecchi G, Pinamonti B, Conte MR, Casazza F, Galderisi M, Maron BJ, Cecchi F. Prognostic significance of left atrial size in patients with hypertrophic cardiomyopathy (from the Italian Registry for Hypertrophic Cardiomyopathy). Am J Cardiol. 2006; 98:960-5

North KN et al. Nemaline myopathy: current concepts. J. Med. Genet. 1997; 34: 705–713

Nowak KJ et al. Mutations in the skeletal muscle α-actin gene in patients with actin myopathy and nemaline myopathy. Nat. Genet. 1999; 23: 208–212

Oakley CE, Hambly BD, Curmi PM, Brown LI. Myosin binding protein C: structural abnormalities in familial hypertrophic cardiomyopathy. Cell Res. 2004; 14: 95-110

Ogut O, Hossain MM and Jin JP. Interactions between nebulin-like motifs and thin filament regulatory proteins. J Biol Chem. 2003; 278: 3089-3097

Olivotto I, Gistri R, Petrone P, Pedemonte E, Vargiu D, Cecchi F. Maximum left ventricular thickness and risk of sudden death in patients with hypertrophic cardiomyopathy. J Am Coll Cardiol. 2003b; 41:315-21

Olivotto I, Maron MS, Autore C, Lesser JR, Rega L, Casolo G, De Santis M,Quarta G, Nistri S, Cecchi F, Salton CJ, Udelson JE, Manning WJ, Maron BJ. Assessment and significance of left ventricular mass by cardiovascular magnetic resonance in hypertrophic cardiomyopathy. J Am Coll Cardiol. 2008a; 52:559-66

Olivotto I, Cecchi F, Gistri R, Lorenzoni R, Chiriatti G, Girolami F, Torricelli F, Camici PG. Relevance of coronary microvascular flow impairment to long-term remodeling and systolic dysfunction in hypertrophic cardiomyopathy. J Am Coll Cardiol. 2006; 47:1043-8

Ottenheijm CA and Granzier H. Lifting the nebula: novel insights into skeletal muscle contractility. Physiology (Bethesda). 2010; 25: 304-310

Ottenheijm CA, Hooijman P, Dechene ET, Stienen GJ, Beggs AH and Granzier H. Altered myofilament function depresses force generation in patients with nebulin-based nemaline myopathy (NEM2). J Struct Biol. 2010; 170: 334-343

Ottenheijm CA, Witt CC, Stienen GJ, Labeit S, Beggs AH and Granzier H. Thin filament length dysregulation contributes to muscle weakness in nemaline myopathy patients with nebulin deficiency. Hum Mol Genet. 2009; 18: 2359-2369

Paulus W et al. Adult-onset rod disease with abundant intranuclear rods. J. Neurol. 1988; 235: 343–347

Pappas CT, Krieg PA and Gregorio CC. Nebulin regulates actin filament lengths by a stabilization mechanism. J Cell Biol. 2010; 189: 859-870

Pappas CT, Bliss KT, Zieseniss A, Gregorio CC. The nebulin family: an actin support group. Trends Cell Biol. 2011; 21(1): 29-37

Pelin K, Hilpela P, Donner K, Sewry C, Akkari PA, Wilton SD, Wattanasirichaigoon D, Bang ML, Centner T, Hanefeld F, Odent S, Fardeau M, Urtizberea JA, Muntoni F, Dubowitz V, Beggs AH, Laing NG, Labeit S, de la CA and Wallgren-Pettersson C. Mutations in the nebulin gene associated with autosomal recessive nemaline myopathy. *Proc Natl Acad Sci U S A* 1999; 96: 2305-2310

Piroddi N, Belus A, Scellini B, Tesi C, Giunti G, Cerbai E, Mugelli A, Poggesi C. Tension generation and relaxation in single myofibrils from human atrial and ventricular myocardium. Pflugers Arch - Eur J Physiol. 2007; 454: 63-73

Poggesi C, Tesi C, Stehle R. Sarcomeric determinants of striated muscle relaxation kinetics. Invited Rev. Pflugers Arch. 2005; 449: 505-517

Rifai Z et al. Intranuclear rods in severe congenital nemaline myopathy. Neurology. 1993; 43: 2372–2377

Ryan MM, Schnell C, Strickland CD, Shield LK, Morgan G, Iannaccone ST, Laing NG, Beggs AH, North KN. Nemaline myopathy: A clinical study of 143 cases. Ann. Neurol. 2001; 50(3): 312-20

Ryan MM, Ilkovski B, Strickland CD, Schnell C, Sanoudou D, Midgett C, Houston R, Muirhead D, Dennett X, Shield LK, De Girolami U, Iannaccone ST, Laing NG, North KN and Beggs AH. Clinical course correlates poorly with muscle pathology in nemaline myopathy. Neurology. 2003; 60: 665-673

Sanoudou D and Beggs AH. Clinical and genetic heterogeneity in nemaline myopathy--a disease of skeletal muscle thin filaments. Trends Mol Med. 2001; 7: 362-368

Scacheri PC et al. A novel ryanodine receptor gene mutation causing both cores and rods in congenital myopathy. Neurology. 2000; 55: 1689–1696

Schiaffino S and Reggiani C. Molecular diversity of myofibrillar proteins: gene regulation and functional significance. Physiol Rev. 1996; 76: 371-423

Shimomura C and Nonaka I. Nemaline myopathy: comparative muscle histochemistry in the severe neonatal, moderate congenital, and adult-onset forms. Pediatr. Neurol. 1989; 5: 25–31

Shy GM et al. Nemaline myopathy. A new congenital myopathy. Brain. 1963; 86: 793–810

Seidman CE & Seidman JG. Gene mutations that cause familial hypertrophic cardiomyopathy. In E. Haber (Ed.), Molecular cardiovascular medicine. 1995; 193–210

Solaro RJ and Van Eyk J. Altered interactions among thin filament proteins modulate cardiac function. J. Mol. Cell Cardiol. 1996; 28: 217-230

Squire JM. Architecture and function in the muscle sarcomere. Curr. Opin. Struct. Biol. 1997; 7: 247-257

Squire JM, Luther PK, Knupp C. Structural evidence for the interaction of C- protein (MyBP-C) with actin and sequence identificatio of a possible actin-binding domain. J. Mol. Biol. 2003; 331: 713-724

Stehle R, Krueger M, Pfitzer G. Force kinetics and individual sarcomere dynamics in cardiac myofibrils following rapid Ca2+ changes. Biophys J. 2002; 83: 2152-61

Stienen GJ, Kiers JL, Bottinelli R and Reggiani C. Myofibrillar ATPase activity in skinned human skeletal muscle fibres: fibre type and temperature dependence. J Physiol. 1996; 493 (Pt 2): 299-307

Sumandea MP, Pyle WG, Kobayashi T, de Tombe PP, Solaro RJ. Identification of a functionally critical protein kinase C phosphorylation residue of cardiac troponin T. J Biol Chem. 2003; 278: 35135-44

Takeda S, Yamashita A, Maeda K, Maeda Y. Structure of the core domain of human cardiac troponin in the Ca(2+) -saturated form. Nature. 2003; 424 (6944): 35-41

Takada F et al. Myozenin: An α-actininand γ-filamin-binding protein of skeletal muscle Z lines. Proc. Natl. Acad. Sci. U. S. A. 2001; 98: 1595–1600

Tardiff JC, Factor SM, Tompkins BD, Hewett TE, Palmer BM, Moore RL et al. A truncated cardiac troponin T molecule in transgenic mice suggests multiple cellular mechanisms for familial hypertrophic cardiomyopathy. Journal of Clinical Investigation. 1998; 101: 2800–2811

Tardiff JC. Thin filament mutations: developing an integrative approach to a complex disorder. Circ Res. 2011; 108: 765-782

Tesi C, Piroddi N, Colomo F, Poggesi C. Relaxation kinetics following sudden Ca2+ reduction in single myofibrils from skeletal muscle. Biophys J. 2002; 83: 2142-2151

Thierfelder L, Watkins H, MacRae C, Lamas R, McKennaW, Vosberg HP et al. α-Tropomyosin and cardiac troponin T mutations cause familial hypertrophic cardiomyopathy: A disease of the sarcomere. Cell. 1994; 77: 701–712

Valle G et al. Telethonin, a novel sarcomeric protein of heart and skeletal muscle.FEBS Lett. 1997; 415: 163–168

Vibert P, Craig R, Lehman W. Steric-model for activation of muscle thin filaments. J Mol Biol. 1997; 266: 8-14

Wallgren-Pettersson C. Congenital nemaline myopathy: a longitudinal study. Commentationes Physico-Mathematicae. 1990; 111: 1–102

Wallgren-Pettersson C, Laing NG. Report of the 70th ENMC International Workshop: nemaline myopathy, 11–13 June 1999, Naarden, The Netherlands. Neuromuscul. Disord. 2000; 10: 299–306

Watkins H, Conner D, Thierfelder L, Jarcho JA, MacRae C, McKenna WJ, Maron BJ, Seidman JG, Seidman CE. Mutations in the cardiac myosin binding protein-C gene on chromosome 11 cause familial hypertrophic cardiomyopathy. Nat Genet. 1995; 11: 434-437

Whitten AE, Jeffries Cm, Harris SP, Trewhella J. Cardiac myosin-binding protein C decorates F-actinin: implications for cardiac function. Proc. Natl. Acad. Sci. U .S. A. 2008; 105: 18360-18365

Witt CC, Burkart C, Labeit D, McNabb M, Wu Y, Granzier H and Labeit S. Nebulin regulates thin filament length, contractility, and Z-disk structure in vivo. EMBO J. 2006; 25: 3843-3855

Wolska BM, Wieczorek DM. The role of tropomyosin in the regulation of myocardial contraction and relaxation. Pflugers Arch.2003; 446: 1-8

Yamaguchi M et al. Nemaline myopathy rod bodies. Structure and composition. J. Neurol. Sci. 1982; 56: 35–56